



# **PLIOCENE TO RECENT SHORTENING OF THE SIWALIK GROUP IN THE HIMALAYAN FORELAND BELT**

***JOHN HIRSCHMILLER***

*DALHOUSIE UNIVERSITY, HALIFAX, NOVA SCOTIA, CANADA, B3H 2J1*

SUBMITTED IN PARTIAL FULFILLMENT OF THE REQUIREMENTS FOR THE DEGREE  
OF BACHELOR OF SCIENCE, HONOURS, DEPARTMENT OF EARTH SCIENCE,  
DALHOUSIE UNIVERSITY, HALIFAX, NOVA SCOTIA  
MARCH 18<sup>TH</sup>, 2013

## Distribution License

DalSpace requires agreement to this non-exclusive distribution license before your item can appear on DalSpace.

### NON-EXCLUSIVE DISTRIBUTION LICENSE

You (the author(s) or copyright owner) grant to Dalhousie University the non-exclusive right to reproduce and distribute your submission worldwide in any medium.

You agree that Dalhousie University may, without changing the content, reformat the submission for the purpose of preservation.

You also agree that Dalhousie University may keep more than one copy of this submission for purposes of security, back-up and preservation.

You agree that the submission is your original work, and that you have the right to grant the rights contained in this license. You also agree that your submission does not, to the best of your knowledge, infringe upon anyone's copyright.

If the submission contains material for which you do not hold copyright, you agree that you have obtained the unrestricted permission of the copyright owner to grant Dalhousie University the rights required by this license, and that such third-party owned material is clearly identified and acknowledged within the text or content of the submission.

If the submission is based upon work that has been sponsored or supported by an agency or organization other than Dalhousie University, you assert that you have fulfilled any right of review or other obligations required by such contract or agreement.

Dalhousie University will clearly identify your name(s) as the author(s) or owner(s) of the submission, and will not make any alteration to the content of the files that you have submitted.

If you have questions regarding this license please contact the repository manager at [dalspace@dal.ca](mailto:dalspace@dal.ca).

Grant the distribution license by signing and dating below.

---

Name of signatory

---

Date

AUTHOR: JOHN HIRSCHMILLER

TITLE: PLIOCENE TO RECENT SHORTENING OF THE SIWALIK GROUP IN THE  
HIMALAYAN FORELAND BELT

DEGREE: B.SC. HONS.

CONVOCATION: MAY

YEAR: 2013

PERMISSION IS HEREWITH GRANTED TO DALHOUSIE UNIVERSITY TO CIRCULATE  
AND TO HAVE COPIED FOR NON-COMMERCIAL PURPOSES, AT ITS DISCRETION,  
THE ABOVE TITLE UPON THE REQUEST OF INDIVIDUALS OR INSTITUTIONS.



---

SIGNATURE OF AUTHOR

THE AUTHOR RESERVES OTHER PUBLICATION RIGHTS, AND NEITHER THE THESIS  
NOR EXTENSIVE EXTRACTS FROM IT MAY BE PRINTED OR OTHERWISE  
REPRODUCED WITHOUT THE AUTHOR'S WRITTEN PERMISSION.

THE AUTHOR ATTESTS THAT PERMISSION HAS BEEN OBTAINED FOR THE USE OF  
ANY COPYRIGHTED MATERIAL APPEARING IN THIS THESIS (OTHER THAN BRIEF  
EXCERPTS REQUIRING ONLY PROPER ACKNOWLEDGEMENT IN SCHOLARLY  
WRITING) AND THAT ALL SUCH USE IS CLEARLY ACKNOWLEDGED.

## ABSTRACT

The 2500 km long Himalayan orogen is characterized by continuity of the principal lithotectonic units. There is evidence for faster convergence rates in the eastern portion the orogen compared to the western portion; in addition, present-day precipitation rates and Late Miocene erosion rates indicate a west-to-east increasing gradient. Further complications are induced by the Shillong Plateau, which is a basement pop-up structure in front of the eastern Himalaya, and the only active structure in the Himalayan foreland that could accommodate or partition 4-7 mm/yr of plate convergence. This study aims to test whether these differences are reflected in the rates of tectonic activity and shortening along the range. To do so I have constructed balanced cross-sections for 10 transects across the Siwalik Group.

The Siwalik Group comprises the deformed part of the Neogene foreland basin along the southern orogen margin. The group consists of synorogenic sediments, which date back to ca. 18.5 Ma and form the youngest and frontal parts of the Himalayan fold-and-thrust belt. Thrust faults in the Sub-Himalaya are splays of a major décollement (the Main Himalayan Thrust), which spans the entire Himalaya thrust belt. Several south-verging thrusts define the deformation and shortening in the Siwalik Group: (1) the Main Boundary Thrust is the backstop of the Siwalik group against the Lesser Himalaya, (2) a succession of duplexes are present within the Sub-Himalaya, and (3) the Main Frontal Thrust is the frontal deformed toe.

During the last 11 myr, convergence rates between the Indian plate and the Eurasian plate were at a steady rate, but with a lateral gradient of ca. 34 mm/yr in the northwest to ca. 44 mm/yr in the northeast of India. Current GPS velocities are consistent with plate convergence velocities, since rates are ca. 10 mm/yr greater in the east than the west. By constructing internally consistent cross-sections, the shortening rates and strain rates obtained helped determine differences in strain rates and shortening rates along the Himalaya. There is a distinct west-to-east increase in strain rate across the Himalaya arc, which correlates with two external parameters.

The exact cause of the west-to-east trend of Pliocene to present shortening can only be determined through quantitative testing of parameters. However, it is seen that rainfall amounts along the Himalayan arc have a direct correlation to strain rates, as there are higher strain rates and rainfall in the west than the east.

# TABLE OF CONTENTS

TABLE OF FIGURES .....	v
LIST OF TABLES.....	4
ACKNOWLEDGMENTS .....	5
<b>1. INTRODUCTION.....</b>	<b>6</b>
1.1. PURPOSE .....	6
1.2. DATA INTEGRITY.....	8
<b>2. GEOLOGICAL SETTING .....</b>	<b>10</b>
2.1. TECTONICS AND CONVERGENCE .....	10
2.2. REGIONAL HIMALAYA GEOLOGY .....	18
2.2.1. LITHOTECTONIC UNITS .....	19
2.2.2. STRUCTURES .....	22
2.3. SIWALIK GROUP .....	24
2.3.1. SEDIMENTOLOGY OF THE SIWALIK GROUP .....	24
2.3.2. DEPOSITIONAL AGE OF THE SIWALIK GROUP .....	29
2.4. STRUCTURE WITHIN THE SIWALIK GROUP .....	32
2.5. MECHANICS OF OROGENIC WEDGES .....	33
2.5.1. MECHANICS OF A BULLDOZER WEDGE .....	34
2.5.2. CRITICAL TAPER MODEL AND COULOMB WEDGES .....	35
2.5.3. EROSION AND FLUX BALANCE IN OROGENIC WEDGES.....	41
2.5.4. OROGENIC WEDGE IN THE SUB-HIMALAYA .....	43
<b>3. BALANCED CROSS-SECTIONS .....</b>	<b>45</b>
3.1. BALANCED CROSS-SECTIONS IN THEORY.....	45
3.2. CONSTANT LENGTH RESTORATION .....	47
3.3. CONSTANT AREA RESTORATION.....	50
3.4. WORKFLOW .....	52
3.5. RESULTS .....	55
3.5.1. BALANCED CROSS-SECTIONS AND MAPS.....	55
3.5.2. SECTION RESULTS.....	73
<b>4. DISCUSSION.....</b>	<b>77</b>
4.1. SEDIMENTATION RATES AND FORMATION LENGTH.....	78
4.2. EROSION AND RAINFALL RATES .....	79
4.3. CRITICAL TAPER MODEL.....	82
4.4. ALONG-STRIKE SHORTENING DIFFERENCES .....	83
4.5. CORRELATION TO PLATE STRAIN RATES .....	85
4.6. CORRELATION TO THE SHORTENING ACROSS THE LHS.....	86
<b>5. CONCLUSIONS AND RECOMMENDATIONS .....</b>	<b>88</b>
5.1. CONCLUSIONS.....	88
5.2. RECOMMENDATIONS AND FURTHER WORK .....	88
<b>6. REFERENCES .....</b>	<b>90</b>
APPENDIX.....	96

## TABLE OF FIGURES

FIGURE 1.1 – GEOLOGICAL OVERVIEW MAP OF THE HIMALAYA .....	8
FIGURE 2.1 - MAP SHOWING THE RECONSTRUCTIONS OF THE TWO SITES ON THE INDIAN PLATE WITH RESPECT TO THE EURASIAN PLATE .....	11
FIGURE 2.2 - CONVERGENCE RATES OF THE HIMALAYAN ARC .....	12
FIGURE 2.3 - GPS VELOCITY MAP OF INDIA.....	14
FIGURE 2.4 - MAJOR STRUCTURAL FEATURES OVERLAIN ON DIGITAL TOPOGRAPHY OF SOUTHERN BHUTAN AND THE SHILLONG PLATEAU AREA.....	15
FIGURE 2.5 - NORTHEAST HIMALAYA AND SHILLONG DISLOCATION MODEL .....	17
FIGURE 2.6 - SCHEMATIC CROSS SECTION AND BLOCK DIAGRAM OF THE HIMALAYA OROGEN .....	19
FIGURE 2.7 – GENERALIZED STRATIGRAPHIC COLUMN OF THE SIWALIKS GROUP IN EASTERN BHUTAN .....	24
FIGURE 2.8 – SCHEMATIC DIAGRAM OF FORELAND BASIN EVOLUTION. ....	25
FIGURE 2.9 - SIWALIK GROUP GENERALIZED STRATIGRAPHIC CHART FROM WESTERN NEPAL .....	28
FIGURE 2.10 - MODERN DAY MEGAFANS AND MAJOR DRAINAGES ON THE SUB-HIMALAYA ALLUVIAL PLAIN IN FRONT OF THE HIMALAYA IN EASTERN NEPAL .....	29
FIGURE 2.11 - GEOLOGICAL OVERVIEW MAP OF THE HIMALAYA WITH STRATIGRAPHIC SECTION LOCATIONS .....	30
FIGURE 2.12 - MAGNETO STRATIGRAPHIC CORRELATION OF THE SIWALIK GROUP ACROSS THE HIMALAYAN ARC .....	31
FIGURE 2.13 - BALANCED CROSS-SECTION THROUGH THE FRONTAL BELT OF WESTERN NEPAL SHOWING THE STYLE OF DEFORMATION IN THE SUB-HIMALAYA.....	33
FIGURE 2.14 - CARTOON DEPICTING THE SELF-SIMILAR GROWTH OF A BULLDOZER WEDGE.....	34
FIGURE 2.15 - BRITTLE AND PLASTIC ROCK STRENGTHS AS A FUNCTION OF DEPTH .....	36
FIGURE 2.16 - GEOMETRY OF AN OROGENIC WEDGE .....	38
FIGURE 2.17 - MOHR DIAGRAM ILLUSTRATING STRESS WITHIN THE OROGENIC WEDGE.....	41
FIGURE 2.18 - AN ERODING OROGENIC WEDGE .....	42
FIGURE 2.19 - VOLUME, MASS, AND TIME TRANSFER CYCLE FOR THE SUB-HIMALAYA WEDGE .....	44

FIGURE 3.1 - RESTORATION OF FAULT TRAJECTORY. A) ADMISSIBLE RESTORED FAULT TRAJECTORY. B) INADMISSIBLE RESTORED FAULT TRAJECTORY .....	45
FIGURE 3.2 - BALANCED CROSS-SECTION AND MAP, USING THE CONSTANT LENGTH METHOD THROUGH THE BHUTAN HIMALAYA FOLD-AND-THRUST BELTS .....	47
FIGURE 3.3 - FLEXURAL SLIP RESTORATION OF A FAULT BENT FOLD.....	50
FIGURE 3.4 - CONSTANT AREA BALANCING OF SECTIONS.....	51
FIGURE 3.5 – LANDSAT GEOCOVER MAP OF THE HIMALAYAN ARC .....	56
FIGURE 3.6 - GEOLOGICAL OVERVIEW MAP OF THE HIMALAYA.....	57
FIGURE 3.7 - GEOLOGICAL MAP OF NORTH WESTERN INDIA (HIMACHAL PRADESH).....	58
FIGURE 3.8 - CROSS-SECTION A. CROSS-SECTION TRACE IS INDICATED ON MAP 1 (FIGURE 3.7) .....	59
FIGURE 3.9 - CROSS-SECTION B. CROSS-SECTION TRACE IS INDICATED ON MAP 1 (FIGURE 3.7) .....	60
FIGURE 3.10 - MAP 2, DETAILED GEOLOGICAL MAP OF THE SIWALIKS FORMATION, WESTERN NEPAL .....	61
FIGURE 3.11 - CROSS-SECTION C. CROSS-SECTION TRACE IS INDICATED ON MAP 2 (FIGURE 3.10).....	62
FIGURE 3.12 - CROSS-SECTION D. CROSS-SECTION TRACE IS INDICATED ON MAP 2 (FIGURE 3.10) .....	63
FIGURE 3.13 - CROSS-SECTION E. CROSS-SECTION TRACE IS INDICATED ON MAP 2 (FIGURE 3.10).....	64
FIGURE 3.14 - CROSS-SECTION F. CROSS-SECTION TRACE IS INDICATED ON MAP 2 (FIGURE 3.10).....	65
FIGURE 3.15 - MAP 3, DETAILED GEOLOGICAL MAP OF THE SIWALIKS FORMATION, EASTERN NEPAL .....	66
FIGURE 3.16 - CROSS-SECTION G. CROSS-SECTION TRACE IS INDICATED ON MAP 3 (FIGURE 3.15) .....	67
FIGURE 3.17 - CROSS-SECTION H. CROSS-SECTION TRACE IS INDICATED ON MAP 3 (FIGURE 3.15) .....	68
FIGURE 3.18 - MAP 4, DETAILED GEOLOGICAL MAP OF THE SIWALIKS FORMATION, EASTERN BHUTAN ...	69
FIGURE 3.19 - CROSS-SECTION I. CROSS-SECTION TRACE IS INDICATED ON MAP 4 (FIGURE 3.18).....	70
FIGURE 3.20 - MAP 5, DETAILED GEOLOGICAL MAP OF THE SIWALIKS FORMATION, ARUNACHEL PRADESH. .....	71
FIGURE 3.21 - CROSS-SECTION J. CROSS-SECTION TRACE IS INDICATED ON MAP 5 (FIGURE 3.20) .....	72
FIGURE 3.22 - GRAPH OF SHORTENING RATE AND STRAIN RATE OF THE SIWALIK GROUP VS. DISTANCE ALONG THE HIMALAYA ARC.....	76
FIGURE 3.23 – SHORTENING VS. DISTANCE OF THE LOWER SIWALIK GROUP ALONG THE HIMALAYA ARC .	76
FIGURE 4.1 – OROGENIC WEDGE RESPONSE TO EROSIONAL EFFICIENCY CHANGES, K.....	80
Pliocene to Recent Shortening of the Siwalik Group in the Himalayan Foreland Belt	2

FIGURE 4.2 - MEAN ANNUAL RAINFALL AVERAGED OVER 10 YEARS ..... 81

FIGURE 4.3 - GRAPH OF SHORTENING RATE AND STRAIN RATE OF THE SIWALIK VS. DISTANCE ALONG THE HIMALAYA ARC WITH TOTAL ANNUAL RAINFALL OVERLAIN ..... 81

FIGURE 4.4 - GRAPH OF THE LENGTHS OF THE SIWALIK SECTIONS VS. DISTANCE ALONG THE HIMALAYA ARC WITH TOTAL ANNUAL RAINFALL OVERLAIN ..... 82

FIGURE 4.5 - TRANSFER ZONES IN WESTERN NEPAL, HIGHLIGHTED WITH TRANSPARENT BOXES. .... 84

FIGURE 4.6 – GRAPH OF SHORTENING RATE SHORTENING AND STRAIN RATE OF THE SIWALIK GROUP AND THE INDIAN PLATE STRAIN RATE VS. DISTANCE ALONG THE HIMALAYA ARC..... 85

FIGURE 4.7 - COMPILATIONS OF SHORTENING ESTIMATES FROM WEST-TO-EAST ACROSS THE HIMALAYAN ARC. .... 86



## **LIST OF TABLES**

TABLE 3.1 - RESULTS FROM THE TEN BALANCED SECTIONS ..... 75

TABLE 4.1 - COMPILATION OF SHORTENING ESTIMATES IN THE SUB-HIMALAYA AND LESSER HIMALAYA... 87

## **ACKNOWLEDGMENTS**

First and foremost I would like to thank my supervisor, Dr. Djordje Grujic, for providing me with the opportunity to work on this challenging project, and inspiring me to understand Himalayan Geology. It was an honour to work with you, and collaborate with you on this project. Without the data provided by Dr. Tank Ojha, Dr. Jean-Louis Mugnier, Dr. Pascale Huyghe, and again Dr. Djordje Grujic, this project would not have been feasible, and thus for I am much indebted. I would also like to thank Midland Valley for the access, and license to MOVE, which allowed me to easily and accurately balance cross-sections. Last but not least, I would like to thank Dr. Martin Gibling for the immense help through the writing process, both with the EARTH 4200 class, and with all the proofreading edits. I am much indebted to you, as this thesis would not have been as near as coherent without your input.

# 1. INTRODUCTION

## 1.1. PURPOSE

The goal of this thesis is to determine if there are differences in shortening rates and amount of shortening along the Himalayan Arc. If so, what are the potential causes of this variability?

Mountain belts are formed by interactions and feedbacks between tectonics and surface processes (erosion and sedimentation). The hypothesis is that the spatial or temporal changes in shortening rates can be correlated with the changes of one or more parameters that control the deformation of the foreland fold-and-thrust belt. Because the Sub Himalayas are the youngest tectonic unit of the Himalayan orogen, the stratigraphic age of the strata, linked to denudation of the orogen, is precisely constrained.

The convergence rates between the Indian and Eurasian plates are well constrained in time and space (Molnar and Stock, 2009). The partitioning of this convergence along the Himalayan Arc is well documented from ongoing GPS measurements (Banerjee et al., 2008). Previous work has also been completed by a number of researchers on climatic parameters (Bookhagen and Burbank, 2010; Grujic et al., 2006).

To test the hypothesis and to achieve the goal of this project, the following specific objectives will be pursued:

1. Interpret cross-sections along the Himalayan foreland arc within the Sub-Himalaya group.
2. Calculate shortening amounts and rates throughout the Himalayan foreland within the Sub-Himalaya group.
3. Suggest factors for the spatial and temporal changes in shortening.
4. Propose a tectonic model which best fits the shortening history.

Number of researchers have constructed balanced sections along the Himalayan Orogen (Coward and Butler, 1985; Srivastava and Mitra, 1994; Mugnier et al., 1999b; Mugnier et al., 1999a; Long et al., 2011a; Schelling and Arita, 1991; Schelling, 1992; Mitra et al., 2010, et al.). Methods and tools of cross-section balancing used by the researchers vary. Due to the varied approach, an accurate qualitative comparison of shortening across the Himalayan Arc is not possible. Once an appropriate picture of the shortening rates along the Himalayan Arc is determined, factors influencing shortening rate can be discussed. Factors may include:

1. Changes in sedimentation and/or erosion rates, (influence from monsoons which influence the erosion and sedimentation).
2. Changes in convergence rate.
3. Changes in partitioning of convergence (e.g., formation of pop-up structures, such as the Shillong Plateau).
4. Changes in the critical taper model which is controlled by the sedimentation and erosion in the orogenic wedge.

Having an internally consistent understanding of the shortening of the Sub-Himalaya group throughout the Himalayan arc allows for discussion on factors which influence the shortening rates.

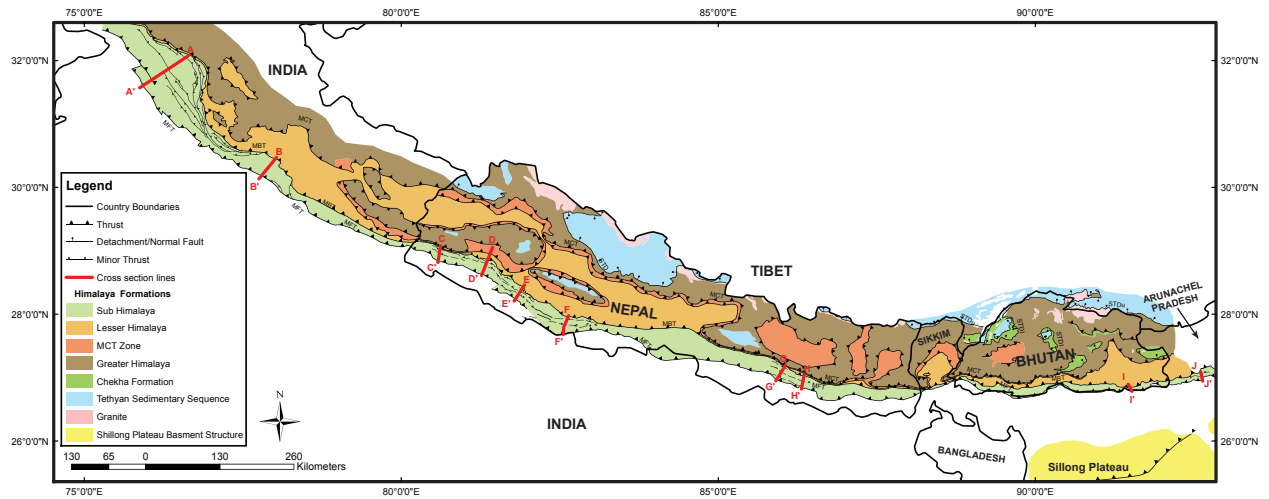


**Figure 1.1 – Geological overview map of the Himalaya. Balanced cross-sections of the Siwalik Group are indicated with red lines. Compiled from McQuarrie et al. (2008), Powers et al., (1998), Chirouze et al., (2012), Mugnier et al., (1999a) and Ojha (personal communication, 2012).**

## 1.2. DATA INTEGRITY

Within the Sub-Himalaya, nine cross-sections have been completed through the Sub-Himalaya and Lesser Himalaya (Coward and Butler, 1985; Srivastava and Mitra, 1994; Schelling and Arita, 1991; Schelling, 1992; Mitra et al., 2010; Long et al., 2011a; Yin, 2010). Mugnier et al. (1999a), Mugnier et al. (1999b) and Powers et al. (1998) also constructed a series of cross-sections through the Sub-Himalaya. Since the sections were completed with distinctive methodologies, and different individuals drawing them, the sections are not internally consistent. These cross-sections were compilations not just

across the Sub-Himalaya, but also the Lesser Himalaya and in some cases, the Greater Himalaya.

Reconstructing sections using historic data, as well as new information, allowed for an internally consistent set of sections and comparison of the sections. Strain rates and shortening rates throughout the Sub-Himalayan arc were calculated. The results of the modeling indicate that there is a west-to-east increase in the strain rate within the Sub-Himalaya across the Himalayan arc. I was able to see a change in strain rates from 7.96 %/myr in the east to 21.96%/myr in the west. It is suggested that rainfall has influenced the strain rates, as there is a greater amount of rainfall in the east.

## **2. GEOLOGICAL SETTING**

### **2.1. TECTONICS AND CONVERGENCE**

Since the collision and closure of the Tethyan Ocean at ca. 50 Ma, the convergence between India and Eurasia has been ongoing. The convergence rate has changed stepwise or continuously and it has been consistently faster in the NE corner than in the NW corner, resulting in the progressive counterclockwise rotation of the Indian plate (Molnar and Stock, 2009; Gan et al., 2007).

The movement of the Indian plate colliding with the Eurasian plate was reconstructed by Molnar and Stock (2009). The position of the Indian plate was mapped using magnetic anomalies and fracture zones, on ocean bottoms, to predict the angular velocity. The reconstructions by Molnar and Stock (2009) combined India, Somalia Nubia, North America and Eurasia to create a reconstruction of the relative positions of the Indian plate with respect to the Eurasian plate.

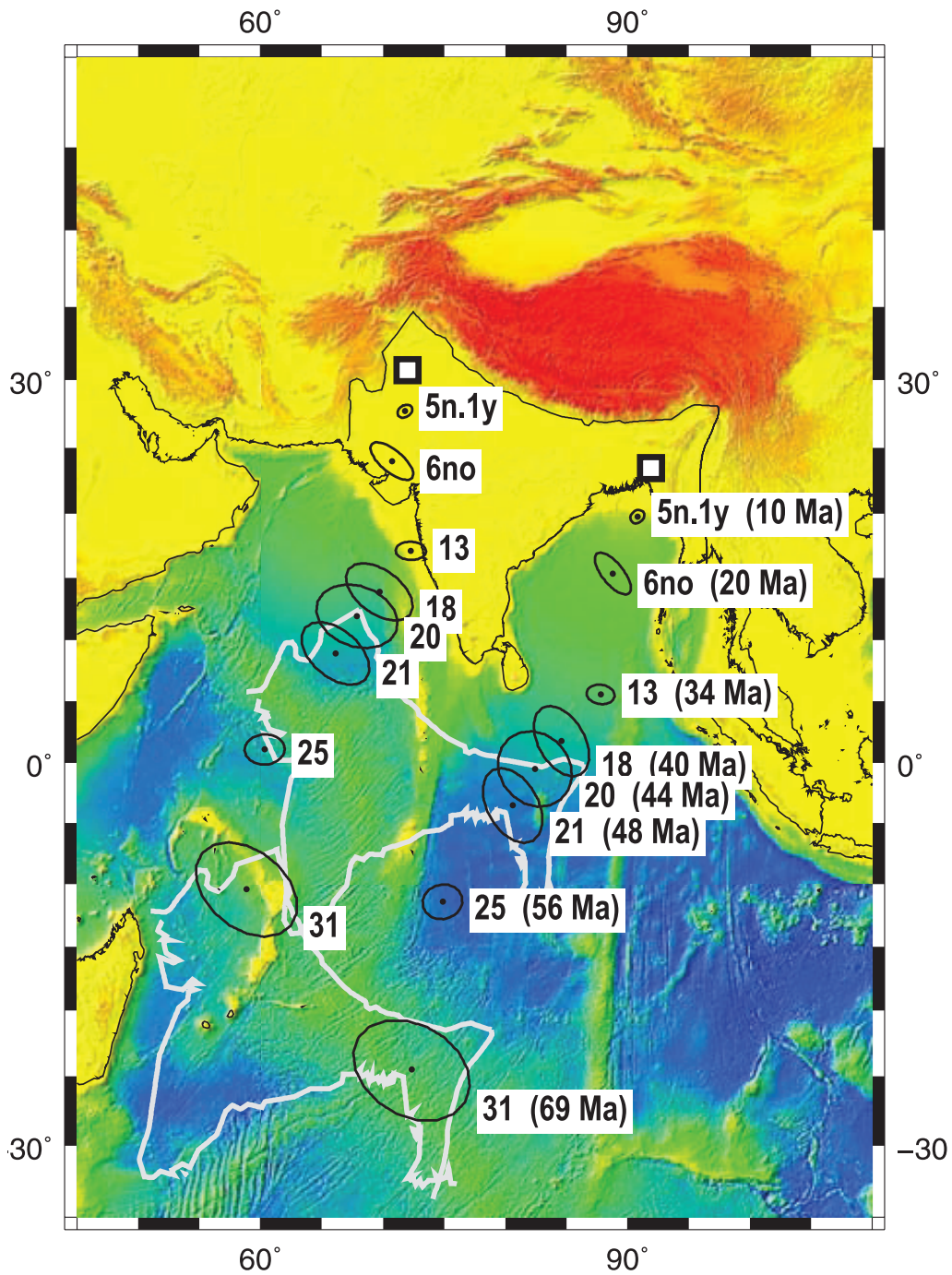
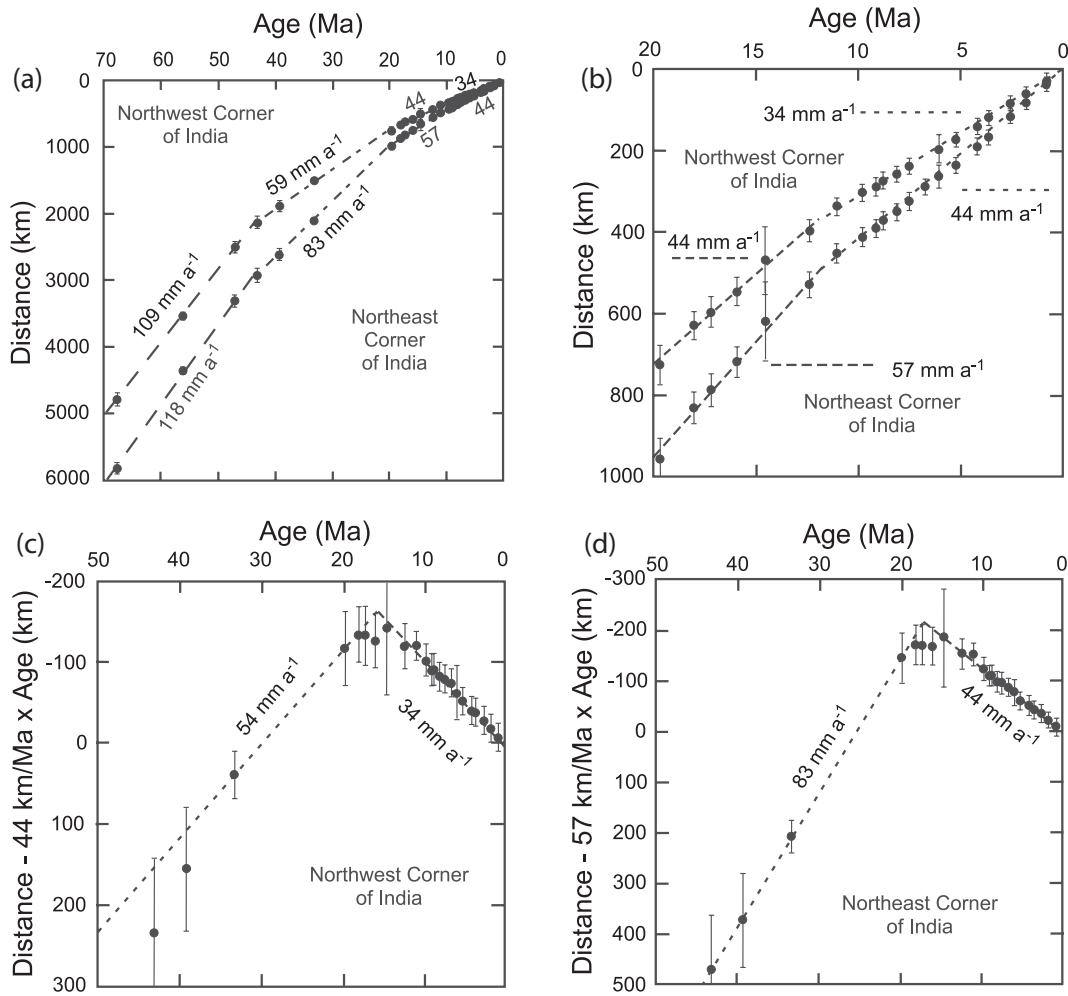


Figure 2.1 - Map showing the reconstructions of the two sites on the Indian plate with respect to the Eurasian plate. The present position is shown with white boxes and the black dots that represent the reconstructions and the ellipses correspond to 95% uncertainty (Molnar and Stock, 2009). India's position is shown through time in the white outline. The white boxes with ages correspond to the position of India at that time. The colors represent the current thickness of the lithosphere, showing the thick Himalayan and Tibetan crust in red, and the thin oceanic crust in blue.





**Figure 2.2 - Convergence rates of the Himalayan Arc (Molnar and Stock, 2009).** (a) Distances of points from current location at different times in the past. The average convergence rates are seen during different intervals, along the Northwest corner and Northeast corner of India. (b) A plot of Figure 2.2a, but zoomed in to the last 20 Ma. (c) & (d) Abrupt change in convergence rate in both NW and NE corner of India. Abrupt slowing of convergence has occurred since ca. 20 Ma, and has been constant since ca. 11 Ma.

The rate of convergence between India and Eurasia has slowed since 45-50 Ma. There was a large drop in the convergence around 20 Ma. Convergence rates at ca. 40-45 Ma changed from 109 to 59 mm/yr in northwestern India and from 118 to 83 mm/yr in northeastern India. Rates dropped ca. 45% between 11 and 20 Ma from 59 to 34 mm/yr in northwest India and from 83 to 44 mm/yr in northeast India. Convergence rates have been constant since ca. 11 Ma with convergence of 34 mm/yr in northwest

India and 44 mm/yr in northeast India (Molnar and Stock, 2009). The last change may have been gradual occurring between 20 and 11 Ma (Figure 2.2 a and b), or may have occurred abruptly at ca. 17 Ma (Figure 2.2 c and d).

GPS data of the shortening rates across the Himalaya arc was collected from 1995-2007 and was interpreted by comparing data from locations of the base stations in India with stations located in the Himalayas and Tibet. To collect the GPS data, a series of stations were sampled within the Himalaya and compared to IGS tracking stations (base station). The stations in the Himalaya were occupied for ca. 5 days and observed for 3-10 years. The movement of the stations in the Himalaya were compared to the IGS tracking station. This difference in distance of the two allows for the velocity to be calculated. With GPS shortening rate, the rates cumulatively increase the further distance away from the base station (Banerjee et al., 2008; Gan et al., 2007). Each part of the Himalaya has different shortening rates. The velocity of the front of the Himalaya compared to the base station is slower than the velocity in the center of the Himalaya compared to the base station. This difference is due to shortening occurring at different parts in the Himalaya rather than along a single fault. With the velocity from the center of the Himalaya to the base station, takes into the account the shortening in other places in-between, the furthest point and base station and displaying a cumulative value of the shortening rates. This constant increase of shortening allows for partitioning of the GPS convergence rates. To calculate the shortening of one specific region of the Himalaya, the shortening convergence rates of the areas closer to the base station must be subtracted first. For example, in Figure 2.3, the red track, which intersects the Pliocene to Recent Shortening of the Siwalik Group in the Himalayan Foreland Belt 13

Shillong plateau, should be reduced by 4-7 mm/yr to calculate the shortening for the Sub-Himalaya (Banerjee et al., 2008).

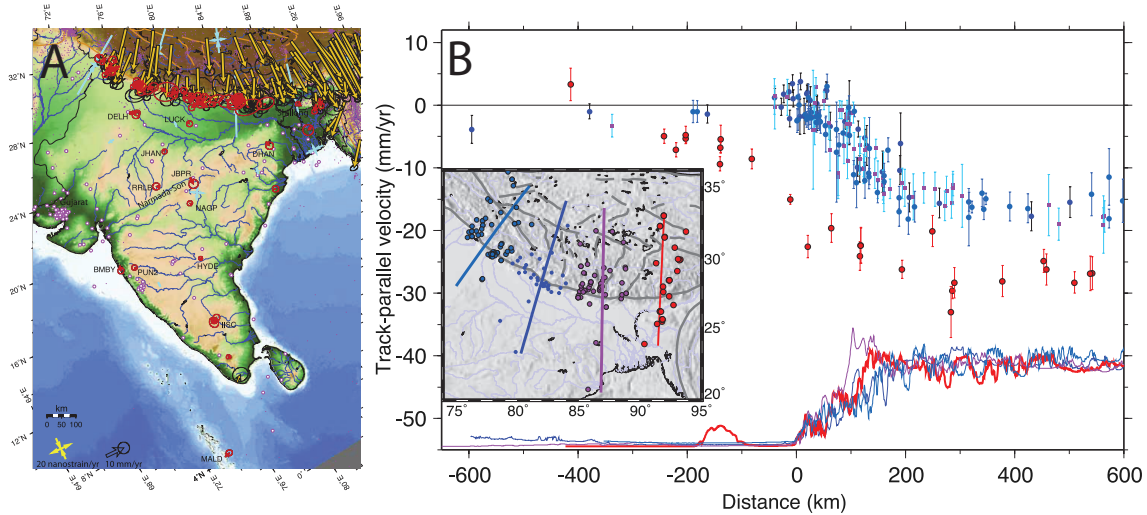


**Figure 2.3 - GPS velocity map of India. (A) Map showing the GPS velocities with respect to the reference frame. Orange arrows have larger rates with respect to India, and Red arrows are GPS velocities of <4mm/yr. Magenta dots represent earthquakes from 1935-2008 (B) GPS velocities with respect to the stable India. Inset map shows the sites included for each of the four profiles. The lines on the bottom of the graph show the topography along each profile line. The three profiles to the west track each other closely. The velocity of the most eastern profile shows convergence rates ca. 10 mm/yr greater than those to the west. This could be due to the Shillong plateau as it moves southward with respect to the India base stations at 4-7 mm/yr (Banerjee et al., 2008).**

The Shillong Plateau is an important part of the shortening history in the eastern portion of the Himalayan arc. The plateau forms the only elevated area in front of the Himalayan orogen.

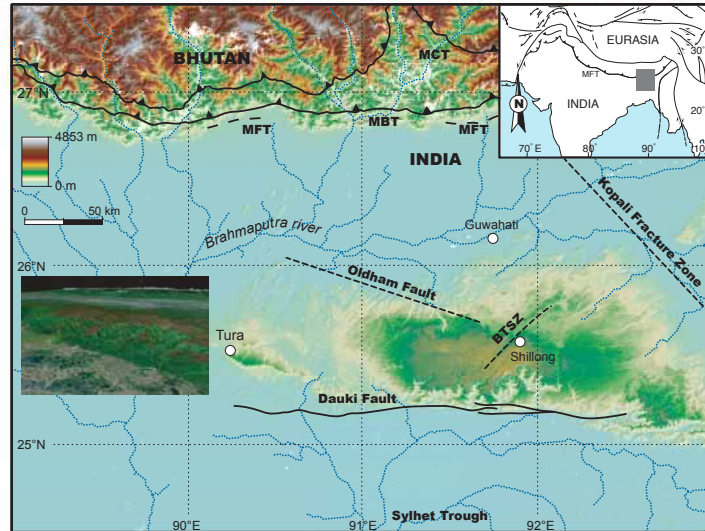


Figure 2.4 - Major structural features overlain on digital topography of Southern Bhutan and the Shillong Plateau area. Modified from Biswas et al. (2007).

The faults bounding it to the north and south are seismically active (Biswas et al., 2007; Bilham et al., 2003; Clark and Bilham, 2008) and the question is to what extent the slip along these faults partitions the convergence rate between India and Eurasia. If there is a strong partitioning, the segment of the Himalayas to the north of the Plateau may undergo slower shortening than the rest of the Himalayas. The first modern analysis of the kinematics of the Shillong Plateau suggested that the shortening rate across the plateau is  $4 \pm 2$  mm/yr assuming that the uplift of the plateau started 2-5 Myr ago (Bilham and England, 2001). According to the estimate of the contraction rate of 18 mm/yr would imply that the faults of Shillong plateau absorb up to one third of the Himalayan contraction rate. Although the sedimentological data indicate that the plateau was submerged until the Pliocene, the thermochronological data (Biswas et al., 2007) indicate that the uplift of the basement of the Shillong plateau started sometime between 15 and 9 Ma. Since the basement of the Plateau was covered by soft Tertiary

sediments, these were easily eroded and the rock uplift and exhumation did not result in surface uplift; only when the hard basement rocks were exposed did surface erosion decrease and the basement rock uplift was converted into surface uplift (Biswas et al., 2007). The surface uplift as estimated by the same thermochronological data is estimated to have started between 5.5 and 3.5 Ma. Taking into account the difference in basement level between the hanging wall (Plateau) and foot wall (Silhet Trough) of the Dauki fault, Biswas et al. (2007) and Clark and Bilham (2008) estimated that the long-term shortening rate across the plateau is actually 0.65–2.3 mm/a, or 1.0- 2.0 mm/a respectively, which represents only 10 – 15% of the Himalayan contraction rate.

Based on more recent GPS measurements the horizontal shortening rates across the Plateau were calculated to be 4 - 7 mm/yr (Bilham et al., 2003; Banerjee et al., 2008), somewhat more precise than the previous estimate of  $6.3 \pm 3.8$  mm/a (Banerjee et al., 2008; Bilham et al., 2003). In addition, the available GPS data for the eastern Himalaya indicate that this segment of the orogen is contracting at ca. 22-24 mm/yr. Although the GPS contraction rates across the Shillong Plateau are larger than the long-term shortening rates, it appears that the contraction rate across the Eastern Himalaya is not lower than for the central segment of the orogen. If the movement along the faults bounding the plateau partition 16 - 30% of plate convergence, removing 4 - 7 mm/yr from 21 - 24 mm/yr yields 14 - 20 mm/yr contraction across the eastern Himalaya which is slightly faster than the central Himalaya (Molnar and Stock, 2009; Banerjee et al., 2008). Consequently, questions emerge.

- a) Is the partitioned convergence a recent pattern or is it a long-term (Late Miocene to present) rate of shortening of the Himalaya?
- b) Did the shortening rate in the eastern Himalaya decrease from a higher value and the recent value is only a coincidence?
- c) Is the shortening rate of the Shillong plateau faster now (GPS) data than in the past (thermochronological data e.g. Biswas et al., 2007), or is the difference in estimated rate biased by the different techniques and time scales of observations?
- d) If the shortening rates across the Himalayas are everywhere the same, how is that reconciled with the different plate convergence rates estimated for the eastern and western corners of the Indian plate, 44 and 34 mm/a respectively over the period of the last 11 Ma (Molnar and Stock, 2009)?

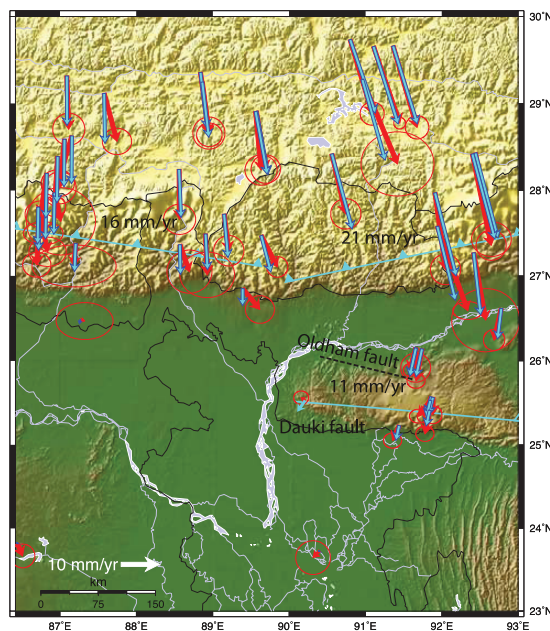


**Figure 2.5 - Northeast Himalaya and Shillong dislocation model. Close-up of NE India and Shillong plateau in Mercator projection with modeled (cyan) velocities and with observed (red). Updip, southern edges of three rectangular dislocations are labeled with optimal model slip rates (Banerjee et al., 2008). The GPS observed and modeled data shows great shortening rates in the Himalayan arc even though there is shortening in the Shillong plateau. Shortening rates from Banerjee et al. (2008) suggest rates of 4-7 mm/yr.**

## **2.2. REGIONAL HIMALAYA GEOLOGY**

The timing of collision of India and Asia is a matter of heated debate, and several criteria have been used to pinpoint the event, but in general it can be assumed that it occurred at 45-55 Ma (Hodges, 2000; Molnar and Stock, 2009). The ongoing convergence between India and Eurasia led to uplift of the Himalayas and Tibet. Shortening occurred in the Himalayas with southward propagating thrusts (Quade et al., 1995). The thickening of the Himalayan crust did not commence until the late Oligocene to early Miocene (Quade et al., 1995).

Molasse-type sediments were shed from the Himalayan highlands and deposited in the foreland basin, stretching continuously from northeast India to northwest Pakistan (Beaumont, 1981; Quade et al., 1995). The sedimentary basin was formed in the foreland of the Himalaya as a result of flexural loading (Quade et al., 1995; Beaumont, 1981). These molassic sediments are known as the Siwalik Group.

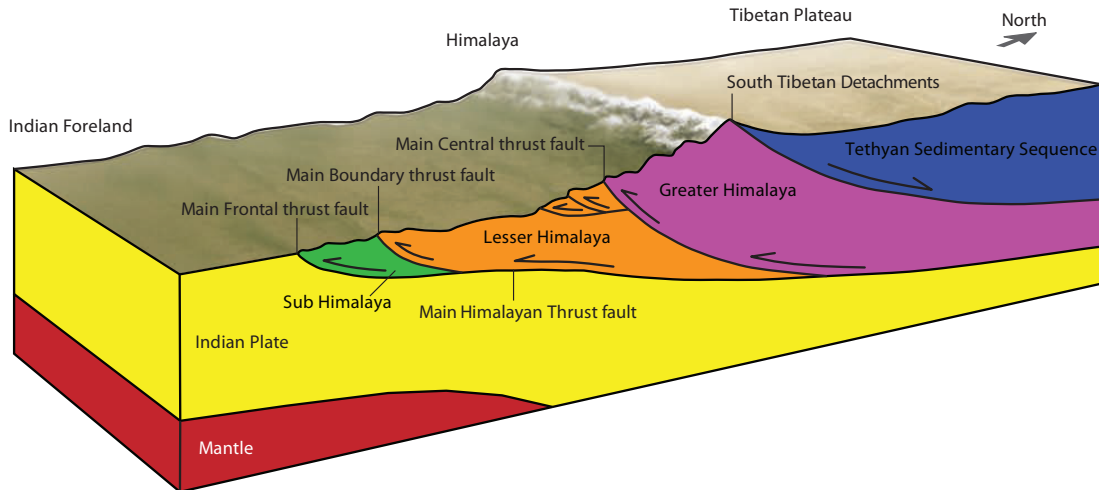


Figure 2.6 - Schematic cross section and block diagram of the Himalaya orogen. Modified from Hodges (2006)

### 2.2.1. LITHOTECTONIC UNITS

From south to north the Himalayan orogen is divided into several lithotectonic units characterized by sediments deposited in different environments at different times and by contrasting Tertiary metamorphism and magmatism. These are separated by north-dipping, south-vergent thrusts; the south most thrusts are brittle faults while the north most thrusts are ductile shear zones.

#### SUB-HIMALAYAN ZONE

The Sub-Himalayan zone is defined as the Neogene and Quaternary foreland basin of the Himalaya. It lies between the Lesser Himalaya and the active Main Frontal Thrust in the front of the Himalaya orogen. There are two different rock groups within the Sub-Himalaya: (1) uppermost Paleocene or Lower Eocene to Lower Miocene marine siltstones and sandstones (Hodges, 2000; Najman et al., 2005) and (2) the Lower



Miocene to Pleistocene alluvial sandstones, mudstones, siltstones, and conglomerates of the Siwalik Group (Hodges, 2000).

Both groups thicken from south to north. Thicknesses range from 2 km in the basin to more than 10 km near the contact zone near the Lesser Himalaya. The west Sub-Himalaya contains both groups, but in the east the Sub-Himalaya contains predominantly the Siwalik Group (Hodges, 2000).

### **LESSER HIMALAYAN SEQUENCE**

Rock types within the Lesser Himalaya Sequence (LHS) include impure quartzites, psammitic phyllites and schists, subordinate impure marbles, meta-mafic rocks, and augen gneisses. The metamorphic grade ranges from Lower greenschist facies in the south and at the base of the LHS to lower-amphibolite-facies grade at the top of the sequence (Long et al., 2011b; Hodges, 2000; Robinson et al., 2001). The rocks of the Lesser Himalaya sequence are deformed into a typical system of fold-and-thrust nappes (Long et al., 2011b; Robinson et al., 2001). The depositional age of the sedimentary rocks ranges from Neoproterozoic to Permian and consequently the rocks are separated in four stratigraphic units, oldest at the top (north) and youngest at the base (south) (Long et al., 2011a; Long et al., 2011b). Thicknesses of the LHS range from 8 to 19 km (Hodges, 2000; Long et al., 2011b).

## **GREATER HIMALAYAN SEQUENCE**

The Greater Himalaya sequence (GHS) is the metamorphic core of the Himalaya. It has been known by other names such as: “Central crystallines”, “Higher Himalayan gneisses” and “Tibetan slab”. The GHS is a continuous belt of amphibolite to granulite grade igneous rocks, metasedimentary rocks and leucogranites. Both the thermal peak of metamorphism and magmatism occurred during the Early and Middle Miocene (Long et al., 2011b; Hodges, 2000).

## **TETHYAN SEDIMENTARY SEQUENCE**

The Tethyan sedimentary sequence (TSS) consists of Proterozoic to Eocene siliciclastic and carbonate sedimentary rocks, which are interbedded with Paleozoic and Mesozoic volcanic rocks. The TSS can be divided into four sub sequences.

1. Pre-rift sequence (Proterozoic to Devonian).
2. Rift and post-rift sequence (Carboniferous–Lower Jurassic).
3. Passive continental margin sequence (Jurassic–Cretaceous).
4. Syn-collisional sequence (Cretaceous–Eocene) (Yin, 2006).

## **2.2.2. STRUCTURES**

### **MAIN FRONTAL THRUST**

The Main Frontal Thrust (MFT) extends across the Himalayan arc. Of all the main structures mentioned here, the MFT is the least well defined because in places, Quaternary sediments cover the MFT (Robinson et al., 2001; Long et al., 2011a). The MFT is the most frontal thrust sheet in the Himalayan arc, and places Siwalik sediments over Quaternary Gangetic and Brahmaputra plain deposits. The MFT is the southern deformation front of the Sub-Himalaya. Movement started at  $2.5 \text{ Ma} \pm 0.5 \text{ Ma}$  and is still active (van der Beek et al., 2006). Rates of slip on the MFT vary depending on methodology used. Published rates on the MFT range from 15-20 mm/yr (Molnar, 1987; Avouac, 2003).

### **MAIN BOUNDARY THRUST**

The Main Boundary Thrust (MBT) places the LHS over the Sub-Himalaya. The timing of movement along the MBT is very poorly constrained. Exhumation of the LHS along the MBT may have started ca. 10 Ma (Yin, 2006). On the other hand, exhumation of the LHS may have resulted in duplexes, and a younger age of activation would be possible, ca. 5 Ma (Yin, 2006; Avouac, 2003). Due to the lack of correlative stratigraphic units, the total magnitude of slip across the fault is not well constrained. Slip along the fault is estimated as >100 km in western and central Himalaya (Yin, 2006), whereas slip along the MBT in eastern Himalaya and Bhutan could be up to 67 km (Long et al., 2011a).

## **RAMGARH THRUST**

Ramgarh thrust creates a duplex system within the Lesser Himalaya sequence (Long et al., 2011a; Robinson et al., 2001). The Shumar Thrust in the eastern Himalaya is equivalent to the Ramgarh thrust in the central and western Himalaya (McQuarrie et al., 2008; Long et al., 2011a). The footwall is composed of predominantly Paleozoic rocks, while the hanging wall is composed of Paleoproterozoic rocks in the eastern Himalaya (Yin, 2006; McQuarrie et al., 2008), and in central and eastern Himalaya, the metamorphic Ramgarh Group is placed on top of the sedimentary Sirmur Group (Godin et al., 2006; Yin, 2006). Activation of the Ramgarh thrust occurred from 10 to 15 Ma (McQuarrie et al., 2008; Godin et al., 2006).

## **MAIN CENTRAL THRUST**

The Main Central Thrust (MCT) is a ductile shear zone that forms the boundary between the Lesser Himalaya sequence and the Greater Himalaya sequence (Godin et al., 2006; McQuarrie et al., 2008). Activation of the MCT varies across the Himalaya resulting in ages from 16 to 23 Ma, with younger ages in the eastern Himalaya (Godin et al., 2006).

## 2.3. SIWALIK GROUP

### 2.3.1. SEDIMENTOLOGY OF THE SIWALIK GROUP

The Siwalik Group consists of synorogenic sediments, which were deposited in the Himalayan foreland basin on the fringe of the Himalayan range. The sediments extend from Assam, India to western Pakistan (Najman et al., 2005; Ojha et al., 2009). Over the entire basin, the sediments are broadly uniform. There are slight differences in the deposition of the Siwaliks over the Himalayan arc. Some nomenclature changes from region to region, but based on lithostratigraphy, the Siwalik Group has been divided into the Lower, Middle and Upper Siwalik Groups (Long et al., 2011b; Ojha et al., 2009).

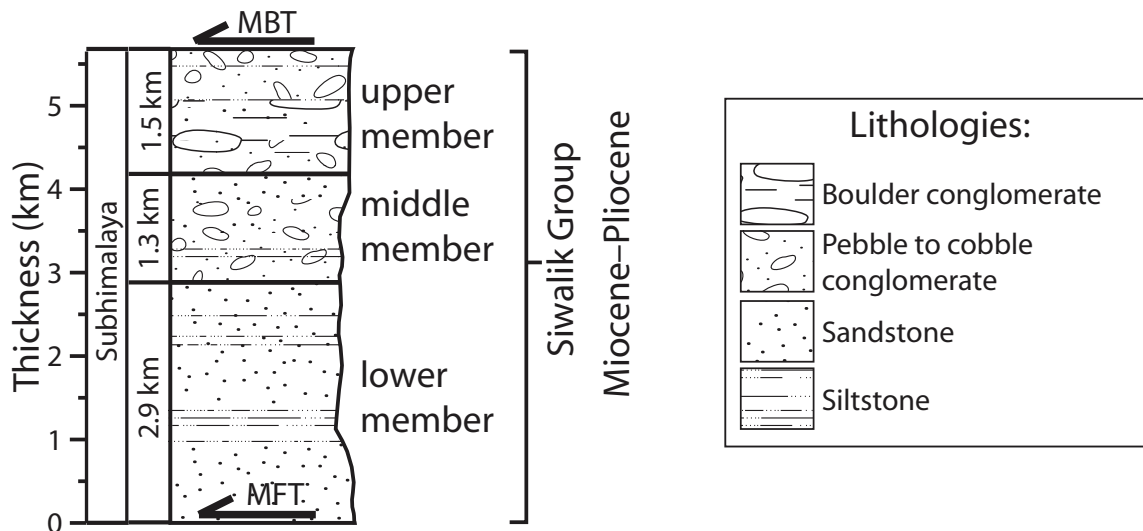


Figure 2.7 – Generalized stratigraphic column of the Siwaliks Group in eastern Bhutan. Modified from Najman et al., (1993) and Long et al, (2011b).

The foreland basin was formed during continental collision, where the over-riding plate (Eurasian) loads the subducting plate (Indian), causing downwarping and associated updoming of the craton creating a forebulge (Figure 2.8). As thrusts continue Pliocene to Recent Shortening of the Siwalik Group in the Himalayan Foreland Belt 24

to elevate crustal rocks, eroded material is deposited into the foreland basin. Deposition of sediments shows a shallowing upwards sequence as deposition rate exceed subsidence. With continued convergence of the plates, the thrusts and associated peripheral forebulge advance cratonwards, and the foreland basin sediments become caught up in the thrusting (Long et al., 2011b; Najman et al., 1993).

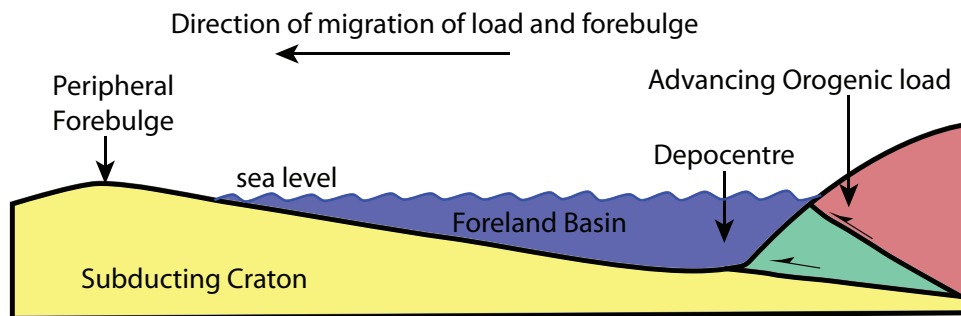


Figure 2.8 – Schematic diagram of foreland basin evolution. See text for explanation. Modified from Najman et al., (1993).

Thickness of the Siwalik Group varies from 2 km to 10 km. Due to faults and erosion, there is no full, intact stratigraphic section (Ojha et al., 2009; Long et al., 2011b). The Siwaliks strata in general coarsen upward from mudstones and siltstones to sandstones and conglomerates in the upper members (Long et al., 2011b; Ojha et al., 2009).

Green-gray, medium-gray and tan siltstones and shales with interbedded sandstones characterize the Lower Siwalik Group. The siltstones and shales are micaceous, laminated and medium- to thick-bedded, whereas the sandstone grains are sub-angular with a high percentage of lithic clasts with a silt-rich matrix (Ojha et al., 2009; Long et al., 2011b). Sandstone beds range from <5 m thick to 30-40 m. These

sandstone beds could be channel bodies, and are indicative of meandering and braided rivers (Quade et al., 1995; Ojha et al., 2009). Low amounts of organics including coal logs and leaf impressions have been found within the Lower Siwaliks (Mugnier et al., 1999b; Quade et al., 1995).

There is a conformable transition into the Middle Siwalik Group from the Lower Siwalik Group (Najman et al., 2005; Mugnier et al., 1999b). The Middle Siwalik Group consists of sandstone and conglomeratic sandstone within minor gray to greenish gray laminated siltstones (Long et al., 2011b; Najman et al., 2005). The sandstone is sub angular medium- to coarse-grained, with a high percentage of lithic clasts (Najman et al., 2005; Long et al., 2011b). These sandstone bodies are mostly between 10-20 m thick, but multistory sandstones occur which are over 45 m thick, indicating an increase in channel-body thickness when compared with the Lower Siwalik Group (Long et al., 2011b; Najman et al., 2005). The conglomerate is generally matrix-supported with pebble- to cobble-sized clasts (Najman et al., 2005; Long et al., 2011b). The appearance of conglomerate marks a change from the Lower Siwaliks to the Middle Siwaliks. In Nepal the first conglomerates found within the Middle Siwalik rocks are composed of metamorphic and sedimentary clasts, which can be compared to the rocks of the LHS and GHS (Quade et al., 1995; Najman et al., 2005) while in Bhutan pebbles are dominantly quartzite and occasionally slate. Sedimentary structures in the sandstones include small- to large-scale channel scours, lamination, tabular and wedge-shaped cross-bedding. Organics can also be found in the clay beds, including wood fragments and leaf impressions (Quade et al., 1995).

The Upper Siwalik Group lies conformably and unconformably on the Middle Siwalik Group due to erosion and deposition on already tilted beds (Mugnier et al., 1999a; Husson et al., 2004). The Upper Siwalik consists of medium- to coarse-grained conglomeratic sandstone and pebble conglomerate. Beds within the Upper Siwalik Group contain matrix-supported conglomerate beds with cobble to boulder-sized clasts and have interbedded siltstones (Long et al., 2011b). The clasts in the conglomerates in the Upper Siwalik deposits are distinctive of their local (i.e, LHS and GHS) provenance as they are composed of granite, lithic sandstone, gneiss and quartzite (Quade et al., 1995; Najman et al., 2005; Long et al., 2011b); in Bhutan the pebbles are dominantly quartzite and no GHS-derived pebbles have been found. Sedimentary structures in the Upper Siwalik Group include trough and tabular cross-bedding, tabular bedding and soft-sediment deformation features (Long et al., 2011b).

Deposition of the Siwalik Group was dominated by a fluvial system with alluvial fans and channels (Ojha et al., 2009). See Figure 2.9 for description summary and environment.



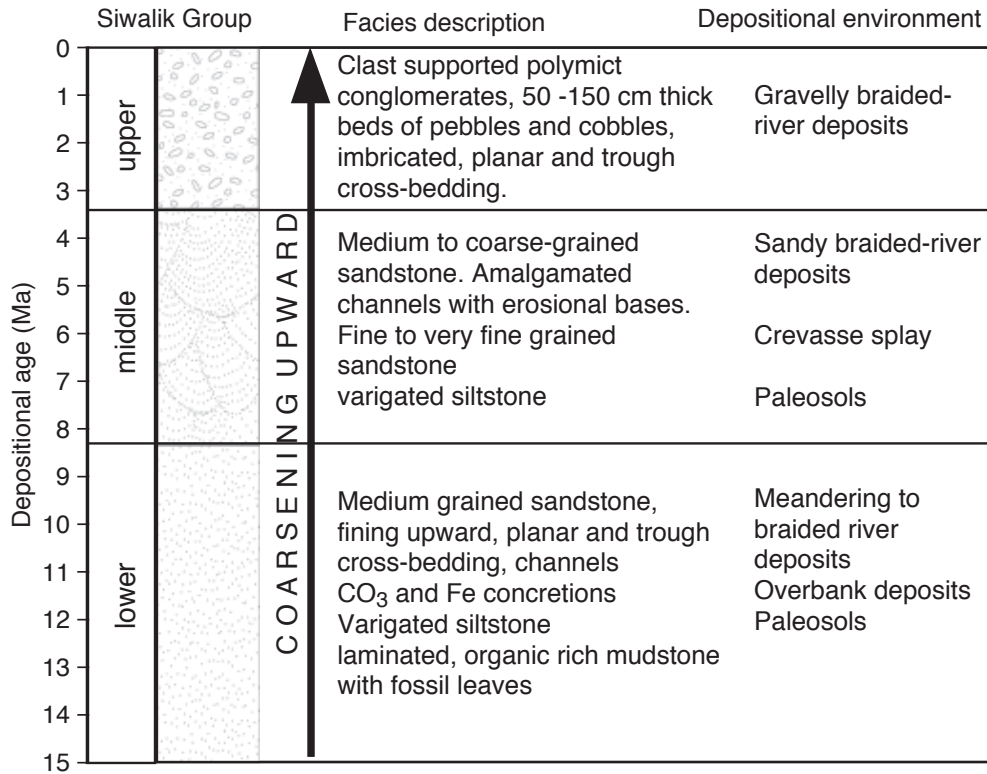


Figure 2.9 - Siwalik Group generalized stratigraphic chart from western Nepal. Short facies description and depositional environments are included. Modified from Bernet et al. (2006).

Indications from paleocurrent and sedimentological data suggest deposition on fluvial megafans which were similar to those currently in the foredeep depozone of the Himalaya foreland basin (Ojha et al., 2009) (Figure 2.10). The Siwalik Group has also been interpreted to represent southward progradation of the foreland deposition with a distal axial river fed by fluvial megafans (Ojha et al., 2009).

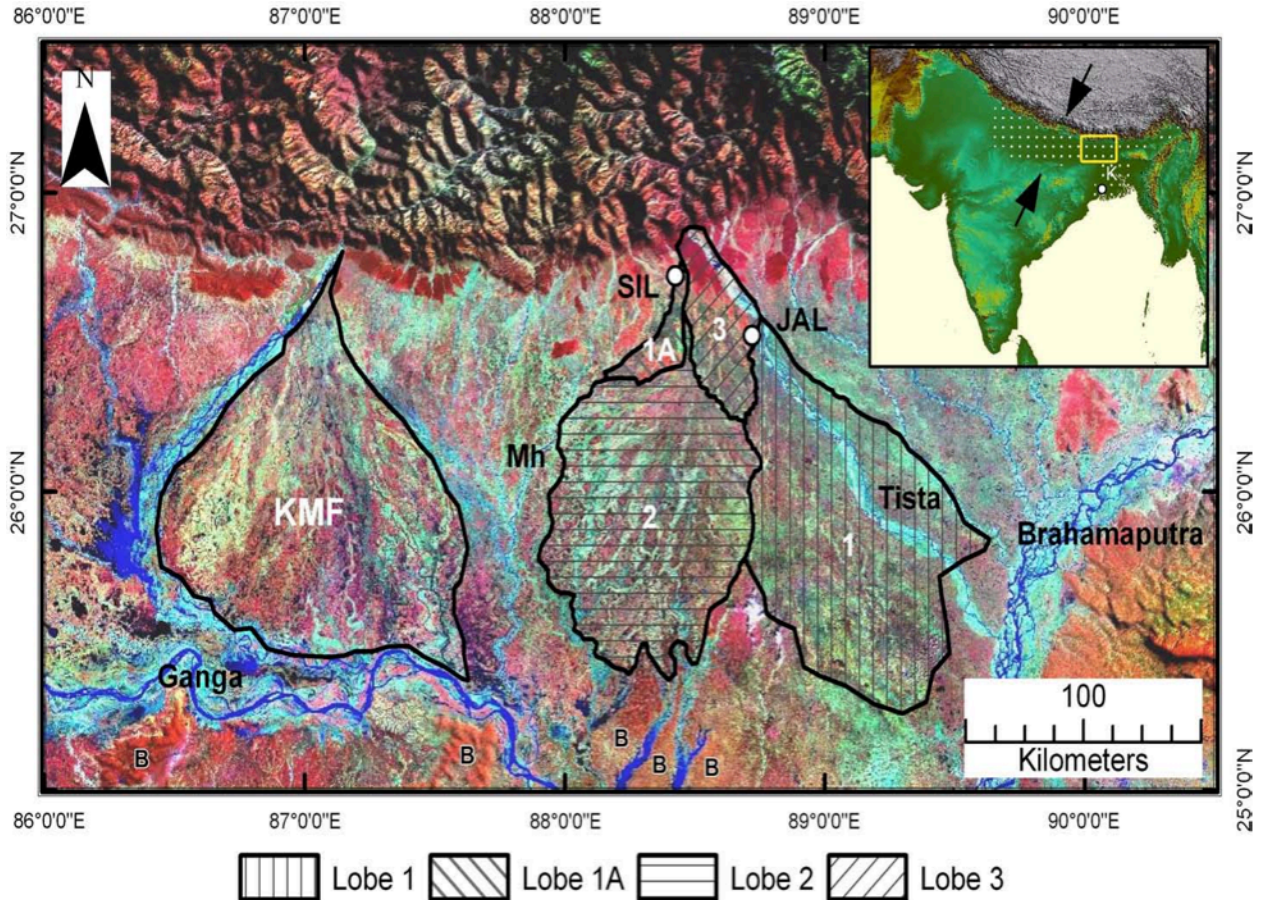
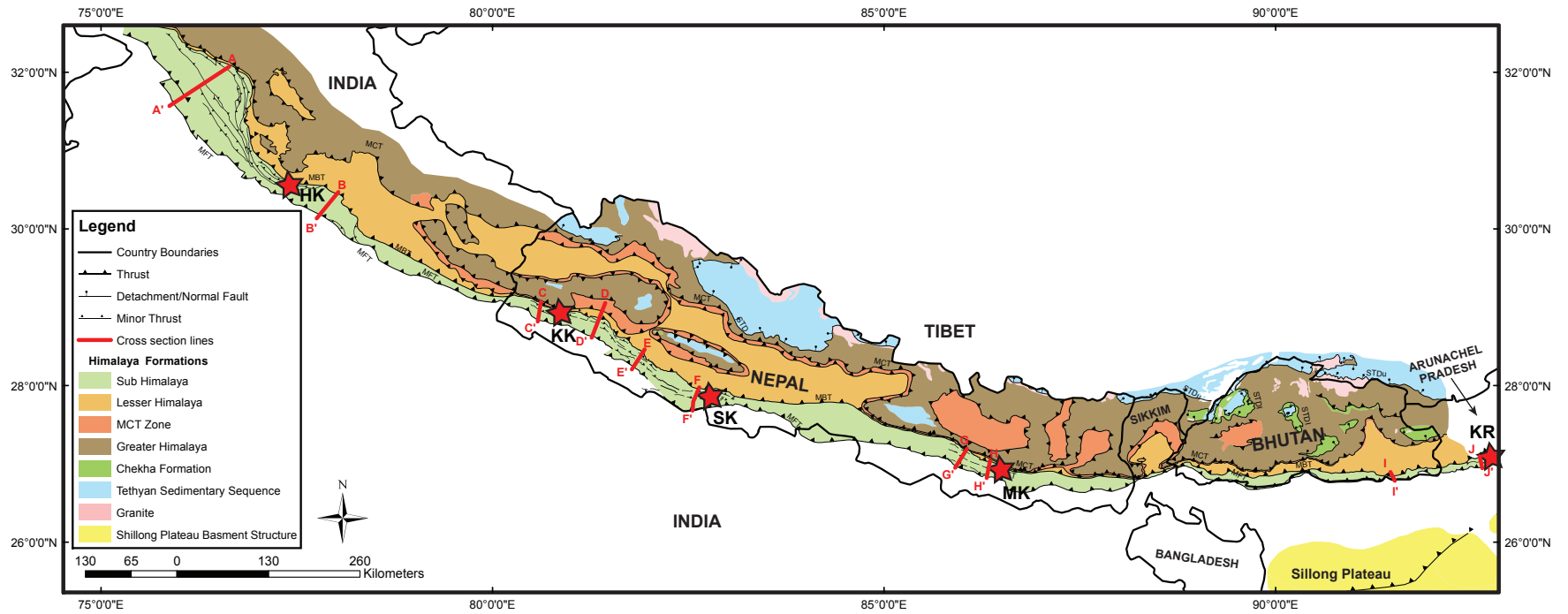


Figure 2.10 - Modern day megafans and major drainages on the Sub-Himalaya alluvial plain in front of the Himalaya in eastern Nepal. The lobes are the Tista and Kosi megafans (Chakraborty and Ghosh, 2010). Deposition of the Siwaliks would have been similar. SIL = Siliguri; JAL = Jalpaiguri; KMF = Kosi megafan; Mh = Mahananda River ; B = marks the basement spurs at the southern margin of the megafan.

### 2.3.2. DEPOSITIONAL AGE OF THE SIWALIK GROUP

Stratigraphic age of the Siwalik Group across the Himalaya arc has been determined using magnetic polarity and carbon isotope methods. The Siwalik Group has been dated and the age ranges from approximately 15 to 1 Ma. In Nepal, the boundary of the Lower to Middle Siwalik is 11.5 to 8 Ma and the Middle to Upper Siwalik boundary is from 4.5 to 2 Ma (Figure 2.11 and Figure 2.12) (Ojha et al., 2009).



**Figure 2.11 - Geological overview map of the Himalaya with stratigraphic section locations. Red stars indicate detailed stratigraphic section locations with magneto stratigraphy. Balanced cross-sections of the Siwalik Group are indicated with red lines. HK; Haripur Khol (Sanyal et al., 2004), KK; Kutia Khol, SK; Surai Khol, MK; Muksar Khol (Ojha et al., 2000; Ojha et al., 2004; Ojha et al., 2009), KR; Kameg River, (Chirouze et al., 2012b). Compiled from McQuarrie et al. (2008), Powers et al., (1998), Chirouze et al., (2012), Mugnier et al., (1999a), Ojha et al, (2009), Sanyal et al., (2004), and Ojha (personal communication, 2012).**

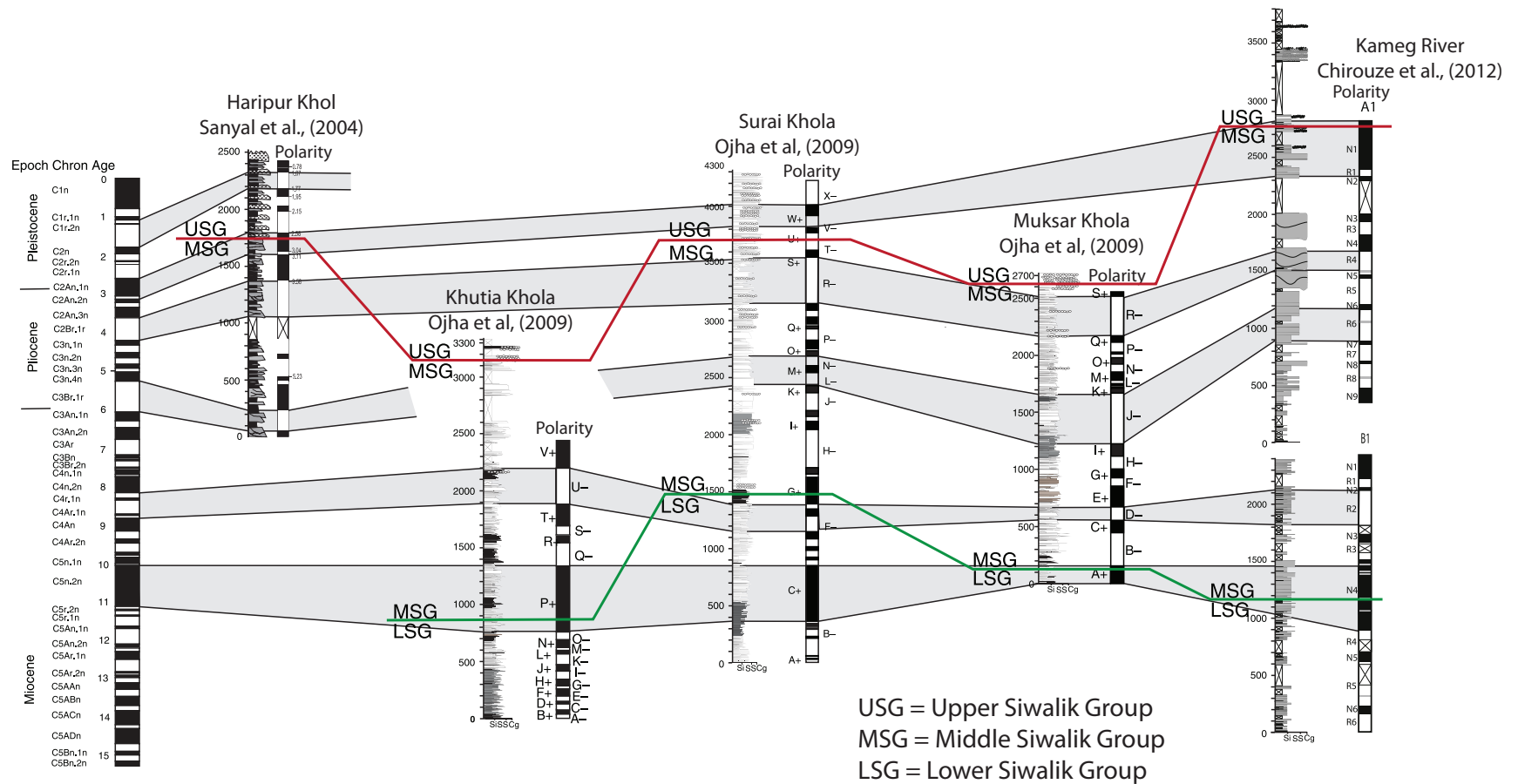


**Figure 2.12 - Magneto stratigraphic correlation of the Siwalik Group across the Himalayan arc. Correlation of the Upper and Middle Siwalik Group contact and the Middle and Lower Siwalik contact are indicated. Locations of the stratigraphic sections can be found on Figure 2.11. Stratigraphic sections and correlations from Ojha et al., (2009), Chirouze et al., (2012) and Sanyal et al., (2004).**

## **2.4. STRUCTURE WITHIN THE SIWALIK GROUP**

The Siwalik Group is constrained between the Main Frontal Thrust to the south and the Main Boundary Thrust to the north (Hodges, 2000). Several southward-verging thrusts lie between the MBT and the MFT. In Nepal these thrusts are grouped together under the name of the Main Dunn Thrust (MDT). The MDT branches out and creates duplexes, horses and “pop-up” structures. Several back-thrusts have also been identified locally. Stratigraphy suggests that these faults do not cross the whole Siwalik Group, but instead branch off décollement levels located within the Lower Siwalik Group and are formed into duplexes (Mugnier and Huyghe, 2006). Folds in the Siwaliks were formed by flexural slip mechanism, are associated with ramps on the thrusts (Yin, 2006; Mugnier et al., 1999b). Unconformities have also been observed in the Siwaliks. The unconformities can be traced uniformly across areas of the Himalaya, and are located at the bottom of the conglomerate facies of the Upper Siwaliks due to the deposition of the synorogenic sediments of the Upper Siwalik on top of already tilted strata (Mugnier et al., 1999b).

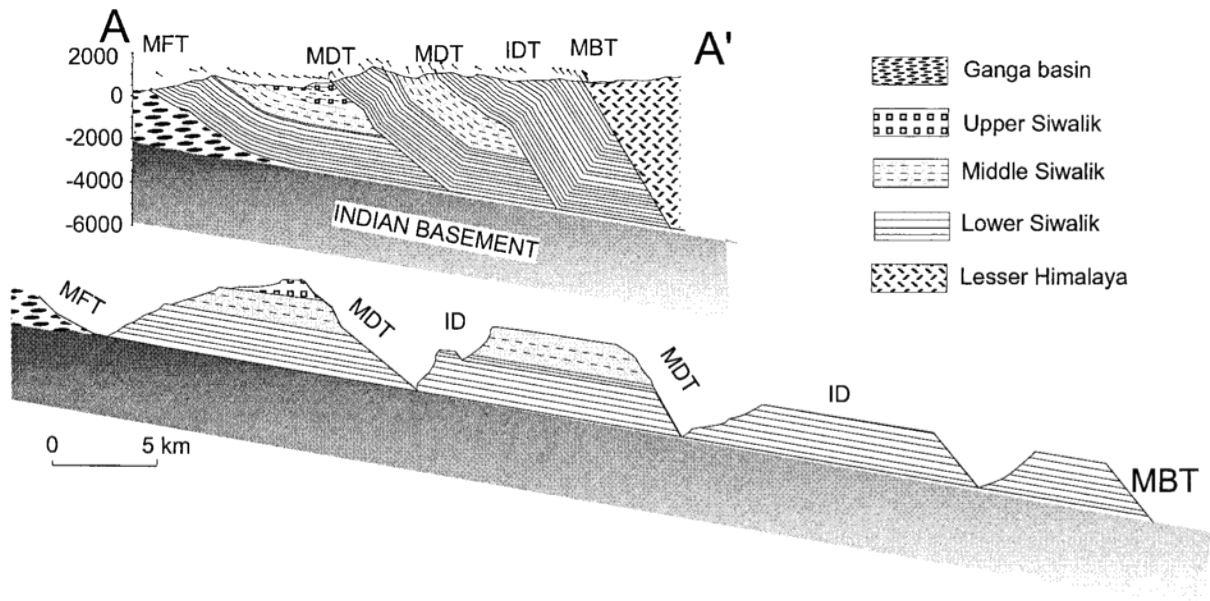


Figure 2.13 - Balanced Cross-section through the frontal belt of western Nepal showing the style of deformation in the Sub-Himalaya. The section shows the Main Frontal Thrust (MFT), Main Dun Thrust (MDT) and Main Boundary Thrust (MBT) (Mugnier et al., 1999b).

## 2.5. MECHANICS OF OROGENIC WEDGES

Orogenic wedges are formed in compressive tectonic regimes, such as the Himalaya. Fold-and-thrust belts show wedge-shape geometry in cross-section and therefore are given the name orogenic wedge. The formation of tectonic wedges is famously made analogous with the bulldozer/snowplow pushing snow (Dahlen, 1990). In an orogenic wedge, the shape of the wedge depends on the force applied to the wedge, gravity, friction along the décollement, internal strength of the material, erosion of the wedge accretion of new material, and in subduction-related wedges, the load of the water column.

The geometry of a wedge tries to maintain the same geometry (Fossen, 2010). The wedge will deform internally with forward and back thrusts to maintain stable shape, i.e., the “critical taper” (Dahlen and Barr, 1989). Dahlen, Suppe, and coworkers, produced a series of papers to understand the mechanics behind orogenic wedges.

### 2.5.1. MECHANICS OF A BULLDOZER WEDGE

Orogenic wedges are equivalent to wedges, which form in front of bulldozers piling up snow. Bulldozer wedges pile up snow until they maintain its critical taper, which is managed by the strength of the material and relative magnitudes of sliding resistance along the base. Increasing the sliding resistance increases the critical taper, while increasing the strength within the wedge decreases it, as seen in Figure 2.14 (Dahlen and Suppe, 1988).

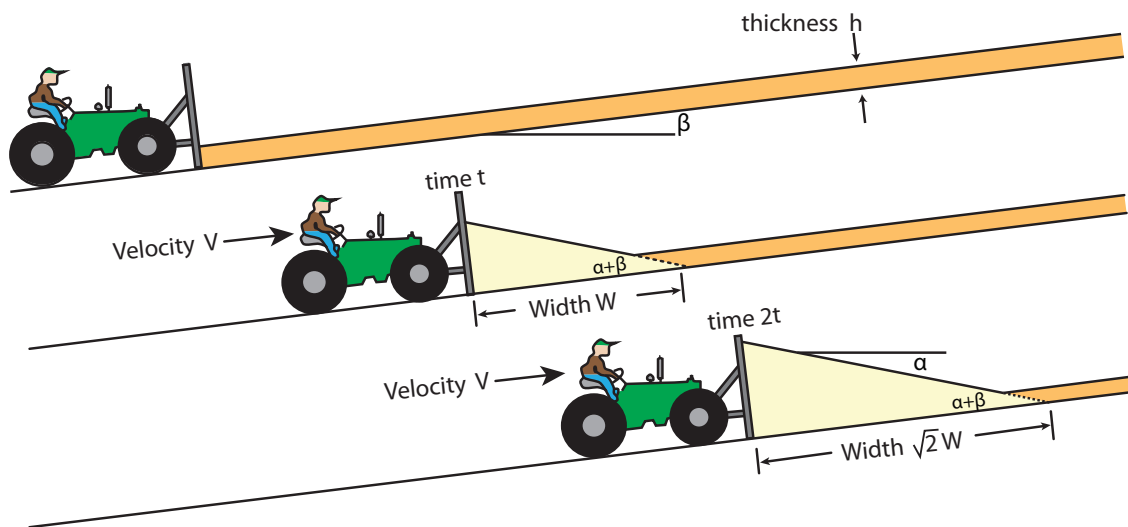


Figure 2.14 - Cartoon depicting the self-similar growth of a bulldozer wedge. Modified from Dahlen (1990). Once the bulldozer starts pushing at time 0 the wedge will start to form. Once it reaches a time  $t$ , the wedge will be the width  $W$ . At a later time  $2t$  the width will be greater, as the height is higher. This is due to the critical angle  $\alpha + \beta$  being kept constant. The angle of the slope of the wedge is maintained with changing size of the wedge. This constant slope is the “critical taper”.

If a bulldozer, the backstop of the wedge, starts at  $t=0$  and starts moving up hill (slope  $\beta$ ) at a uniform velocity  $V$ , pushing sand, a critically tapered wedge will start to form in front of the bulldozer. The wedge forming in front of the bulldozer will have a slope  $\alpha$ . The critical angle at the toe of the wedge is  $\alpha+\beta$ . Assuming that density,  $\rho$ , is constant, and that  $\alpha+\beta$  will not change in time, we can calculate the width,  $W$ ;

Equation 1

$$W = \left[ \frac{2hVt}{\tan(\alpha + \beta)} \right]^{1/2} \approx \left[ \frac{2hVt}{\alpha + \beta} \right]^{1/2}$$

Where  $h$  is height,  $V$  is velocity and  $t$  is time. The final approximation in the formula above is valid for a wedge with a narrow taper,  $\alpha+\beta \ll 1$  (Dahlen, 1990).

### 2.5.2. CRITICAL TAPER MODEL AND COULOMB WEDGES

A key assumption for orogenic wedges is that the stress within the wedge is everywhere equal to the rock strength (Dahlen, 1990). The taper is “critical” in the sense that the rock strength will be exceeded by compressive strength in the (subcritical) wedge, so the wedge will fail and deform by thickening to its critical taper. This will in turn allow for a thicker (supercritical) wedge, which is strong enough to slide stably over the basal décollement without internal failure of deformation. This is not the case. An orogenic wedge will keep building and deforming, thus a failure law was developed (Dahlen and Suppe, 1988).

Stress within the lithosphere is thought to be controlled by a variety of deformation mechanisms, including: brittle fracture, frictional sliding at low pressures, thermally activated processes, dislocation climb and pressure solution. Brittle behavior



is stress-limiting in the upper 10 to 15 km of the crust for most materials except evaporites, which display plastic behaviors at shallower depths (Dahlen and Suppe, 1988).

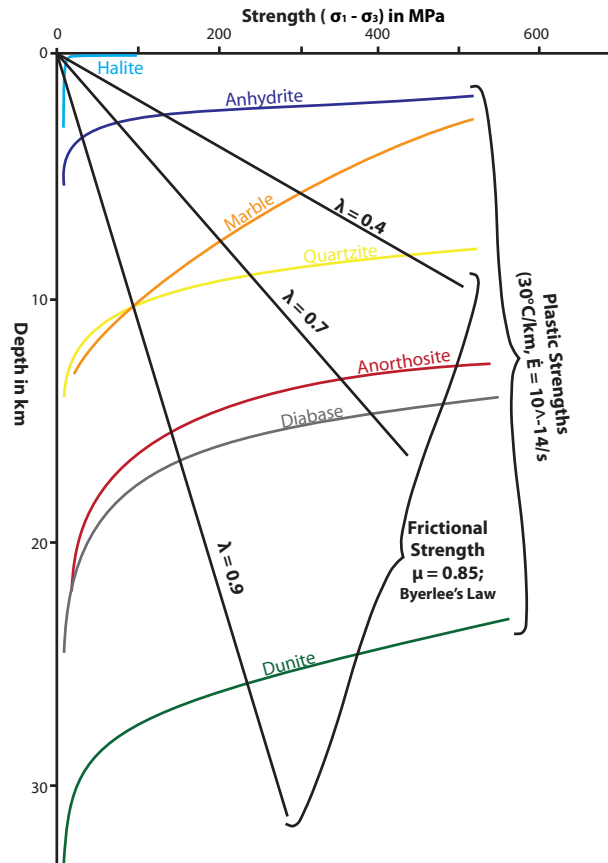


Figure 2.15 - Brittle and plastic rock strengths as a function of depth. Brittle friction is largely independent of rock type, while plastic strengths vary considerably. Thus in turn, variation in depth of brittle-plastic transitions is: 0-5 km for evaporites, 10-15 km for carbonate and quartz rich rocks, 15-20 km for quartz free feldspar-bearing rocks, and 25-30km for olivine-rich rocks (redrawn from Dahlen & Suppe 1988).  $\lambda$  is the pore fluid ratio found in equation 3. Strength of rocks deforming brittlely increase with depth (with increasing confining pressure = Coulomb materials), while the strength of rocks deforming plastically decreases with depth (with increasing  $T$  = thermally activated deformation processes).

Mathematical relationships between Critical Taper and Coulomb material have been developed (Davis et al., 1983; Dahlen et al., 1984; Lehner, 1986; Barcion, 1987; Zhao et al., 1986; Dahlen and Suppe, 1988; Dahlen and Barr, 1989; Barr and Dahlen, 1989; Dahlen, 1990; Dahlen, 1984). Below is a simplified representation of the Critical

Taper model in Coulomb wedges; the more detailed description is beyond the scope of this thesis. For derivations of the formulae see Dahlen et al. (1984), Barcilon (1987), Dahlen and Barr (1989) and Dahlen (1990). We can assume a constant gradient of cohesion  $k$ , is equal to the cohesion (the solidness) of the wedge,  $S_0$  (Zhao et al., 1986):

**Equation 2**

$$S_0 = k_z$$

In the idealised Coulomb wedge model, the wedge is perfectly triangular. The surface slope is  $\alpha$ , the basal dip  $\beta$ , and axes  $x$ ,  $z$  are aligned with the upper surface of the wedge (Figure 2.16). The wedge density is  $\rho$ , the overlying water density (if present) is  $\rho_w$ , acceleration due to gravity is  $g$ ,  $P_f$  is fluid pressure and  $\sigma_z$  is strength in the  $z$  direction. These parameters lead to the pore fluid pressure ratio  $\lambda$  (Dahlen and Suppe, 1988)

**Equation 3**

$$\lambda = \frac{P_f - \rho_w g D}{\sigma_z - \rho_w g D}$$

In this equation  $D$  is water depth. For subaerial wedges density  $\rho_w$  is considered to be of air, and is negligible (Dahlen and Suppe, 1988).

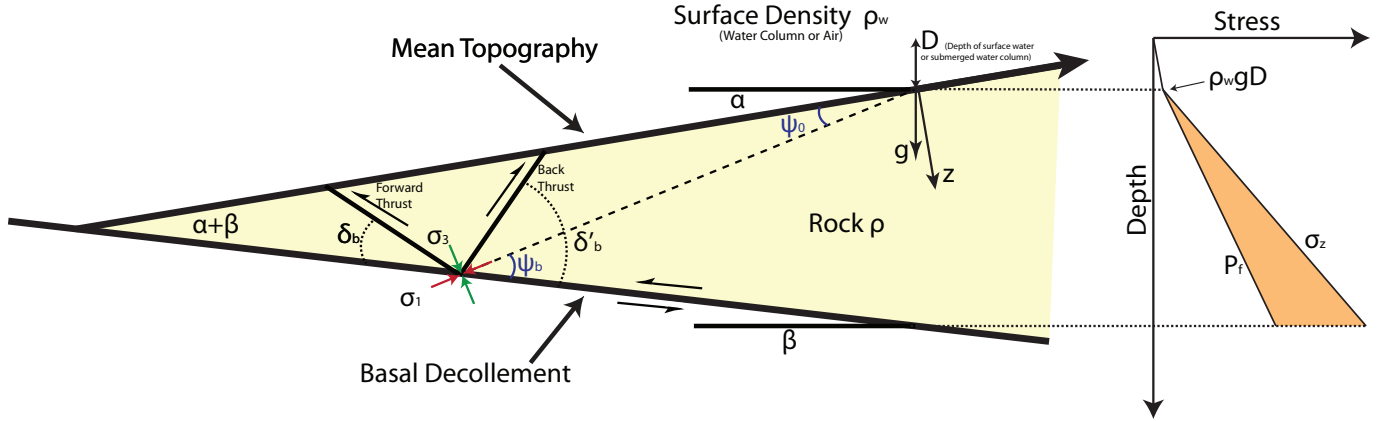


Figure 2.16 - Geometry of an orogenic wedge showing: the Cartesian coordinates  $x, z$ , the angles  $\alpha$  (surface slope angle),  $\beta$  (angle to décollement),  $\psi_0, \psi_b$  (angles with respect to forces acting on the wedge and surface slope),  $\delta_b$  (forward thrust),  $\delta'_b$  (back thrust) which define the taper, and the forces acting on the wedge  $\sigma_1, \sigma_3$ . The diagram on the right shows the effective stress  $\sigma_z - P_f$  (lithostatic pressure – pore fluid pressure) in the shaded area. Compiled from Dahlen & Suppe (1988) and Dahlen et al. (1984).

The basal décollement is assumed to have a different sliding friction  $\mu_b$  and pore fluid pressure  $\lambda_b$ , which may differ from the wedges  $\mu$  and  $\lambda$  (Dahlen and Suppe, 1988). Within the orogenic wedge, uniform constant properties required are: rock density  $\rho$ , water density  $\rho_w$ , coefficient of friction  $\mu$ , basal coefficient of sliding friction  $\mu_b$ , pore-fluid pressure ratio  $\lambda$ , basal pore-fluid pressure ratio  $\lambda_b$ , gravity  $g$ , cohesion gradient  $k$ , and the internal friction angle  $\phi$  (Dahlen and Suppe, 1988; Dahlen, 1990). The critical taper of a wedge can be calculated by:

Equation 4

$$\alpha + \beta = \psi_b - \psi_0$$

where:

Equation 5

$$\psi_0 = \frac{1}{2} \arcsin \left[ \left( 1 + \frac{1}{\mu^2} \right)^{1/2} \sin \alpha' \right] - \frac{1}{2} \arctan \mu'_b$$

Equation 6

$$\psi_b = \frac{1}{2} \arcsin \left[ \left( 1 + \frac{1}{\mu'_b{}^2} \right)^{-1/2} \left( \frac{(k/\rho g \mu) \cos 2\psi_0 + \left( 1 + \frac{1}{\mu^2} \right)^{1/2} \cos \alpha}{(k/\rho g \mu) + (1 - \lambda) \cos \alpha} \right) \right] - \frac{1}{2} \arcsin \mu'_b$$

where the variables  $\alpha'$ ,  $\mu'_b$  and  $\mu$  are defined by (Dahlen and Suppe, 1988; Dahlen, 1990):

Equation 7

$$\alpha' = \arctan \left[ \frac{(1 - \rho_w/\rho) \sin \alpha}{(k/\rho g \mu) + (1 - \lambda) \cos \alpha} \right]$$

Equation 8

$$\mu'_b = \arctan \left[ \frac{(1 - \lambda_b)}{(1 - \lambda)} \mu_b \right]$$

Equation 9

$$\mu = \tan \phi$$

The state of stress orientation is the same everywhere in the wedge, and therefore angles  $\psi_o$  and  $\psi_b$  (Figure 2.16) are the same throughout the wedge, as they are related to angles of the principal compressive stress (Dahlen and Suppe, 1988). An approximation of  $\alpha + \beta$  in a dry sand wedge can be obtained (Dahlen, 1990):

Equation 10

$$\alpha + \beta \approx \left( \frac{1 - \sin \phi}{1 + \sin \phi} \right) (\beta + \mu_b)$$

Using small-angle approximation, which is applicable to many thin-skinned fold-and-thrust belts, the wedge has a narrow taper:  $\alpha \ll 1$ ,  $\beta \ll 1$ ,  $\psi_b \ll 1$ , and  $\psi_o \ll 1$ . By having  $\psi_b \ll 1$  implies the principal compressive stress  $\sigma_1$  is quasi-horizontal (Figure 2.16), and the basal décollement is very weak [ $\mu_b(1 - \lambda_b) \ll \mu(1 - \lambda)$ ]. The equation, which takes in account of pore fluid-pressure, and usually is a sub-marine wedge (Dahlen, 1990) is:

Equation 11

$$\alpha + \beta \approx \frac{(1 - \rho_f/\rho) \beta + \mu_b(1 - \lambda_b)}{(1 - \rho_f/\rho) + 2(1 - \lambda) \left( \frac{\sin \phi}{1 - \sin \phi} \right)}$$

Shear failure (faults) within a Coulomb wedge occur along conjugate shear planes. Because of the similarity, these slip surfaces have the same orientation

Pliocene to Recent Shortening of the Siwalik Group in the Himalayan Foreland Belt 39

everywhere within the wedge. Forward-verging thrusts step up from the décollement at an angle defined by (Dahlen and Suppe, 1988):

Equation 12

$$\delta_b = \frac{1}{2} \arctan(1/\mu) - \psi_b$$

and back thrusts step up at a steeper angle (Dahlen and Suppe, 1988):

Equation 13

$$\delta'_b = \frac{1}{2} \arctan(1/\mu) + \psi_b$$

Failure stress  $|\tau|$  at the point where they fail and ramp up into a thrust is given by:

Equation 14

$$|\tau| = (\rho - \rho_w)gz \sin \alpha \left[ \frac{(1 + \mu^2)^{-1/2}}{\sin 2\psi_0} \right]$$

while the frictional resistance  $[\tau_b = \mu'_b(\sigma_n - P_f)]$  on the décollement at the same point is:

Equation 15

$$\tau_b = (\rho - \rho_w)gz \sin \alpha \left[ \frac{\sin 2\psi_b}{\sin 2\psi_0} \right]$$

For every fold-and-thrust belt with an orogenic wedge the ratio of décollement strength to wedge strength  $\chi$  must be in the range  $0 \leq \chi \leq 1$  for the wedge to be sustained. The ratio is seen below (Dahlen and Suppe, 1988; Dahlen, 1990):

Equation 16

$$\chi = \frac{\tau_b}{|\tau|} = (1 + \mu^2)^{1/2} \sin 2\psi_b$$

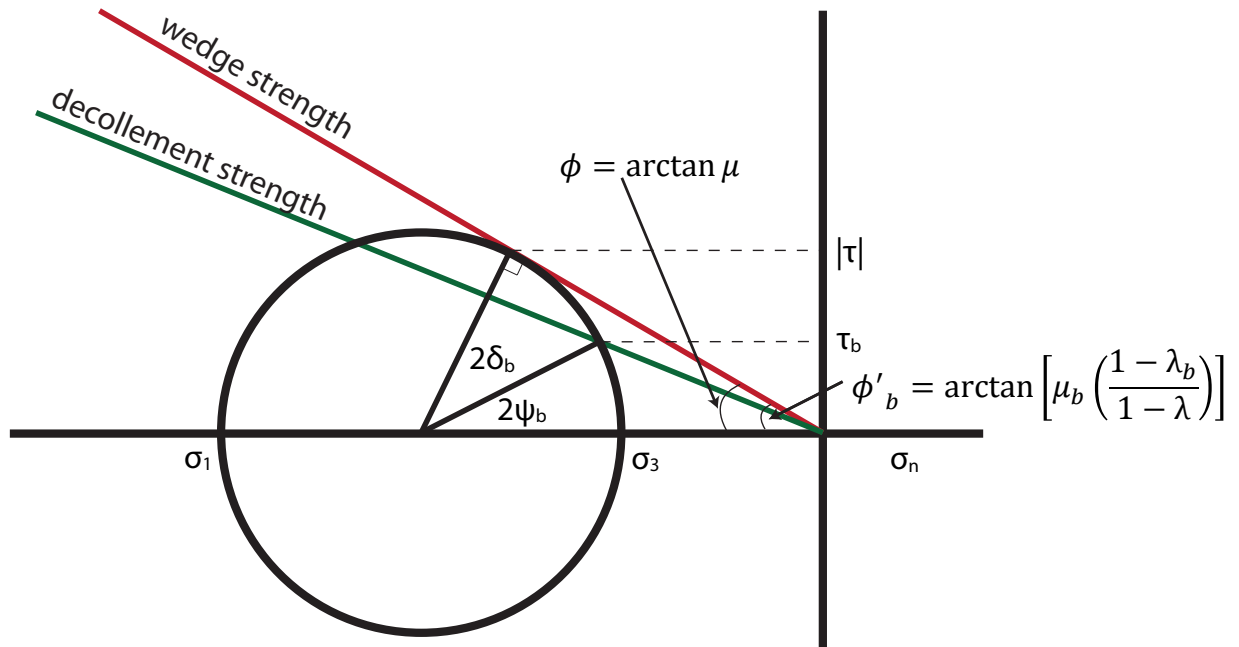


Figure 2.17 - Mohr diagram illustrating stress within the orogenic wedge modified from Dahlen (1990).

### 2.5.3. EROSION AND FLUX BALANCE IN OROGENIC WEDGES

Erosion is an important factor for an orogenic wedge. The eroding wedge will keep adjusting itself by creating thrusts to allow for the wedge to grow, maintaining the critical angle. The erosive efflux balances the influx rate of fresh material into the toe of the wedge. This allows for a steady-state width of a uniformly eroding wedge in a bulldozer model and is demonstrated by (Dahlen, 1990):

Equation 17

$$\dot{\epsilon}W \sec(\alpha + \beta) \approx \dot{\epsilon}W = hV$$

where  $\dot{\epsilon}$  is the rate of erosion. The steady-state wedge must continually deform to both accommodate the influx of fresh material at the toe, and maintain the critical taper against erosion (Dahlen, 1990).

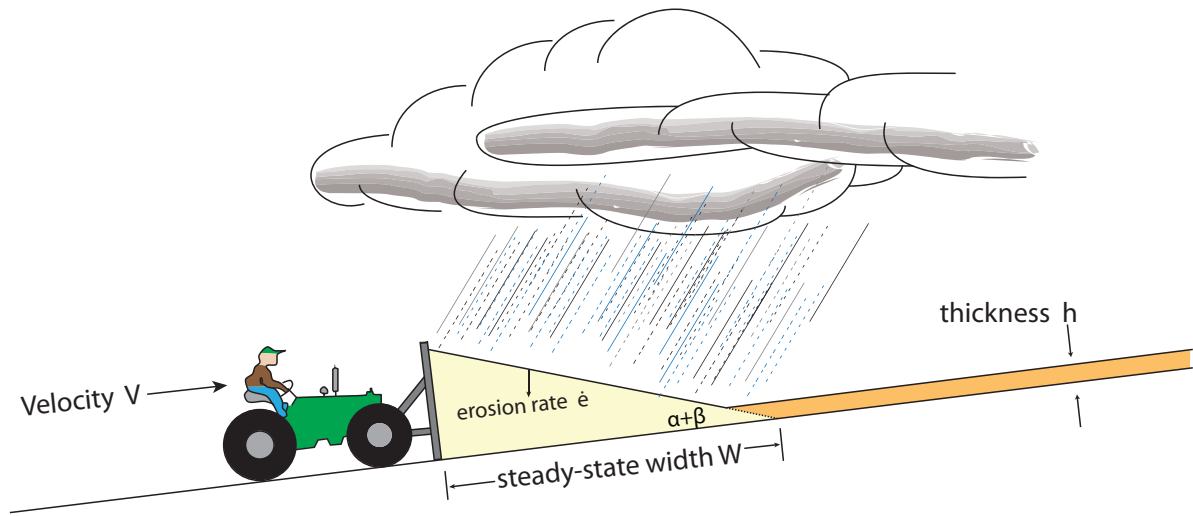


Figure 2.18 - An eroding orogenic wedge. The wedge must attain a dynamic steady-state width given by  $\dot{e}W = hV$  (modified from Dahlen, 1990).

The steady-state Coulomb wedge is affected by more than just erosion. Accretion influx,  $\dot{A}$ , at the toe of the wedge, underplating material entering the wedge,  $\dot{b}$ , along the lower portions of the décollement, and erosion,  $\dot{e}$ , at the surface, must balance for the wedge to be steady state. The equation has to balance with the total flux entering on the left and the material leaving on the right (Equation 18) for steady state to be obtained:

Equation 18

$$\dot{A} + \sec \psi_b \int_{x_0}^x \dot{b} dx = \sec \psi_0 \int_{x_0}^x \dot{e} dx + \int_{x_0 \tan \psi_0}^{x_0 \tan \psi_b} u dz$$

where:

Equation 19, Equation 20, and Equation 21

$$\int_{x_0 \tan \psi_0}^{x_0 \tan \psi_b} u dz = \dot{A} \quad u \sin \psi_b - v \cos \psi_b = \dot{b} \quad u \sin \psi_0 - v \cos \psi_0 = \dot{e}$$

and:

Equation 22

$$\mathbf{u} = u\hat{x} + v\hat{z}$$

$\psi_b$  and  $\psi_0$  correspond to angles within the wedge,  $x$  and  $x_0$  are planar boundaries in the front and back of the wedge, and  $\mathbf{u}$  is the Eulerian velocity of the overriding plate where  $u$  and  $v$  are the  $x$  and  $z$  vectors of the velocity respectively (Dahlen and Barr, 1989). Further reading, explanation and formulae concerning into the balance of forces and material within the orogenic wedge can be found in the two-part paper by Dahlen & Barr (1989), and Barr & Dahlen (1989) and a newer and updated version of erosion acting on an accretionary wedge in Whipple (2004) and Whipple (2009).

#### **2.5.4. OROGENIC WEDGE IN THE SUB-HIMALAYA**

The active orogenic wedge of the Himalaya can be thought of as just the Sub-Himalaya with the MBT as the backstop. Sediment transfer within the wedge is an important part of the Sub-Himalaya. Erosion acts as a major control on the Himalayan fold-and-thrust belt. The wedge identifies the stress of unloading sediments. This unloading of sediments controls the activation and reactivation regimes of the Main Dunn Thrusts (Husson et al., 2004).

Sediment transfer in the Sub-Himalaya is thought to be in a steady-state regime in the wedge. The input volume of accretion to the toe equals the output volume of the erosion. Some of the material is 'captured' as duplexes being underthrust below the MBT or accreted along the footwall of the MBT (Husson et al., 2004). These features were observed using structural maps and balanced cross-sections by Mugnier et al. (1999).



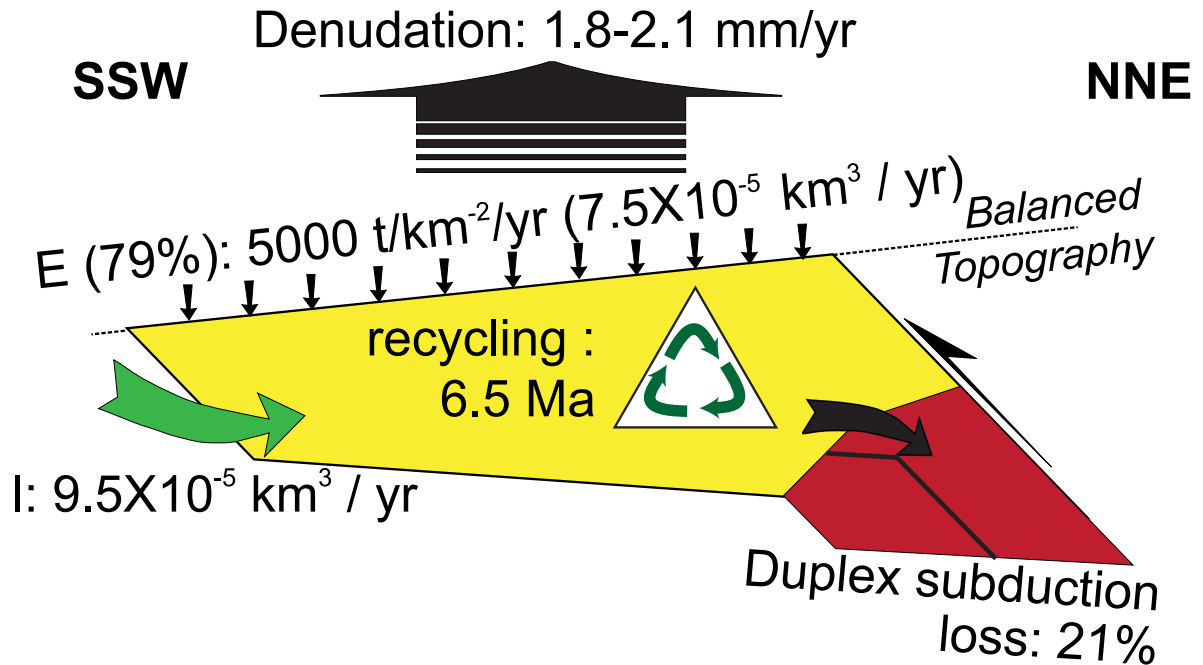


Figure 2.19 - Volume, mass, and time transfer cycle for the Sub-Himalaya wedge. I: the accreting material from the MFT; E: erosion which equals the output minus the loss from duplex subduction. Denudation is evaluated assuming a steady state volume and steady critical taper angle of the wedge. Modified from Husson et al. (2004).

Accretion is the only current input of material into the Sub-Himalaya. The rate of accretion is ca.  $9.5 \times 10^{-5}$  km<sup>3</sup>/yr at the front of the Himalayan belt in western Nepal. About 21% of the accreted material is removed as duplexes of the Lower Siwalik Group beneath the MBT. The residence time of the sediments, which undergo the burial and exhumation cycle, is estimated to be 6.5 Ma. Assuming a steady-state wedge, erosion rate is then calculated on the order of 1.8-2.1 mm/yr (Husson et al., 2004).

### 3. BALANCED CROSS-SECTIONS

#### 3.1. BALANCED CROSS-SECTIONS IN THEORY

**Balancing** is the interpretation or construction of a geologic profile, which can be retrodeformed by geologically realistic processes to a geologically sound undeformed state.

**Restoration** involves working a cross-section backward to its undeformed or **retrodeformed** state. The layers must be coherent for a realistic restoration, which means that the section has no or minimum overlaps and gaps, fault offsets are removed, and sedimentary layers are unfolded and rotated to horizontal and planar layers. The geological section is not balanced until an adequate restored version is offered (Fossen, 2010).

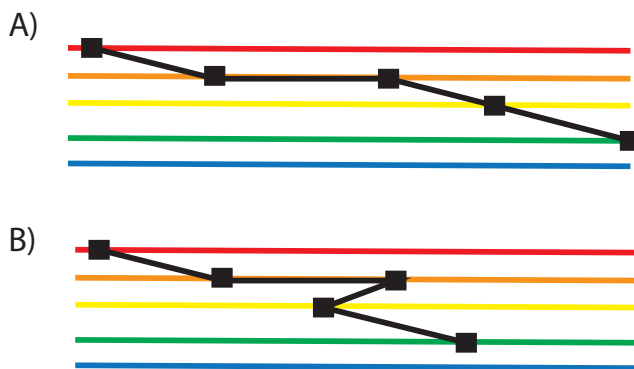


Figure 3.1 - Restoration of fault trajectory. A) Admissible restored fault trajectory. B) Inadmissible restored fault trajectory because the fault trajectory changes directions of propagation once the section is restored. Modified from Woodward et al. (1989).

Instead of restoring a section to its original state, it is possible to start with the undeformed model and deform it until it looks like the interpreted section; this is known

as **forward modeling**. With the forward modeling method we can understand the deformation history and the role of deformation parameters better (Fossen, 2010).

Balancing helps us ensure that the interpretation is realistic and helps determine the amount of shortening or extension in the section. A balanced cross-section is not always correct, but it is more likely to be correct than other sections, which are not balanced (Fossen, 2010).

The simplest way to balance is to use **stratigraphic markers**. When making sections with more than one stratigraphic marker, a two-dimensional cross-section is obtained. At the start of a section, a **pinpoint** must be placed as a point of reference. The pinpoint is usually selected to be a point at the end of the sections where no deformation has taken place. Conditions for balancing should include:

- The interpretation is geologically sound.
- Balanced sections are admissible, which means that the cross-section is valid.
- Sections must be restorable.
- There is plane strain deformation (i.e., no movement of material points in an out of the section plane).
- Sections are parallel to the tectonic transport direction.
- The structures in the section must be kinematically compatible with respect to each other.
- Deformation choices must be reasonable based on the tectonic setting.
- Results must be geologically reasonable based on observations (Fossen, 2010).

### 3.2.CONSTANT LENGTH RESTORATION

The most common method used in fold-and-thrust belts is the constant length method also known as line balancing. Constant length balancing assumes that stratigraphic markers will be restored to their initial length and have been extended and shortened only through observable separations and overlaps such as faults and folds. Any area, which is dominated by thin-skinned tectonics, is a good region to apply constant length balancing. If used correctly with enough stratigraphic markers, a constant length method will also preserve area (Fossen, 2010).

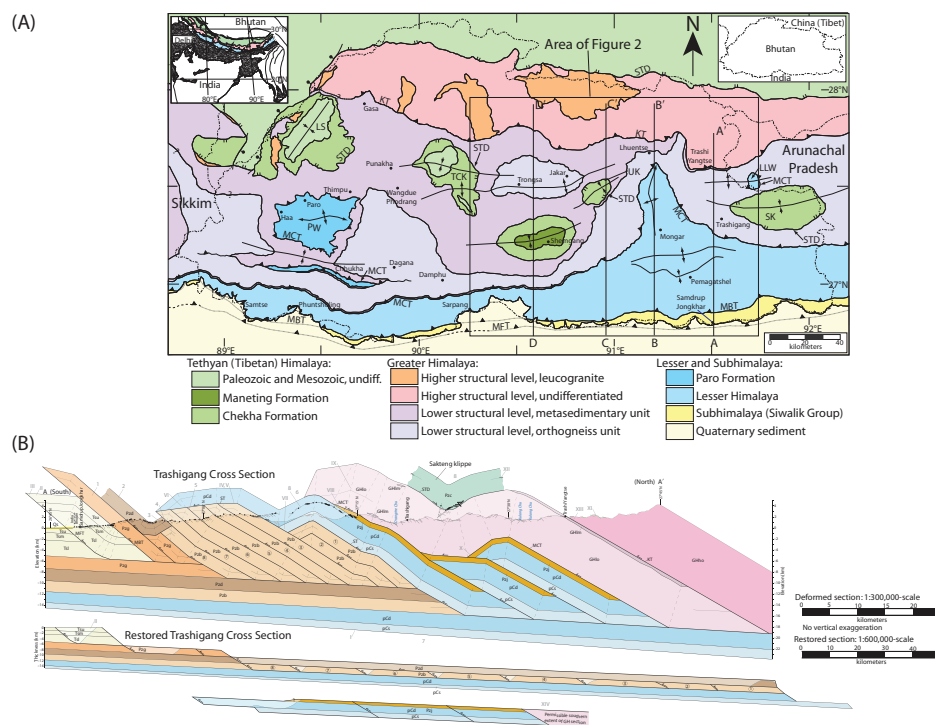


Figure 3.2 - Balanced Cross-section and map, using the constant length method through the Bhutan Himalaya fold-and-thrust belts. (A) Map of sections through Eastern Bhutan, (B) Eastern Bhutan, Tashigang section A (cross-section trace A on map). Deformed and retrodeformed sections are shown (Long et al., 2011a).

Guidelines, rules and assumptions which must be used when line balancing include (Woodward et al., 1989):

1. Constant length of lines.
2. Constant thickness of beds throughout the section.
3. Stratigraphic thickness is known for the area, and assumed to be constant.  
Stratigraphic thickness of beds can be found from either measured sections or three point problems to calculate thickness.
4. The regional section restoration should always begin at an undeformed foreland pin.
5. The section should be parallel to the tectonic transport direction. In addition the assumed strain geometry must be near to perfect plane strain, ie. no movement of material points in and out of the section plane.
6. Geometric and kinematic fold and fault models should be appropriate to the local geology. Folds formed by flexural slip or flexural shear are restorable while the passive shear folds are not.
7. Dips along the section should be projected to the section and adjusted the appropriate dip angle parallel to the section.
8. Drawn horizons at surface must have the same or similar dip as the projected measured dips.
9. Depth of basement (i.e., basal décollement geometry) of the section must be known from geophysical or bore hole data, or inferred from the total stratigraphic thickness.

10. The section must have reasonable geological features such as duplexes, faults and folds.
11. Thrusts in the section must have a forward imbrication assumption, in which younger faults are closer to the foreland.
12. The restored section must have an admissible solution.

Constant length restoration requires consistency of lengths in a restored section. In foreland fold-and-thrust belts, such as the Sub-Himalaya, equal bed lengths sometimes do not occur (Woodward et al., 1989). Younger synorogenic sediment is deposited on the already shortened strata, or sintectonically resulting in shorter bed lengths. The pre-orogenic sediments, such as the Lower Siwalik, will be fully restorable, and the synorogenic sediments will yield a shorter restored length (Husson et al., 2004; Woodward et al., 1989).

Flexural-slip folding mechanism is crucial in constructing and interpreting cross-sections for line balancing. Flexural slip provides both preservation of the line length and preservation of bed thickness. Slip happens parallel to the bedding only (Figure 3.3). When balancing fault-bend folds and fault-propagation folds, flexural slip is convenient (Fossen, 2010).

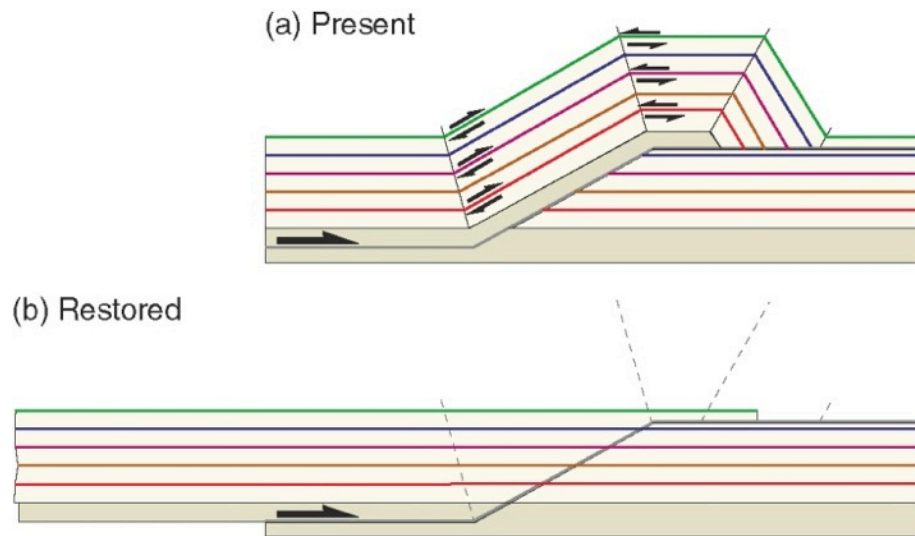


Figure 3.3 - Flexural slip restoration of a fault bent fold. Constant length and area are assumed during the restoration. The individual stratigraphy was moved and rotated to match the stratigraphy in the footwall (Fossen, 2010).

### 3.3.CONSTANT AREA RESTORATION

It many cases the lengths of the lines will change during deformation, which makes line balancing inapplicable. Instead, the area needs to be constant in order for the section to balance. The theory behind area balancing is simple, but the application is involved. The deformed area of the section must equal the undeformed area of the section. Same assumptions as for the line balancing must be made while area balancing. Compaction, pressure solution, or movement in or out of the section cannot occur for equal area balancing to work. On the other hand, layers can change thickness within the section, and both flexural slip and flexural shear folding within the section can happen (Fossen, 2010).

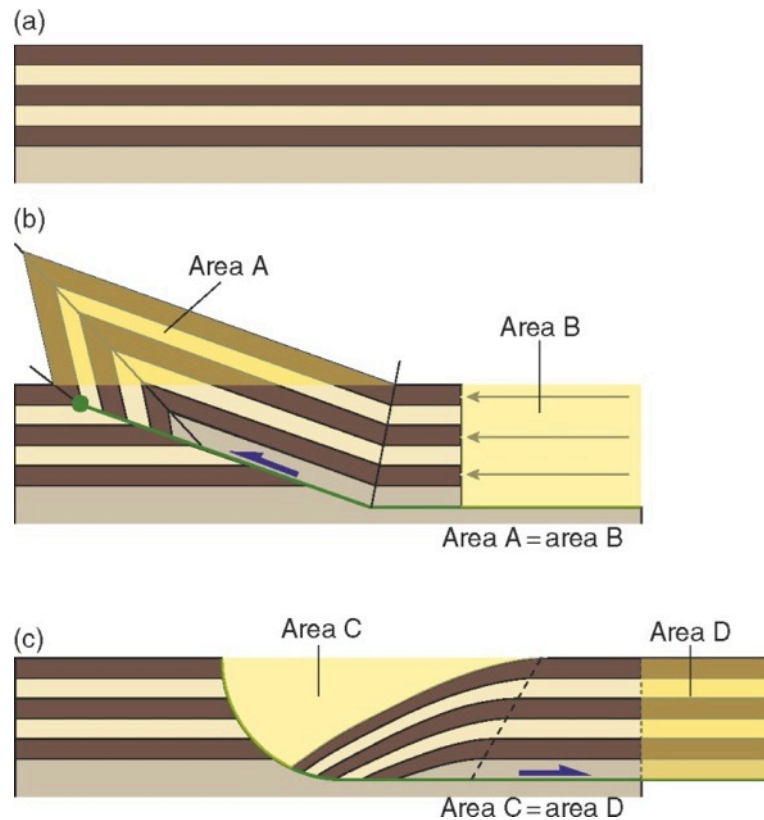


Figure 3.4 - Constant area balancing of sections. a) Undeformed section, b) fault propagation fold with the deformed area A equaling the original undeformed area B, c) listric extensional fault where the original undeformed area C equals the extensional area D. Bed lengths and thickness will change if the internal strain is shear, but the section is balanced since area is constant (Fossen, 2010).

In this thesis line balancing was performed. The deformation of the Sub-Himalayan sediments occurred at temperatures less than 100 °C, there is no observable volumetric strain (e.g. pressure solution, extensive veining, development of a new planar fabric), the wavelength/thickness ratio of folds is small, all of which suggest that the flexural slip folding mechanism and plane strain deformation are reasonable assumptions of deformation mechanisms and strain geometry.



### **3.4. WORKFLOW**

A step-by-step guide and short course to balancing geological cross-sections can be found in Woodward et al. (1989). The suggested workflow was adjusted to the modern software and data availability. Below is a list of steps, which were used in this thesis to be complete balanced sections applying line-balancing method.

1. Acquire published geological maps and cross-sections for the area and compile with own field observations.
2. Georeference and merge maps together using ArcGIS.
3. Digitize faults, polygons of the formations, structures, strikes and dips, etc. into shapefiles using ArcGIS.
4. Import digitized shapefiles into Midland Valley – Move.
5. Acquire digital elevation models (DEM) and import them into Move.
6. Identify which structural measurements belong to which formation, and label accordingly using Move.
7. Project dip data to the surface of the DEM, so there will be an elevation associated with the data.
8. Draw a line in map view of where a cross-section is to be drawn.
9. Project the cross-section line to the DEM, so the line will have surface elevations on it.
10. Project dip data to the line from a reasonable distance away. The projected dip data must use apparent dips to the section.

11. Project surface intersections of formation contacts and faults onto the cross-section trace.
12. If a published cross-section is available, import a picture, in .png format, to the new cross-section and scale it to fit the section to use as a reference for the type of structures that may be present in the region.
13. Review the stratigraphy of the area, so the constant thickness of the formations is known.
14. Draw the décollement with appropriate dip value towards the hinterland.
15. Draw a layercake of the formations in front of the deformation front, so the undeformed stratigraphy is known, and the assumed depth to the décollement is justified.
16. Draw a pin line in the undeformed strata in front of the deformation. The pin line is used as a reference point of strata to which the section will be restored to.
17. Continue the intersections of the surface faults to depth. (e.g. Project the faults from their surface trace to depth.)
18. Draw formations in the cross-section, keeping in mind constant thickness of the beds, and reasonable geological features, such as duplexes. The whole area from surface to décollement must be filled with strata.
19. Attempt to restore the cross-section into a retrodeformed state. If the older layers are longer than the younger layers, and faults are all propagating in

foreland or hinterland direction, thrust and back thrust respectively, the section is balanced.

20. Measure the total length of a key horizon in the retrodeformed section and the length of the horizon present from the pin to the end of where it is present in the deformed section.
21. Calculate the total shortening of that horizon in both total distance and also in percentage.
22. Export cross-sections, and save as a .pdf file.
23. Import the cross-section and retrodeformed section into Adobe Illustrator.
24. Merge the two sections documents together into the same file.
25. Clean up images by drawing neater scales, and adding color to the formations.
26. Look up stratigraphic data from published papers and works on the ages of key horizons in the area to acquire the age of that horizon. Determine the depositions age of the key horizon from the published data. Use a deeper horizon, as upper horizons may be synorogenic sediments.
27. Assuming deformation is still ongoing, calculate the shortening per year of that horizon using the total shortening in length and the age of the horizon.

Repeat and compare for additional cross-sections.

### **3.5. RESULTS**

Along 2000 km of the Himalayan orogen, ten balanced cross-sections were constructed across the Sub-Himalaya. Total shortening is the product of elapsed time and strain rate. Strain rate is imposed. If the deformation started at the same time everywhere there should be no difference between the shortening rate and strain rate. However if the deformation started at variable times there will be a difference between % shortening and strain rates. Shortening distance, shortening %, shortening rate, and strain rate were calculated for each section using local stratigraphic ages from published papers.

#### **3.5.1. BALANCED CROSS-SECTIONS AND MAPS**

An overview geological map of the Himalaya, local geology maps of the Siwalik Group, and balanced cross-sections are displayed in Figure 3.6. The scales of the maps are different due to paper size restrictions but are provided in the digital appendix at the same scale. Cross-section A is at a smaller scale than the other 9 cross-sections due to the paper length. All the maps and cross-sections are provided in the Appendix. All the cross-sections are at the same scale in the Appendix.

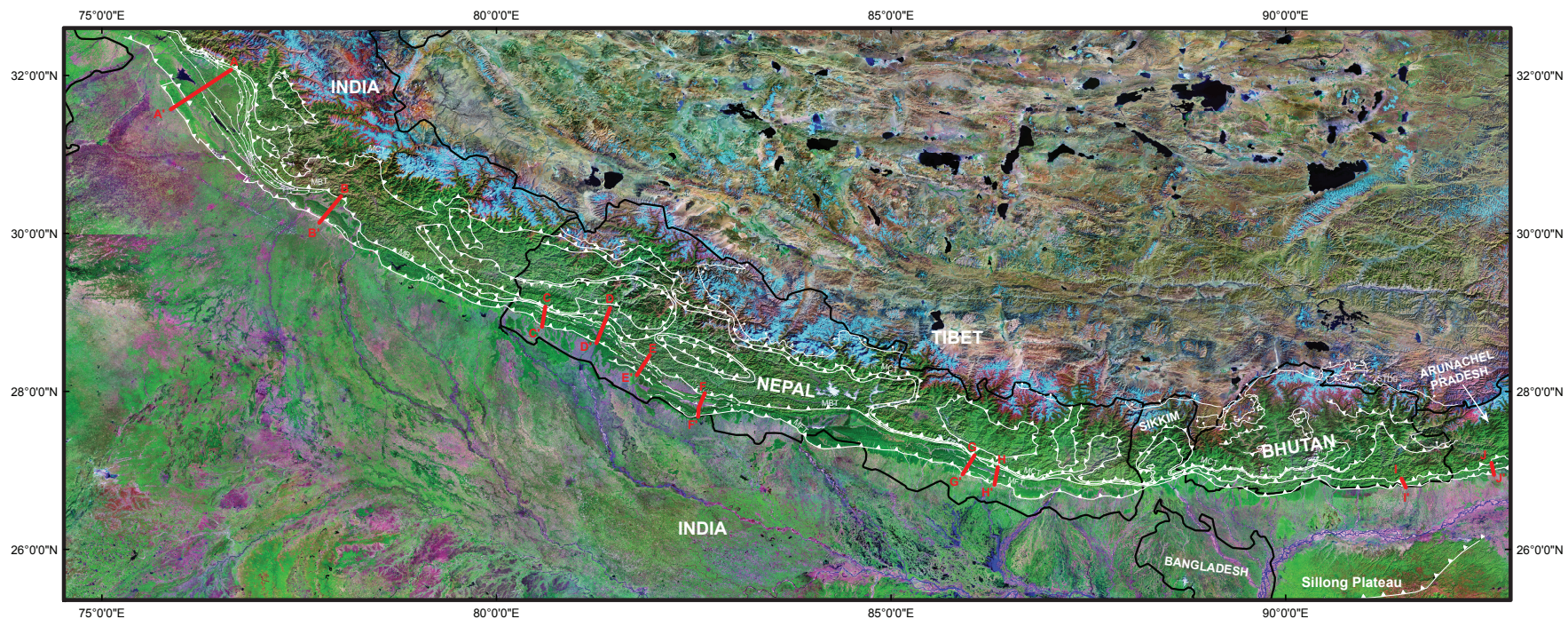


**Figure 3.5 – Landsat Geocover map of the Himalayan arc. The imagery shows topographic differences in the Indo-Gangetic plains of India, and the drainage systems (in purple) on the plains with the topography of the Himalaya and Tibetan Plateau. Cross-sections are indicated with red lines, and major faults and shear zones are displayed in white and compiled from McQuarrie et al. (2008), Powers et al., (1998), Chirouze et al., (2012), Mugnier et al., (1999), Yin et al., (2010) and Ojha (personal communication, 2012).**

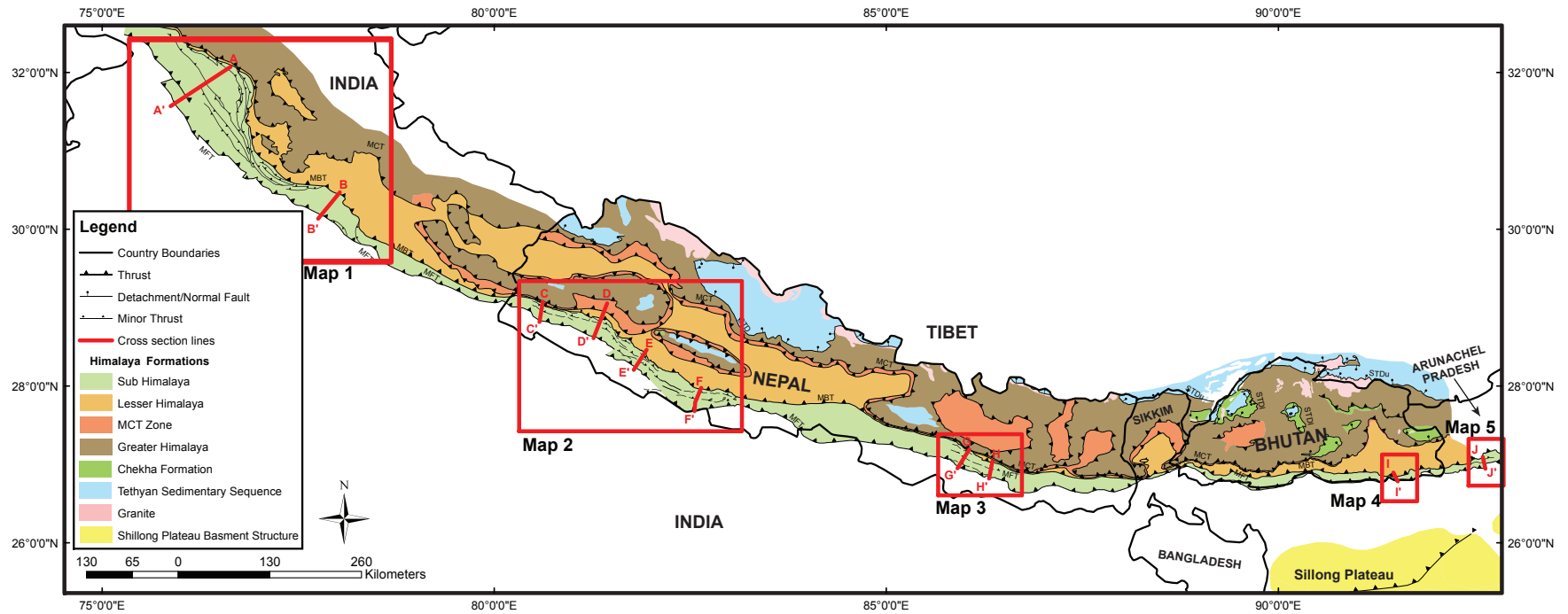


**Figure 3.6 - Geological overview map of the Himalaya. Red boxes indicate detailed geological map areas of the Sub-Himalaya and Siwalik Group. Balanced cross-sections of the Siwalik Group are indicated with red lines. Compiled from McQuarrie et al. (2008), Powers et al., (1998), Chirouze et al., (2012), Mugnier et al., (1999), Yin et al., (2010) and Ojha (personal communication, 2012).**

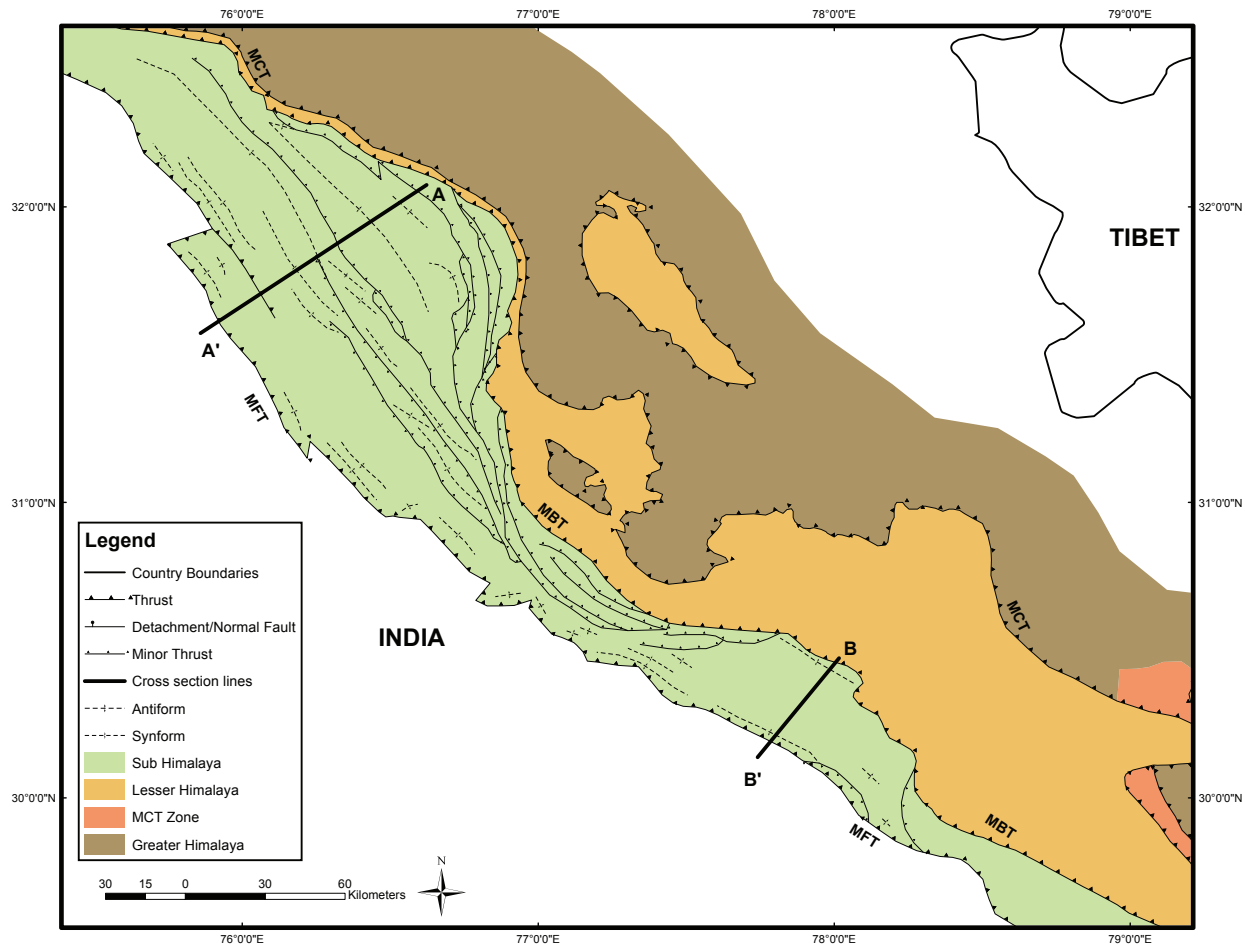
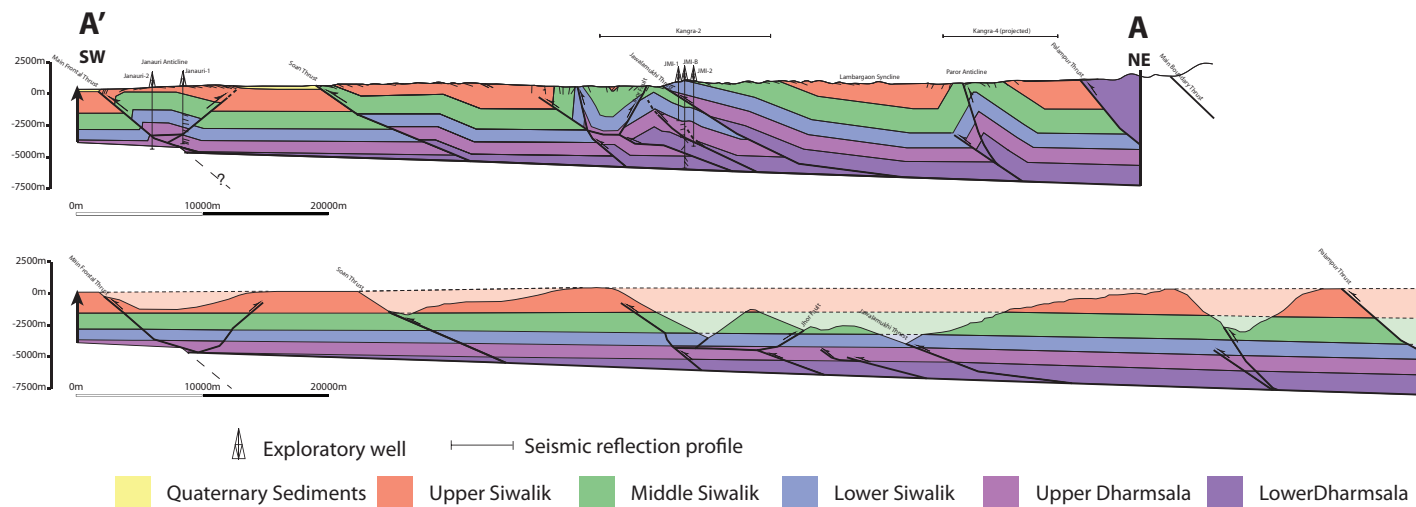


Figure 3.7 - Geological map of North Western India (Himachal Pradesh). Structures in the Sub-Himalaya are well mapped. Cross-sections (Powers et al., 1998) were constructed using seismic and bore hole data. Map is modified from Powers et al., (1998).



**Figure 3.8 - Cross-section A.** Cross-section trace is indicated on Map 1 (Figure 3.7). Section completed with seismic and bore hole data, and modified from Powers et al., (1998), and ages from Sanyal et al. (2004).

For cross-section A, the Middle/Lower Siwalik boundary has a deformed length of 83.9 km, retrodeformed length of 106.8 km, which results in shortening of  $23.0 \pm 3.47$  km and  $21.5 \pm 3.24$  %. Assuming that deformation started at the Middle/Upper Siwalik boundary,  $2.70 \pm 0.30$  Ma, will result in shortening rates of  $8.5 \pm 1.60$  mm/yr and strain rates of  $2.54e-15 \pm 4.73e-16$  s<sup>-1</sup>.



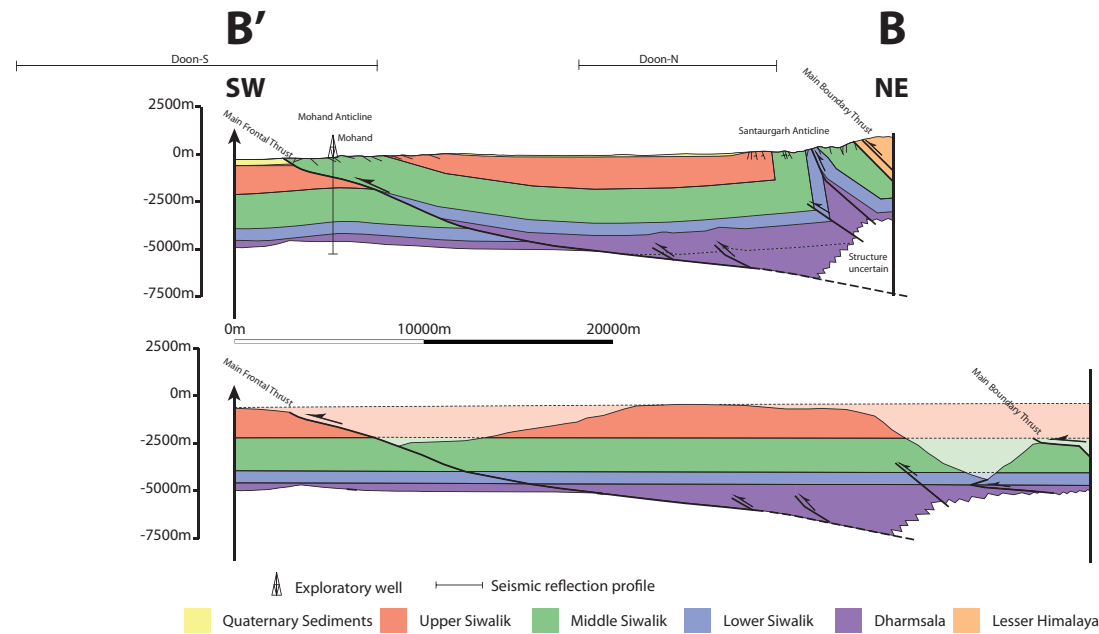


**Figure 3.9 - Cross-section B.** Cross-section trace is indicated on Map 1 (Figure 3.7). Section completed with seismic and bore hole data, and modified from Powers et al., (1998) and ages from Sanyal et al. (2004).

For cross-section B, the Middle/Lower Siwalik boundary has a deformed length of 34.75 km, retrodeformed length of 45.34 km, which results in shortening of  $10.60 \pm 2.67$  km and  $23.4 \pm 5.89$  %. Assuming that deformation started at the Middle/Upper Siwalik boundary,  $2.70 \pm 0.30$  Ma, will result in shortening rates of  $3.93 \pm 1.08$  mm/yr and strain rates of  $2.75e-15 \pm 7.56e-16$  s<sup>-1</sup>.

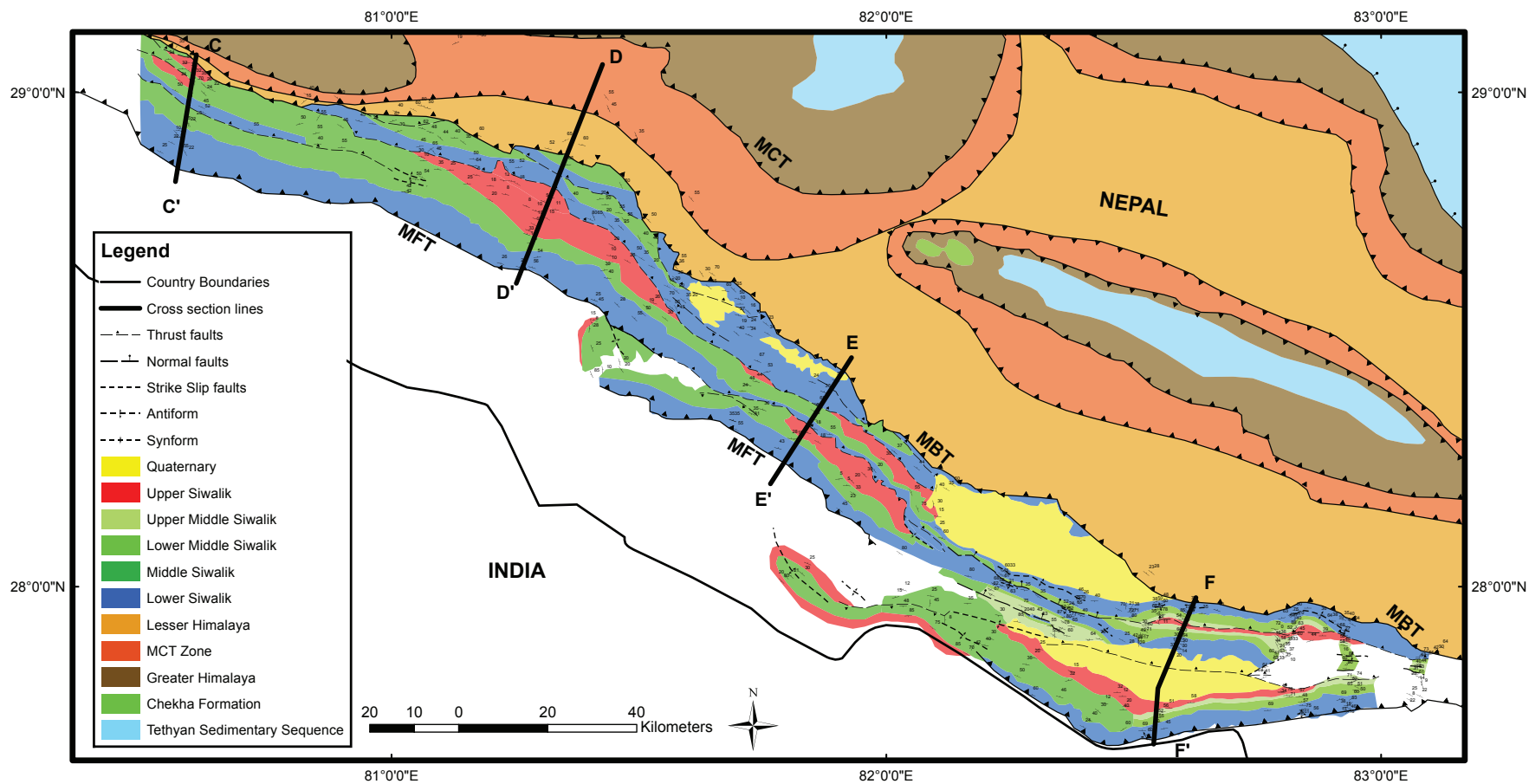
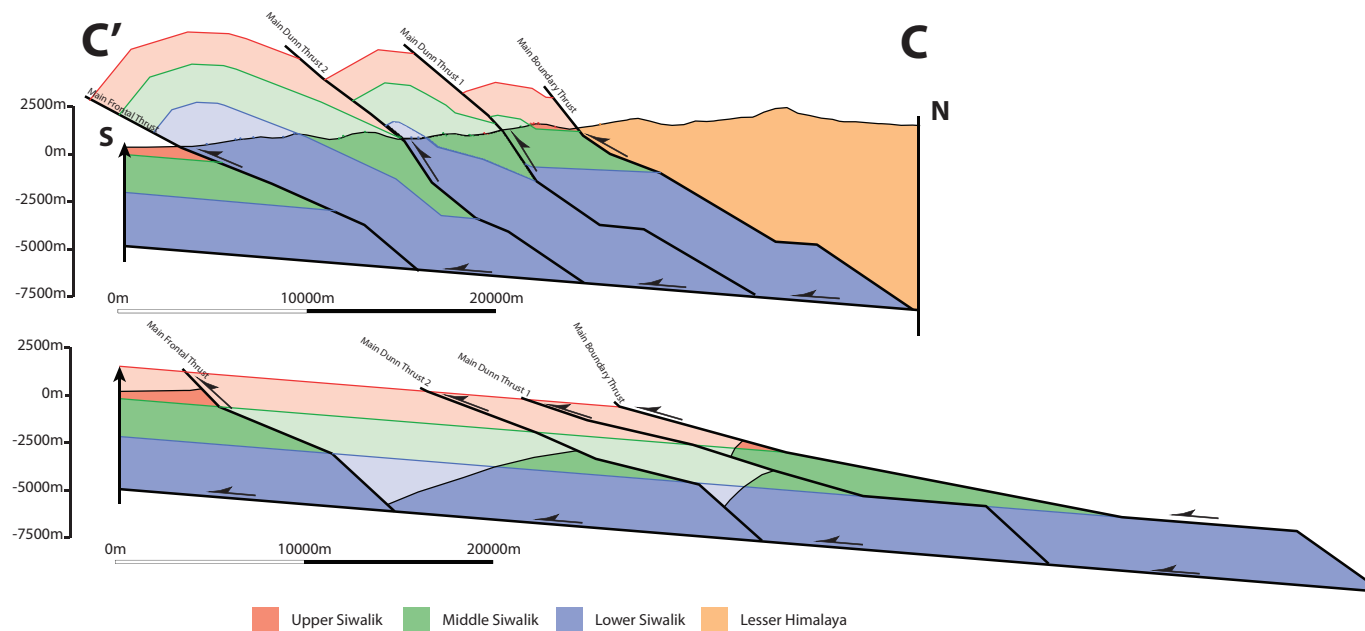


Figure 3.10 - Map 2, detailed geological map of the Siwaliks formation, Western Nepal. Balanced and retrodeformed cross-sections along transects D to F are found on the map. Structural data from Mugnier et al. (199b), in western Nepal, Ojha, (personal communication, 2012), and McQuarrie et al. (2008).



**Figure 3.11 - Cross-section C.** Cross-section trace is indicated on Map 2 (Figure 3.10). Map and structural data from Mugnier et al., (1999a), and ages from Ojha et al., (2009). For cross-section C, the Middle/Lower Siwalik boundary has a deformed length of 36.8 km, retrodeformed length of 62.50 km, which results in shortening of  $25.7 \pm 2.21$  km and  $41.1 \pm 3.53$  %. Assuming that deformation started at the Middle/Upper Siwalik boundary,  $4.83 \pm 1.00$  Ma, will result in shortening rates of  $5.32 \pm 1.19$  mm/yr and strain rates of  $2.70e-15 \pm 6.05e-16$  s<sup>-1</sup>.

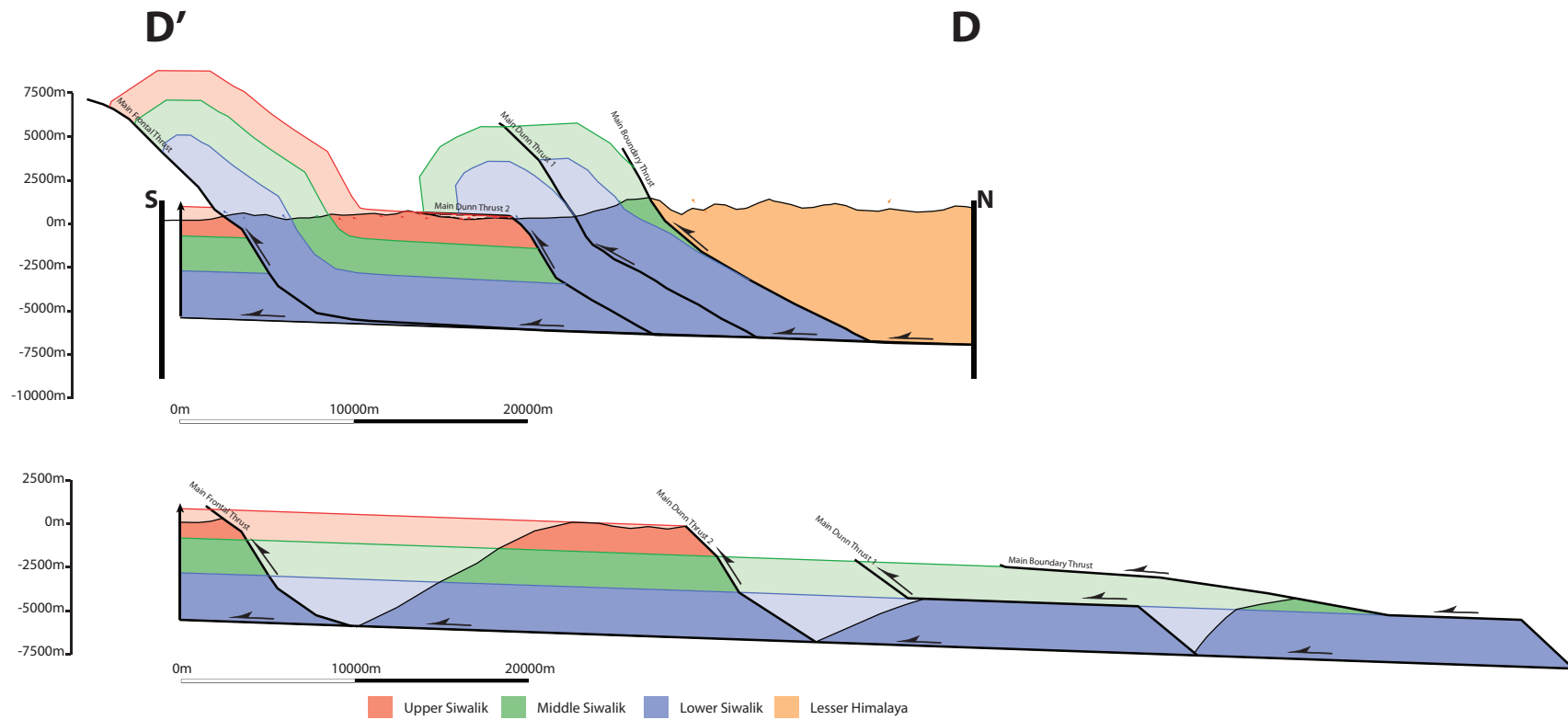
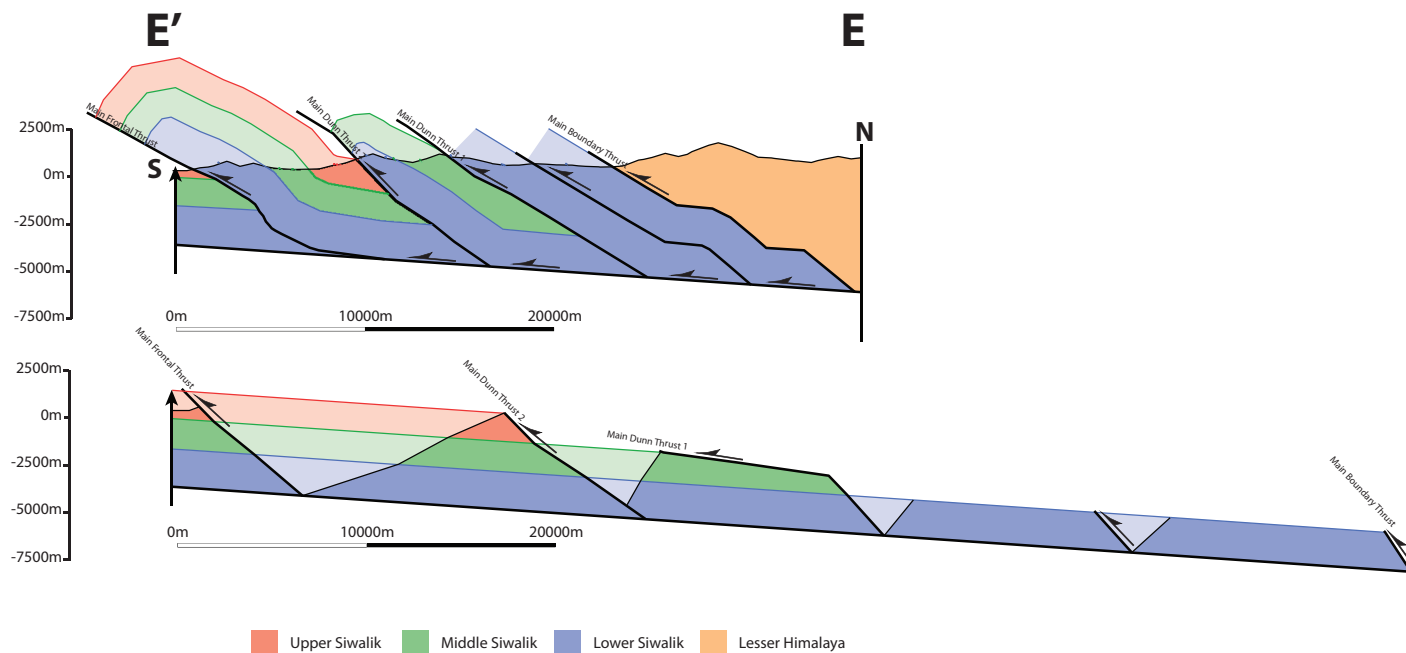


Figure 3.12 - Cross-section D. Cross-section trace is indicated on Map 2 (Figure 3.10). Map and structural data from Mugnier et al., (1999a), and ages from Ojha et al., (2009).

For cross-section D, the Middle/Lower Siwalik boundary has a deformed length of 39.6 km, retrodeformed length of 77.3 km, which results in shortening of  $37.7 \pm 8.77$  km and  $48.8 \pm 11.4$  %. Assuming that deformation started at the Middle/Upper Siwalik boundary,  $4.83 \pm 1.00$  Ma, will result in shortening rates of  $7.81 \pm 2.43$  mm/yr and strain rates of  $3.20e-15 \pm 9.97e-16$  s<sup>-1</sup>.



**Figure 3.13 - Cross-section E.** Cross-section trace is indicated on Map 2 (Figure 3.10). Map and structural data from Mugnier et al., (1999a), and ages from Ojha et al., (2009).

For cross-section E, the Middle/Lower Siwalik boundary has a deformed length of 33.3 km, retrodeformed length of 64.4 km, which results in shortening of  $31.1 \pm 3.22$  km and  $48.2 \pm 4.99$  %. Assuming that deformation started at the Middle/Upper Siwalik boundary,  $3.22 \pm 0.30$  Ma, will result in shortening rates of  $9.66 \pm 1.35$  mm/yr and strain rates of  $4.74e-15 \pm 6.61e-16$  s<sup>-1</sup>.

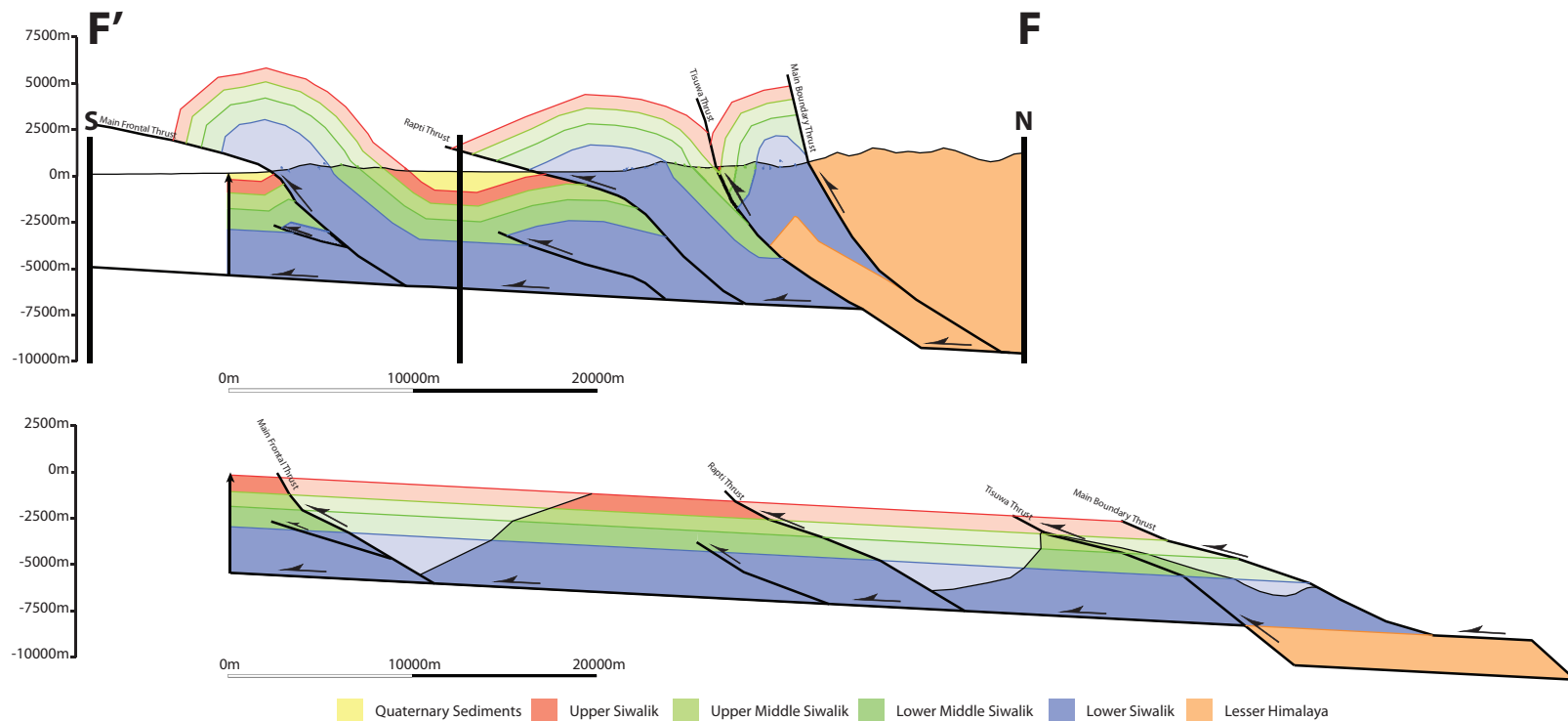


**Figure 3.14 - Cross-section F.** Cross-section trace is indicated on Map 2 (Figure 3.10). Map and structural data from Ojha, (personal Communication, 2012), and ages from Ojha et al., (2009).

For cross-section F, the Middle/Lower Siwalik boundary has a deformed length of 31.6 km, retrodeformed length of 58.6 km, which results in shortening of  $27.0 \pm 2.98$  km and  $46.1 \pm 5.09$  %. Assuming that deformation started at the Middle/Upper Siwalik boundary,  $3.22 \pm 0.30$  Ma, will result in shortening rates of  $8.39 \pm 1.21$  mm/yr and strain rates of  $4.54e-15 \pm 6.55e-16$  s<sup>-1</sup>.

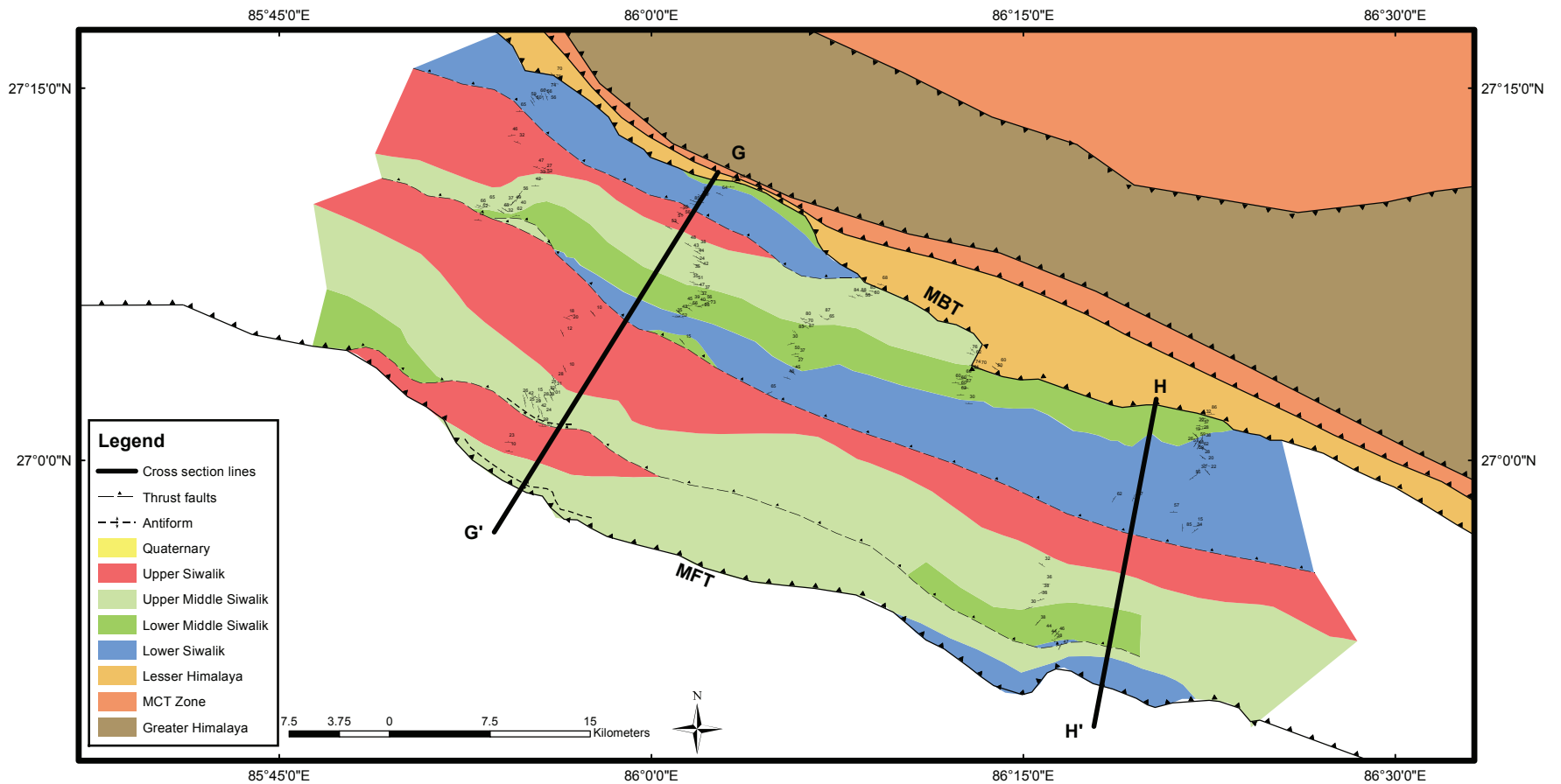
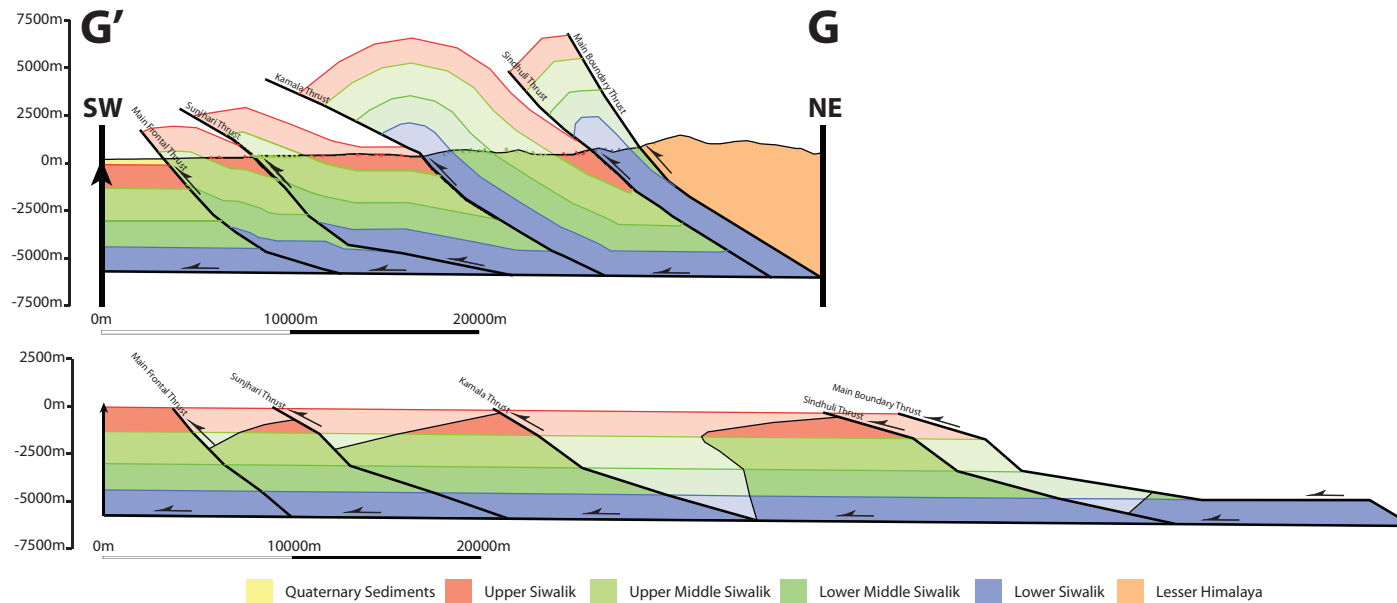


Figure 3.15 - Map 3, detailed geological map of the Siwaliks formation, Eastern Nepal. Balanced and retrodeformed cross-section along transects G and H are found on the map. Structural data from Ojha, (personal communication, 2012) and McQuarrie et al., (2008), and ages from Ojha et al., (2009).



**Figure 3.16 - Cross-section G.** Cross-section trace is indicated on Map 3 (Figure 3.15). Map and structural data from Ojha (personal communication, 2012), and ages from Ojha et al., (2009).

For cross-section G, the Middle/Lower Siwalik boundary has a deformed length of 38.1 km, retrodeformed length of 67.4 km, which results in shortening of  $29.3 \pm 1.52$  km and  $43.5 \pm 2.26$  %. Assuming that deformation started at the Middle/Upper Siwalik boundary,  $3.42 \pm 0.60$  Ma, will result in shortening rates of  $8.57 \pm 1.57$  mm/yr and strain rates of  $4.03\text{e-}15 \pm 7.37\text{e-}16$  s<sup>-1</sup>.



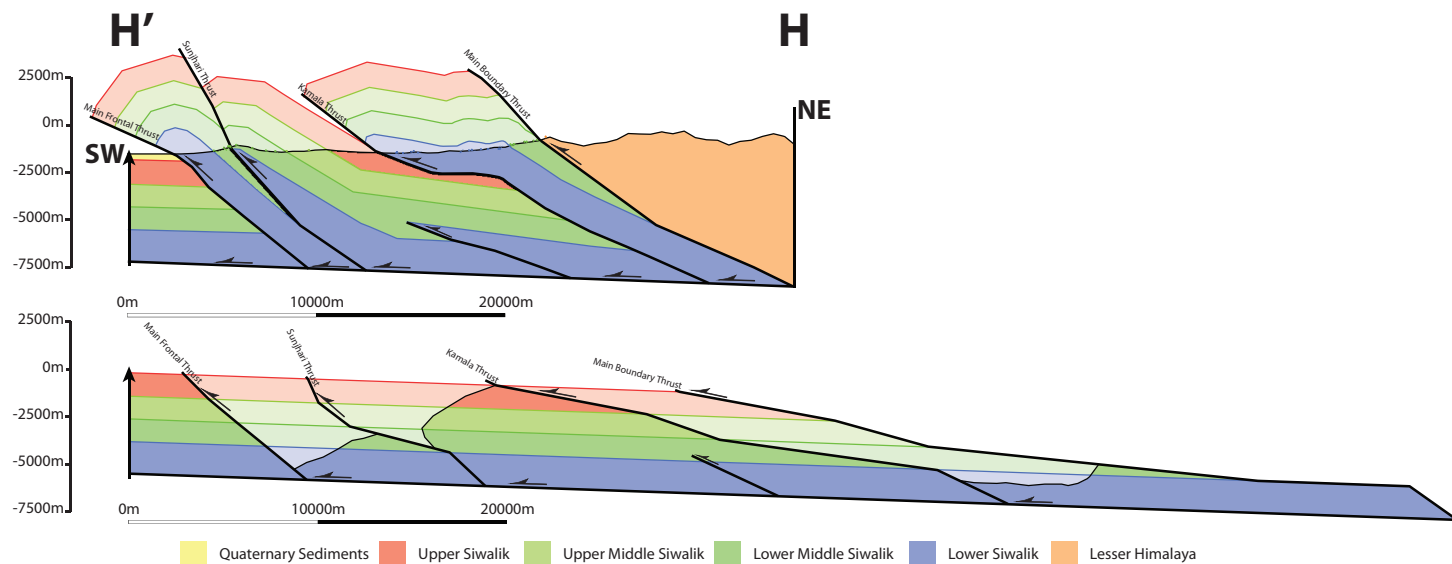


**Figure 3.17 - Cross-section H.** Cross-section trace is indicated on Map 3 (Figure 3.15). Map and structural data from Ojha (personal communication, 2012), and ages from Ojha et al., (2009).

For cross-section H, the Middle/Lower Siwalik boundary has a deformed length of 35.2 km, retrodeformed length of 67.8 km, which results in shortening of  $32.6 \pm 2.29$  km and  $48.1 \pm 3.38$  %. Assuming that deformation started at the Middle/Upper Siwalik boundary,  $3.42 \pm 0.60$  Ma, will result in shortening rates of  $9.53 \pm 1.80$  mm/yr and strain rates of  $4.46e-15 \pm 8.42e-16$  s<sup>-1</sup>.

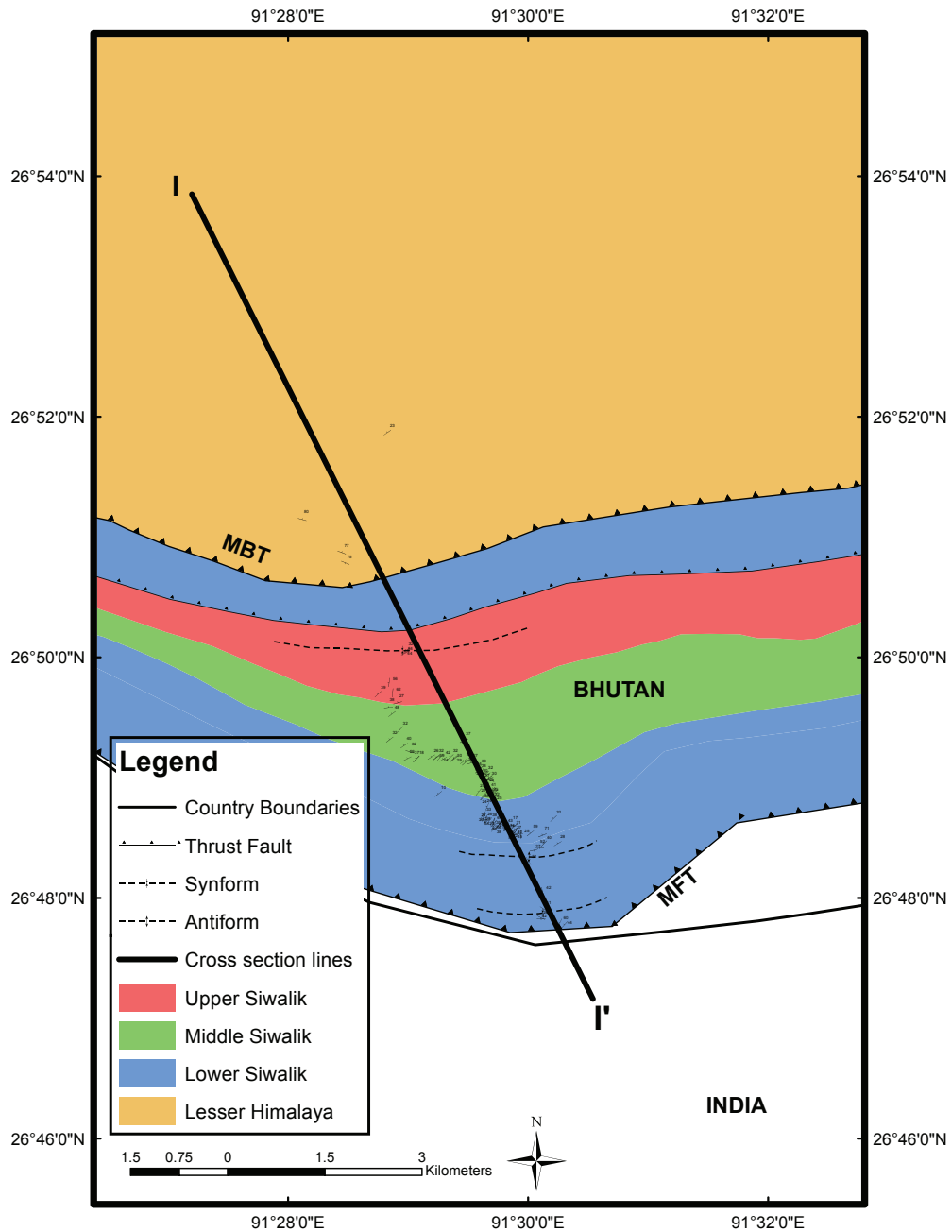


**Figure 3.18 - Map 4, detailed geological map of the Siwaliks Formation, Eastern Bhutan. Section I is found on the map. Structural data from Grujic, (personal communication, 2012)**

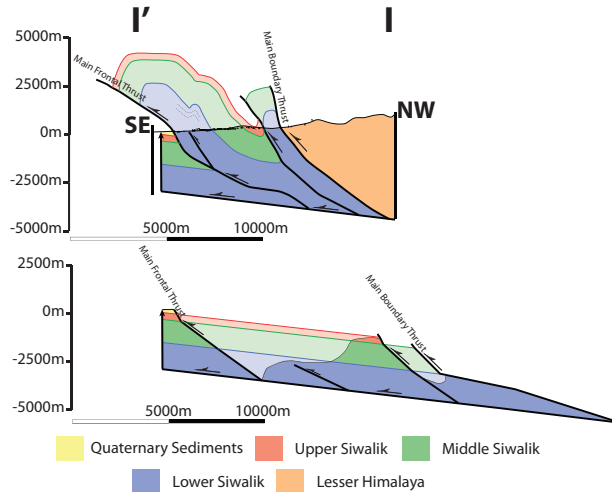


**Figure 3.19 - Cross-section I.** Cross-section trace is indicated on Map 4 (Figure 3.18). Map and structural data from Grujic (personal communication, 2012), and ages from (Chirouze et al., 2012b).

For cross-section I, the Middle/Lower Siwalik boundary has a deformed length of 6.19 km, retrodeformed length of 14.55 km, which results in shortening of  $8.31 \pm 1.45$  km and  $57.1 \pm 9.96$  %. Assuming that deformation started at the Middle/Upper Siwalik boundary,  $2.60 \pm 0.30$  Ma, will result in shortening rates of  $3.20 \pm 0.67$  mm/yr and strain rates of  $6.96e-15 \pm 1.46e-15$  s<sup>-1</sup>.

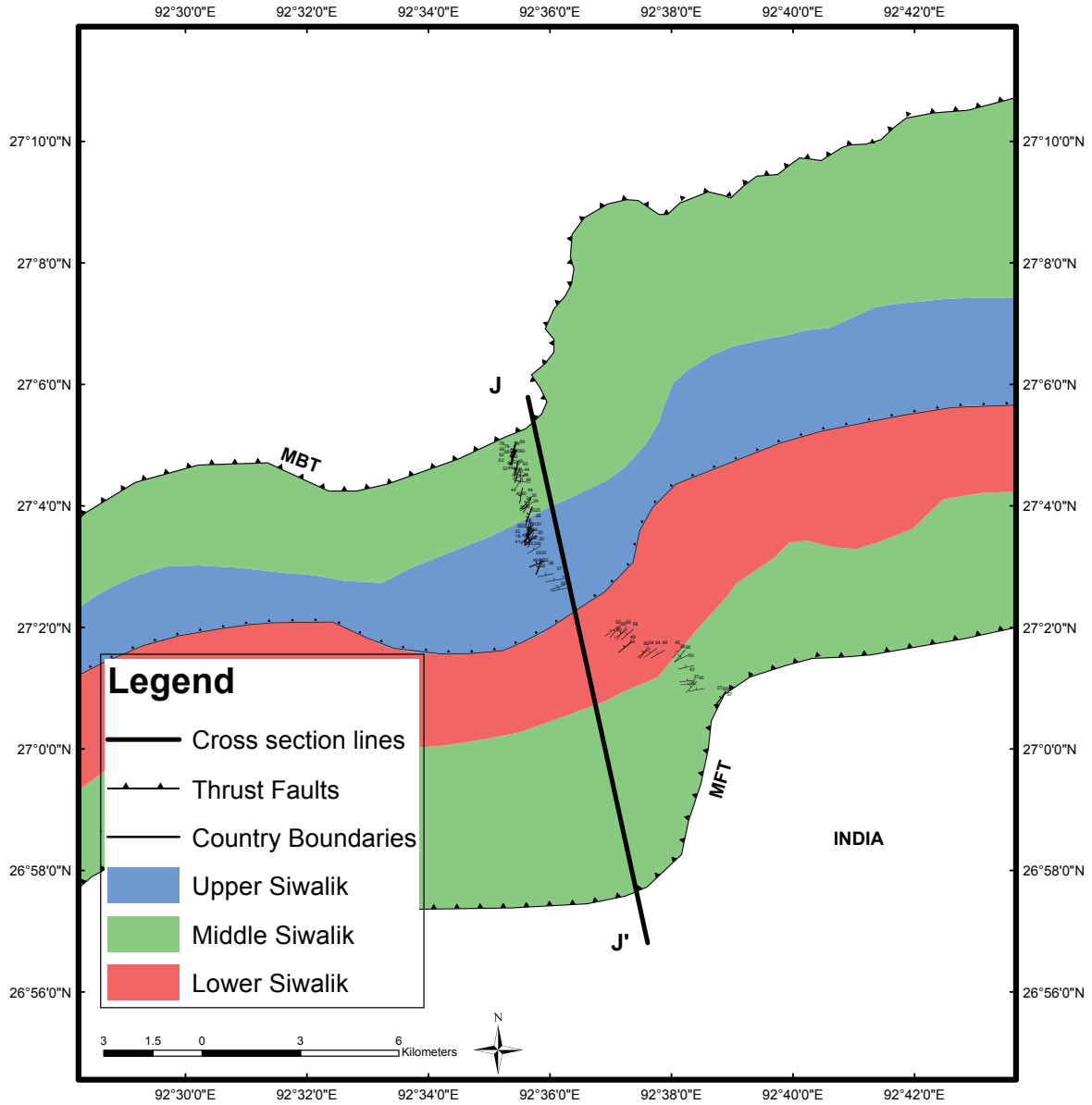


**Figure 3.20 - Map 5, detailed geological map of the Siwaliks Formation, Arunachal Pradesh. Section I is found on the map. Structural data from Chirouze and Huyghe, (personal communication, 2012) and map modified from (Chirouze et al., 2012a).**

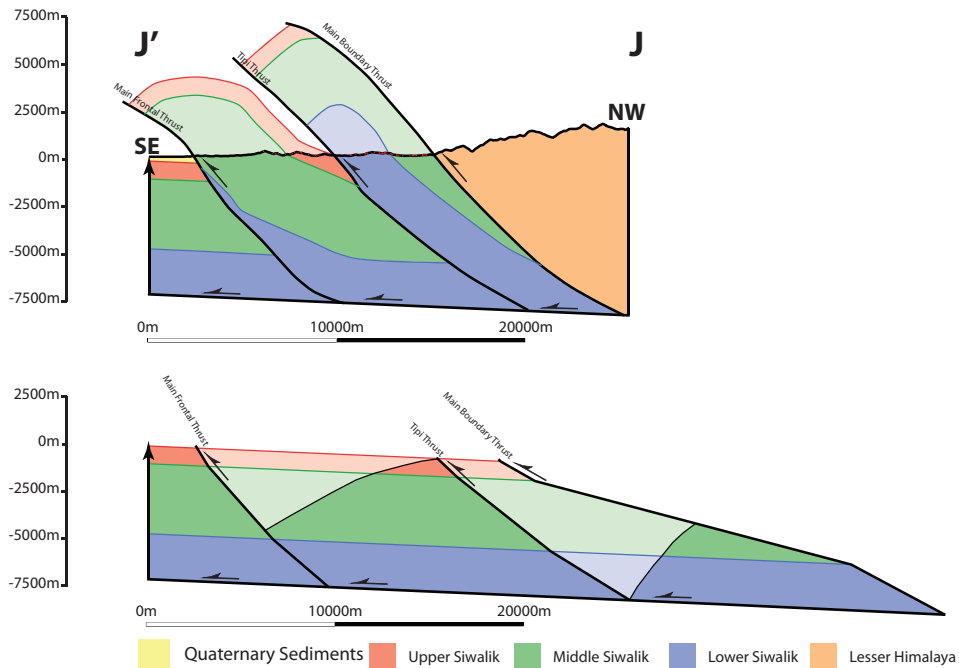


**Figure 3.21 - Cross-section J. Cross-section trace is indicated on Map 5 (Figure 3.20). Structural data from Chirouze and Huyghe, (personal communication, 2012) and map modified from (Chirouze et al., 2012a).**

For cross-section J, the Middle/Lower Siwalik boundary has a deformed length of 20.8 km, retrodeformed length of 37.3 km, which results in shortening of  $16.5 \pm 1.91$  km and  $44.3 \pm 5.13$  %. Assuming that deformation started at the Middle/Upper Siwalik boundary,  $2.6 \pm 0.30$  Ma, will result in shortening rates of  $6.35 \pm 1.04$  mm/yr and strain rates of  $5.40e-15 \pm 8.82e-16$  s<sup>-1</sup>.

### 3.5.2. SECTION RESULTS

The results and calculations of the cross-sections are displayed in Table 3.1. The shortening distance and percentage was calculated using the Lower Siwalik Group. This was used because it is the lowest and most complete formation, and therefore it has accumulated all the strain within the Sub-Himalaya. The onset of deformation in the Siwaliks is not precisely determined. In this work, it was assumed that the deformation started at the Upper/Middle Siwalik Boundary as discordance is observed in places between the layers. Consequently the shortening rates were calculated using the local age of the Upper/Middle Siwalik Boundary.

Cross-section A to H were drawn in locations in the Himalaya where there are no structures between the foreland belt and the foreland basin. Cross-sections I and J were drawn in locations of the foreland belt where the Shillong Plateau is in the foreland basin.

Among the ten cross-sections constructed, results varied widely. Total shortening ranges from 8.31km to 37.7km. Percentage shortened was quite uniform, and has an increasing gradient from west-to-east with a range of 21.5 to 57.2%. Shortening rates vary from 3.20 to 9.66 mm/yr. Strain rates also display a west-to-east increasing gradient with values ranging from  $2.52\text{E-}15$  to  $6.96\text{E-}15$  s<sup>-1</sup>. All results are displayed in Table 3.1, Figure 3.22, and Figure 3.23.

The errors in shortening rate and strain rate were calculated by propagating the errors of both the cross-sections and stratigraphic age. Error propagation formula is:

**Equation 23**

$$R \pm \delta R = \frac{X}{Y}$$

where:

**Equation 24**

$$\delta R = |R| * \sqrt{\left(\frac{\delta X}{X}\right)^2 + \left(\frac{\delta Y}{Y}\right)^2}$$

where X, Y and R are arbitrary values, and  $\delta$  is the error associated with the value. Analysis of error in the cross-sections was completed using area balancing error method (Judge and Allmendinger, 2011). The difference in shortening length of the line balancing and the area balancing is the error of the section. The age of the Upper/Middle Siwaliks boundary was estimated to have a 0.3 Ma error. A generic error of 0.3 Ma was used due to measuring of the correlation of the absolute ages given by Ojha et al. (2009), Sanyal et al. (2004), and Chirouze et al., (2012), and the placement of the Upper/Middle Siwaliks boundary. The Khutia Khola stratigraphic section may have ages younger than what are used in this study. Originally, the Upper/Middle Siwalik boundary was inferred using sedimentation rates. Magneto stratigraphic data was not available for the upper portion of the Middle Siwaliks, so a correlation could not be done, therefore the error of 1.0 Ma is used for the Khutia Khola section, as it is an inferred age. Similarly, the Muksar Khola magnetostrat data ends at the Upper/Middle Siwalik boundary, and error may be greater, thus an error of 0.6 Ma was used.

Cross-sections C and D should be looked into further, as the stratigraphic ages of the sections are not as well constrained due to using the Khutia Khola stratigraphic age.

Table 3.1-. Results from the ten balanced sections. Deformation is assumed to have started at the beginning of the deposition of the Upper Siwalik, as there is discordance in some places, as well as the appearance of conglomerates.

<b>Section</b>	<b>Shortening of the Lower Siwalik (km)</b>	<b>Shortening of the Lower Siwalik (%)</b>	<b>Age of Upper/Middle Siwalik Boundary from Magneto Stratigraphy (Ma)</b>	<b>Shortening Rate from Age of Top of Middle Siwalik (Lower Siwalik Shortening) (mm/yr)</b>	<b>Strain Rate of the Lower Siwalik (strain/sec)</b>
A	23.0 ± 3.47	21.5 ± 3.24	2.70 ± 0.30	8.52 ± 1.60	2.52E-15 ± 4.73E-16
B	10.6 ± 2.67	23.4 ± 5.89	2.70 ± 0.30	3.93 ± 1.08	2.75E-15 ± 7.56E-16
C	25.7 ± 2.21	41.1 ± 3.53	4.83 ± 1.00	5.32 ± 1.19	2.70E-15 ± 6.05E-16
D	37.7 ± 8.77	48.8 ± 11.35	4.83 ± 1.00	7.81 ± 2.43	3.20E-15 ± 9.97E-16
E	31.1 ± 3.22	48.2 ± 4.99	3.22 ± 0.30	9.66 ± 1.35	4.74E-15 ± 6.61E-16
F	27.0 ± 2.98	46.1 ± 5.09	3.22 ± 0.30	8.39 ± 1.21	4.54E-15 ± 6.55E-16
G	29.3 ± 1.52	43.5 ± 2.26	3.42 ± 0.60	8.57 ± 1.57	4.03E-15 ± 7.37E-16
H	32.6 ± 2.29	48.1 ± 3.38	3.42 ± 0.60	9.53 ± 1.80	4.46E-15 ± 8.42E-16
I	8.31 ± 1.45	57.1 ± 9.96	2.60 ± 0.30	3.20 ± 0.67	6.96E-15 ± 1.46E-15
J	16.5 ± 1.91	44.3 ± 5.13	2.60 ± 0.30	6.35 ± 1.04	5.40E-15 ± 8.82E-16



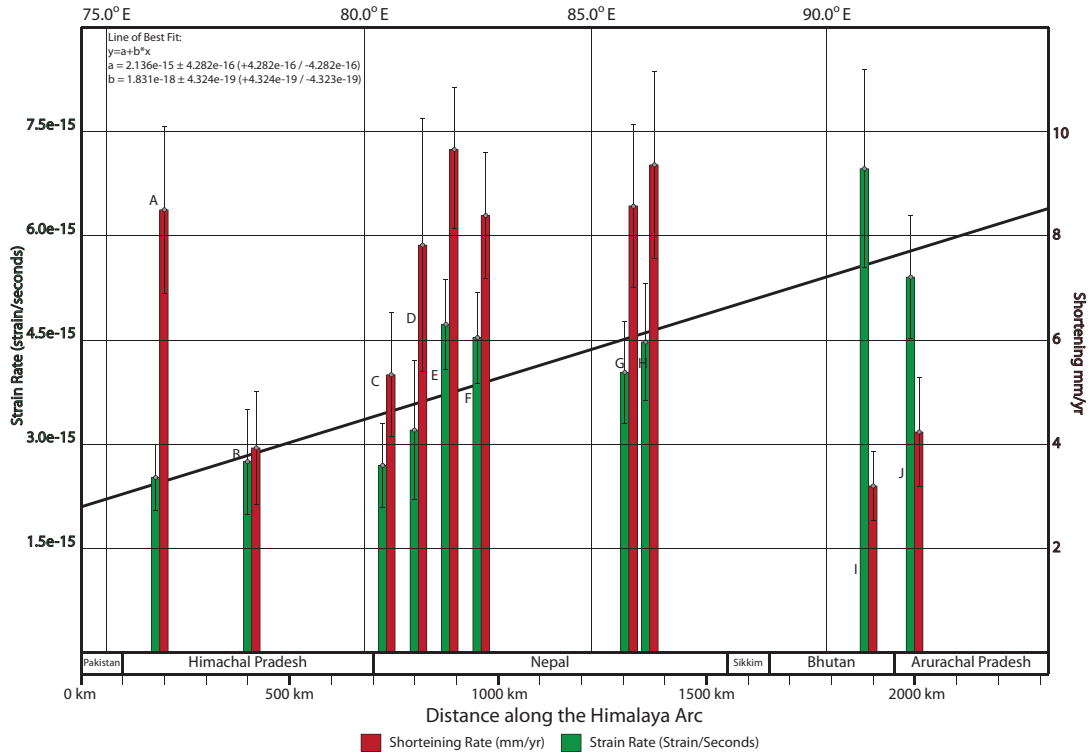


Figure 3.22 - Graph of shortening rate and strain rate of the Siwalik Group vs. distance along the Himalaya arc. The shortening and strain rate was calculated using the length and % shortened of the Lower/Middle Siwalik in the sections and the time since deformation was assumed to begin. Line of best fit is for strain rate.

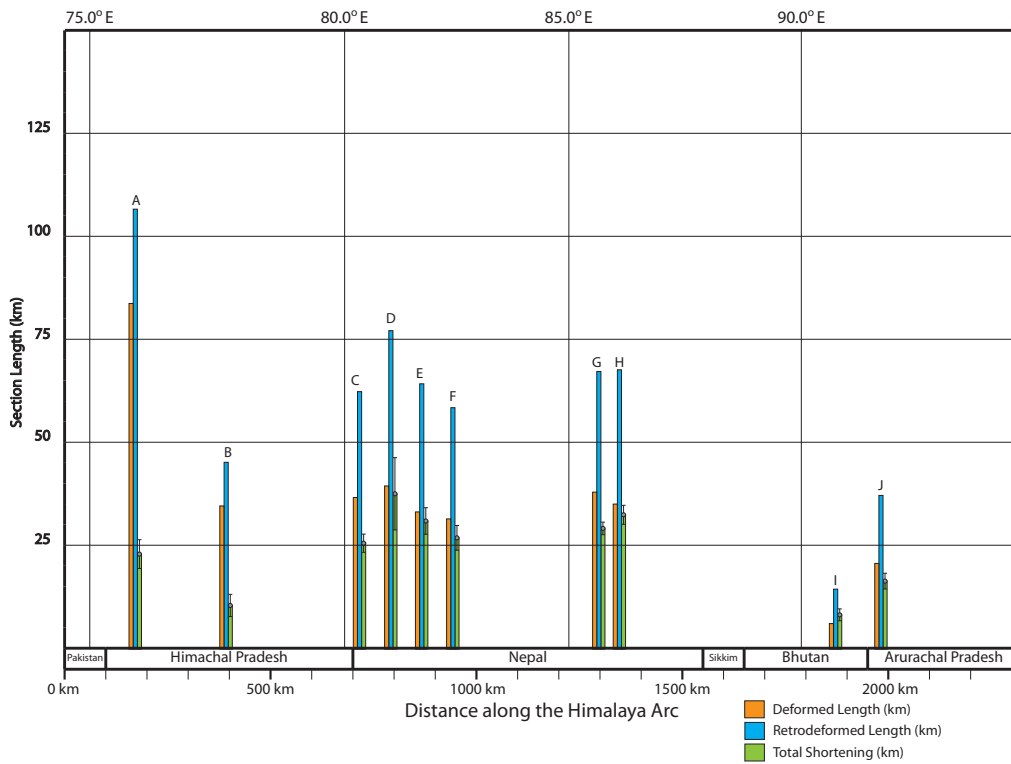


Figure 3.23 – Shortening vs. distance of the Lower Siwalik Group along the Himalaya arc.

## 4. DISCUSSION

Along strike, changes of shortening rates and strain rates pose questions for the causes of these trends.

During the last 11 myr, convergence rates of the Indian plate colliding with the Eurasian plate were constant, but varied laterally from ca. 34 mm/yr in the northwest to ca. 44 mm/yr in the northeast of India (Molnar and Stock, 2009). Current GPS velocities are consistent with the trend of plate convergence velocities, since rates are ca. 10 mm/yr greater in the east than the west (Banerjee et al., 2008). It is found with the cross-sections drawn that there is a west-to-east increase in strain rate. Finally, there is also a pronounced trend of mean annual precipitation rates in the foothills of the Himalaya which increase from the west-to-east (Bookhagen and Burbank, 2010). Shortening rates and strain rates are not perfectly consistent with each other since the strain rates have a linear trend and the shortening rates are more variable. In turn, factors which influence shortening and strain rates were examined, are:

1. Sedimentation rates, amount of sedimentation and formation length.
2. Erosion and rainfall rates.
3. Critical Taper Model and differences in parameters of the model across the Sub-Himalaya.
4. Effects of transfer zones and strike-slip structures.

Furthermore, additional questions arise to why Bhutan has the lowest shortening rate but highest strain rate in the Sub-Himalaya. Did deformation in the Sub-Himalaya and Foreland Basin of the western Himalaya occur later than the rest of the Himalaya? Are there other factors influencing differences in shortening?

#### **4.1. SEDIMENTATION RATES AND FORMATION LENGTH**

The length of the undeformed section varies substantially throughout the Siwalik Group along the Himalayan arc. In the west and central Himalaya, the undeformed sections are quite long reaching lengths of over 100 km. In the east, the retrodeformed sections range from 8.31 to 16.5 km. However there is a clear W-E trend in the undeformed length of the Sub-Himalayan basin. This relationship may be related to the elastic thickness of the undergoing plate, which with the constant lithospheric thickness can be correlated with the convergence rate. The simple observations of the shape of the current foredip and bulge indicate an eastward narrowing and deepening of the Himalayan foredip (Bilham et al., 2003). This drastic variation in the formation length is difficult to assess for variations in shortening as there are substantially different shortening distances.

Ojha et al., (2009) analyzed deposition rates. Sediment accumulation ranges from 0.28 – 0.56 mm/yr, generally with rates increasing upward throughout the section. Younger sediments are more proximal, coarser and thus the accumulation rates are higher. These increased sedimentation rates suggest there is a lateral propagation of a major thrust system (i.e. MBT) in the frontal Lesser Himalaya. It is seen, in Nepal, that there is a slight decrease of sedimentation rates from west-to-east, as well as sediments Pliocene to Recent Shortening of the Siwalik Group in the Himalayan Foreland Belt 78

get younger eastward. These observations of sedimentation rates may be related to wedge forming processes.

#### **4.2. EROSION AND RAINFALL RATES**

Erosion plays an important role in the critical taper model of orogenic wedges. The angle of the orogenic wedge has to stay constant for the wedge to maintain a constant shape. The wedge will have to compensate and adjust to the temporal changes in erosion rate, to stay at a steady angle, which is achieved by activation of new thrusts (Equation 17-21) (Dahlen, 1990; Dahlen and Suppe, 1988; Dahlen and Barr, 1989; Barr and Dahlen, 1989).

Rainfall during the Indian summer monsoon throughout the Himalaya is the principal factor for erosion. There is a distinct east-to-west gradient in rainfall, with the warm tropical climates to the east, and desert climates to the west. Over the Himalayan foothills, the annual rainfalls range from over 4 meters in the east to less than 0.5 m in the west (Bookhagen and Burbank, 2010).

There is a clear correlation between the rainfall and the strain rates (Figure 4.3). The correlation with the shortening rates is less clear but it is present, and is the same as the strain rate correlation when the two outliers, section A and J are omitted. In addition, there is an inverse correlation between the wedge width (deformed length in Figure 3.23) and the precipitation. A higher erosional efficiency,  $K$ , will favor a narrower wedge (Whipple, 2009).

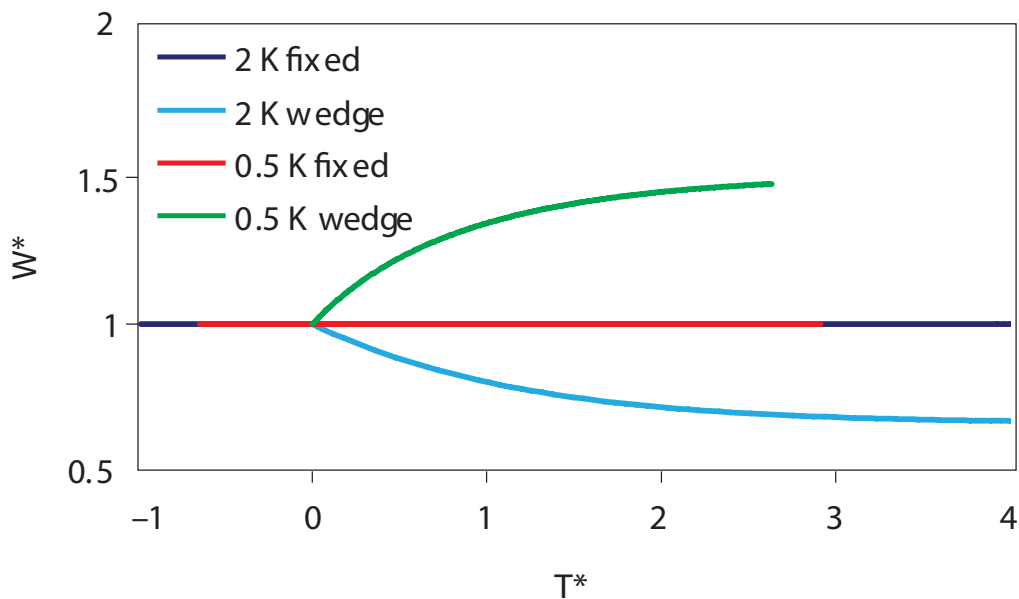


**Figure 4.1 – Orogenic wedge response to erosional efficiency changes,  $K$ . Response to an increase (twice, 2K) and decrease (half, 0.5K) in erosional efficiency are tested using an analytical model. The model predicts half-width ( $W^*$ ) plotted against a dimensionless time ( $T^*$ ) (Whippe, 2009).**

Because the monsoonal precipitation always proceeds from east to west, the same gradient of precipitation (though with different absolute values) can be expected for any period in the past regardless of the potential periods of monsoonal precipitation. The main difference is in the Bhutan Himalaya where a significant decrease of precipitation has likely occurred due to the surface uplift of the Shillong plateau and establishment of the rain shadow in its lee (Biswas et al., 2007). However this change has most likely occurred before or at the onset of deformation in the Siwaliks.

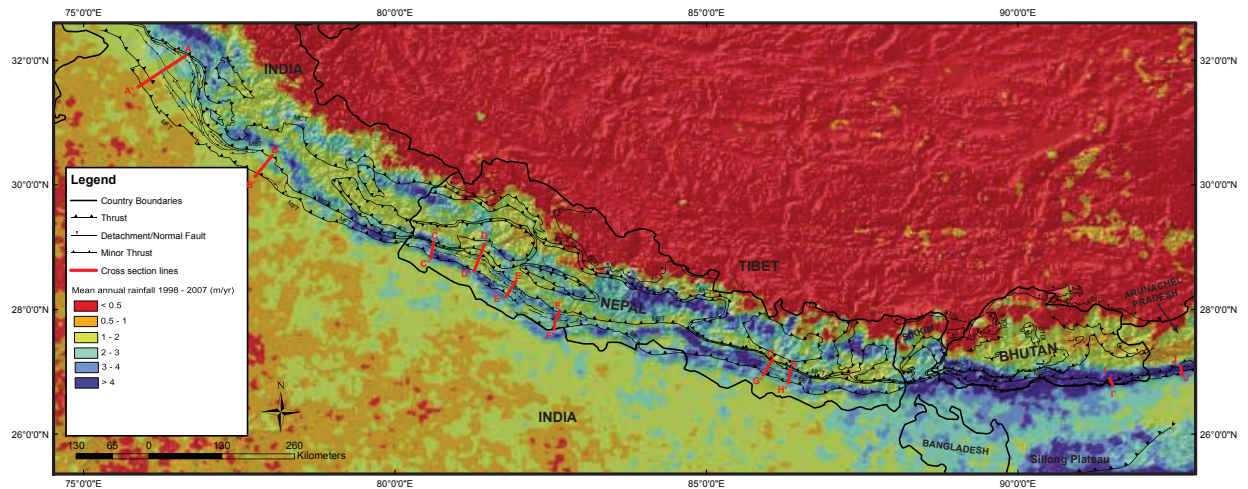


Figure 4.2 - Mean annual rainfall averaged over 10 years. Rainfall calibrated from TRMM 2B31 data (Bookhagen and Burbank, 2010). Note there is a distinct gradient from the east to the west for rainfall amount. There is also an inner and outer band within the topographic of the Himalaya.

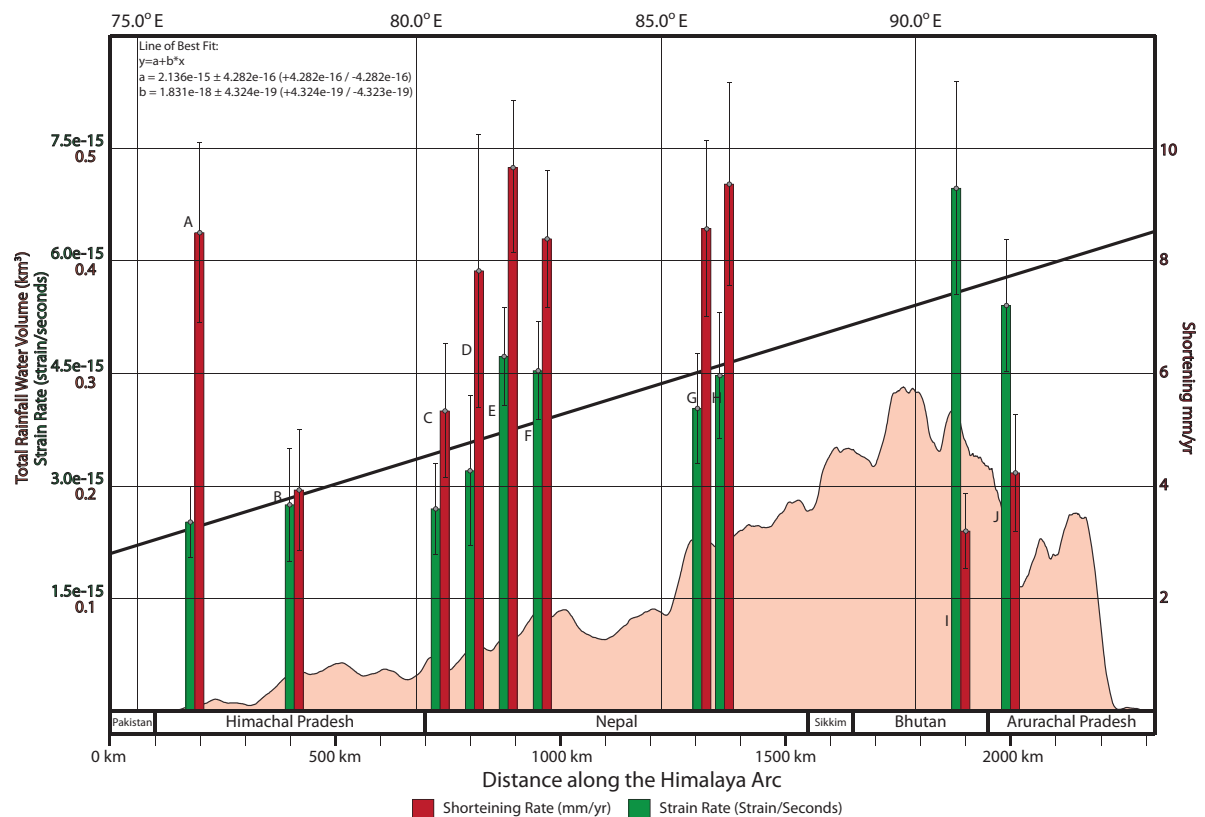


Figure 4.3 - Graph of shortening rate and strain rate of the Siwalik vs. distance along the Himalaya arc with total annual rainfall overlain. There are correlations between the strain rates and the annual amount of rainfall at elevations less than 500m. There is an evident correlation of a west-to-east increase both in strain rate and rainfall. Rainfall data from Bookhagen et al., (2010). The line of best fit is for strain rates.

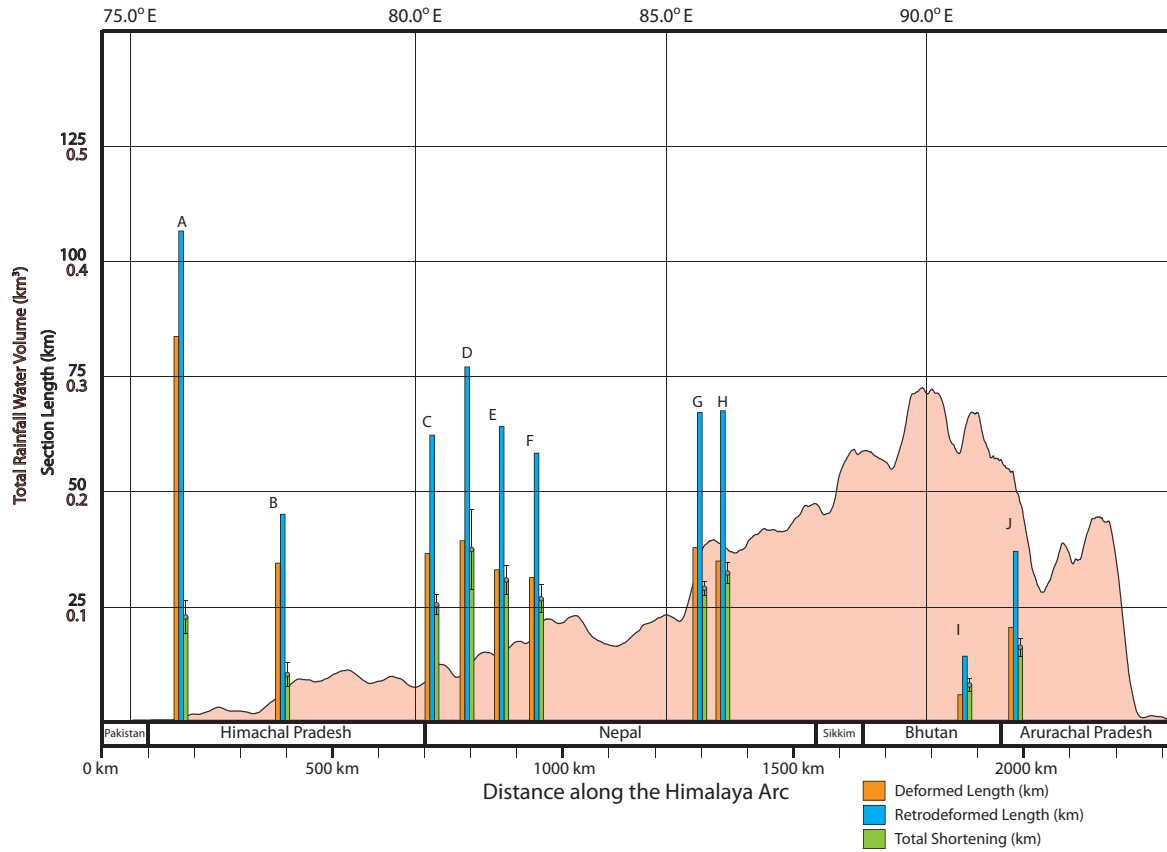


Figure 4.4 - Graph of the lengths of the Siwalik sections vs. distance along the Himalaya arc with total annual rainfall overlain. There is an inverse correlation between the retrodeformed length and deformed length and the annual amount of rainfall at elevations less than 500m. Rainfall data from Bookhagen et al., (2010).

### 4.3. CRITICAL TAPER MODEL

In the critical taper model, erosion plays an important role in the % of shortening in a section and the width of the wedge. The orogenic wedge will try to maintain a constant angle ( $\alpha+\beta$ ). As for the angle of the wedge, to have a steeper angle, in general, the orogenic wedge must have stronger material in the wedge, or on the décollement. Therefore, the angle is maintained by the properties of the material in the orogenic wedge. If erosion rates increase the wedge will have to shorten to keep the angle

constant by creating a series of thrust faults (Dahlen, 1990; Whipple, 2004; Whipple, 2009) (Figure 4.1).

In the Sub-Himalaya, it is seen that there is an eastward increase in precipitation rates. Due to the inverse correlation of precipitation rates and wedge shape, it is safe to conclude the Sub-Himalaya orogenic wedge follows the critical taper model, in which higher erosion rate causes a narrow wedge and greater shortening %. On the other hand strain rates are externally imposed and are related to plate convergence rates.

#### **4.4. ALONG-STRIKE SHORTENING DIFFERENCES**

Within areas where there is a high concentration of cross-sections, e.g. western Nepal, there is variation in the shortening within the sections, and the trends described until now are not smooth but appear to be stepwise. Mugnier et al. (1999a) suggested these differences may be due to propagating faults and orogen-perpendicular transfer zones. There may be strike slip movement within the transfer zone, which in turn accommodates differential shortening. These transfer zones are displayed by a main fault stopping and stepping out, e.g. the Main Frontal Thrust in Figure 4.5.



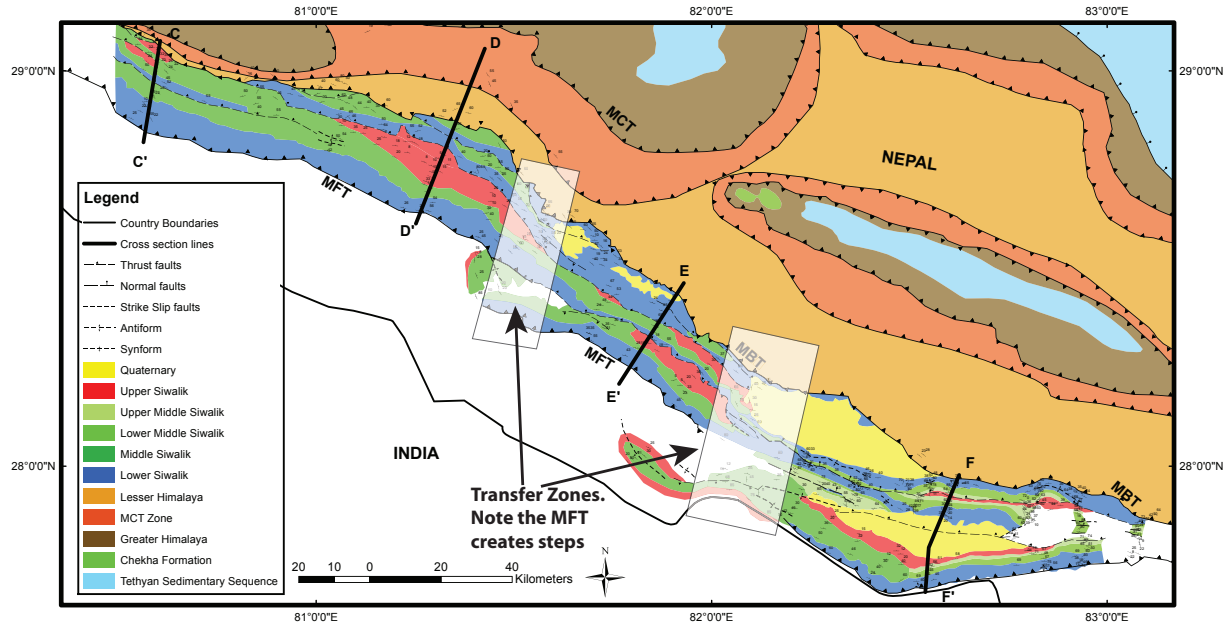


**Figure 4.5 - Transfer Zones in Western Nepal, highlighted with transparent boxes. There is a distinct shift in the major faults to the south within the transfer zones. These zones may accommodate shortening, and account for differences in shortening. Transfer zones modified from Mugnier et al. (1999a) and structural data from Mugnier et al. (1999b), in western Nepal, Ojha, (personal communication, 2012), and McQuarrie et al. (2008).**

There is a distinct difference in the shortening and strain rates between eastern Nepal and Bhutan. In Sikkim and western Bhutan there is a number of seismically active strike slip faults in Sikkim (De and Kayal, 2004). These strike slip faults may act as a transfer zones and allow for a step like difference in strain and shortening rates between eastern Nepal and Bhutan. Further field-work will have to be completed to conclude if there is a correlation between strike slip faults and differences in strain and shortening rates.

The Shillong Plateau is another structure under investigation. The Shillong Plateau is a pop up structure in front of the eastern Himalaya (Biswas et al., 2007). The Shillong Plateau, accommodates some of the convergence of the Indian plate. In this thesis it has been demonstrated that there is a constant west-to-east increasing

gradient of strain rates in the foreland belt, thus we can conclude the foreland belt shortening and strain rates are independent from the Shillong Plateau.

#### 4.5. CORRELATION TO PLATE STRAIN RATES

The strain rates of the convergence of the Indian plate correlate extremely well to the cross section strain rates. The Indian plate strain rates were calculated from Molnar and Stocks (2009) plate convergence rate. The strain was calculated using a generic 200 km thick lithosphere value (Fossen, 2010).

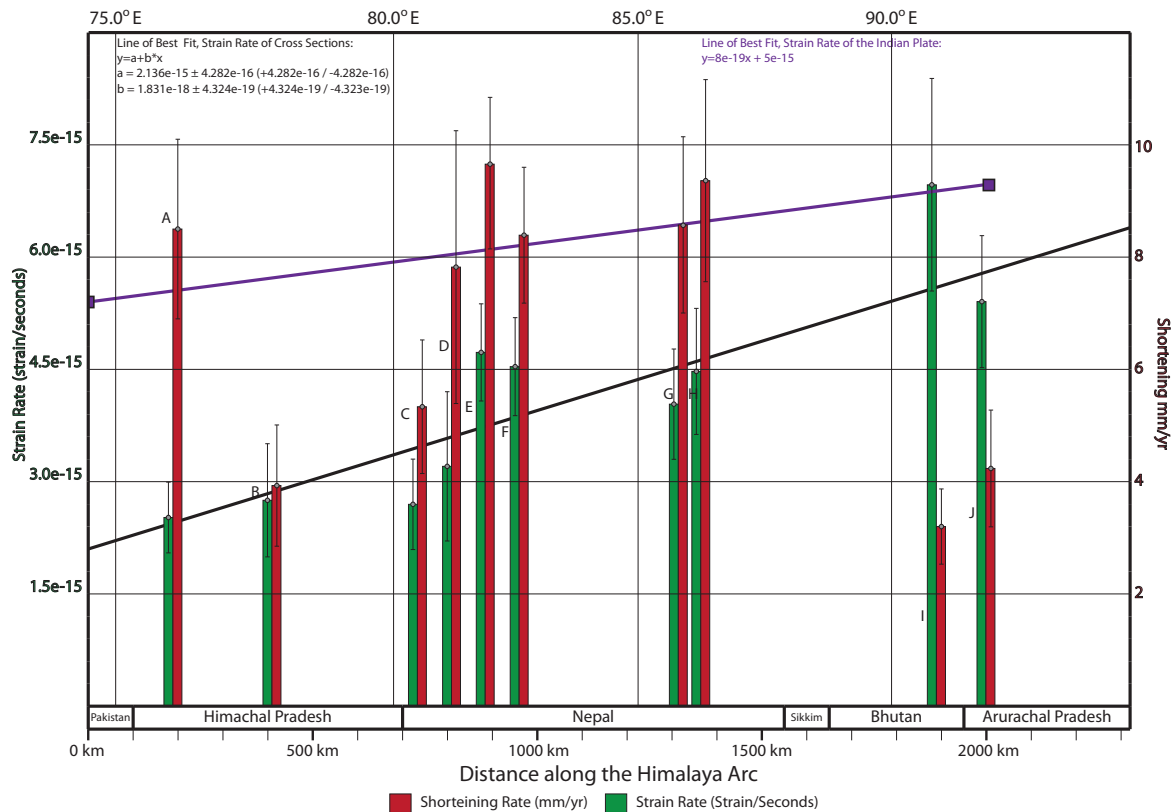


**Figure 4.6 – Graph of shortening rate shortening and strain rate of the Siwalik Group and the Indian plate strain rate vs. distance along the Himalaya arc. There is an evident correlation of a west-to-east increase both in strain rate of the Siwalik Group and the strain rate of the Indian plate. The black line is the line of best fit for the strain rate of the Sub-Himalaya, and the purple line is the line of best fit for strain rate of the Indian plate. The Indian plate strain rates are from Molnar and Stock (2009).**

#### 4.6. CORRELATION TO THE SHORTENING ACROSS THE LHS.

The total shortening in the Sub-Himalaya as determined in this thesis is small compared to the shortening estimated in the LHS. Several authors have constructed balanced cross-sections across the Himalayan orogen. Many of these however do not meet the minimum requirement for balanced cross-sections, in particular when attempting to construct them for the metamorphic core of the Himalaya, the GHS. Short discussion on this can be found in Fossen et al., (2010). For these reasons I have extracted only the estimates of shortening across the LHS and along the MBT excluding the displacement along the MCT and any higher unit or structure.

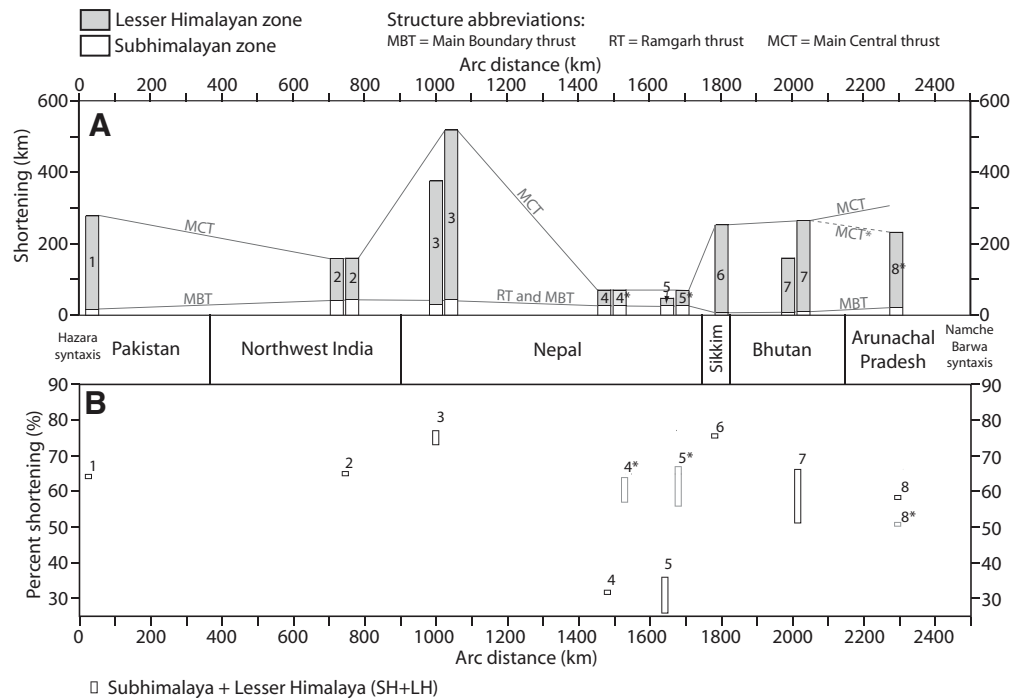


Figure 4.7 - Compilations of shortening estimates from west-to-east across the Himalayan arc modified from (Long et al., 2011a). (A) The total amount of shortening within the sections. The numbers of the sections correlate to the sections in table 4.1. The MBT and MCT are shown on the figure and where they lie within the sections. (B) Compilation of Percent shortening ranges across the Himalayan arc. The numbers correspond to the section in table 4.1.

**Table 4.1 - Compilation of shortening estimates in the Sub-Himalaya and Lesser Himalaya modified from (Long et al., 2011a). Abbreviations SH – Sub-Himalaya, LH- Lesser Himalaya. Section can be seen in the figure above, with respective locations.**

**\*Calculated by adding 122-193 km shortening to LH zone**

**\*\* Calculated by subtracting 75 km shortening from LH zone**

Section Number	Section Location	Shortening SH+LH (km)	Shortening SH+LH (%)	Reference
1	Pakistan	288	64	(Coward and Butler, 1985)
2	India, Kumaon and Garhwal	160	65	(Srivastava and Mitra, 1994)
3	Western Nepal	378-517	74-77	(Robinson et al., 2006)
4	East-central Nepal	73	32	(Schelling, 1992)
4*	East-central Nepal	73	57-64	(Schelling, 1992)
5	Eastern Nepal	50	26-36	(Schelling and Arita, 1991)
5*	Eastern Nepal	70	56-67	(Schelling and Arita, 1991)
6	Sikkim	255	76	(Mitra et al., 2010)
7	Central and eastern Bhutan	160-263	52-66	(Long et al., 2011a)
8	Western Arunachal Pradesh	-	58	(Yin et al., 2010)
8**	Western Arunachal Pradesh	232	51	(Yin et al., 2010)

The pattern of total shortening and the % shortening is not clear. The reasons may be multiple, and may include: the differences in construction of balanced cross-sections between about dozen geologists, high uncertainties in structures within the LHS and uncertainties in the position of the basal detachment.

## **5. CONCLUSIONS AND RECOMMENDATIONS**

### **5.1. CONCLUSIONS**

The shortening amount, shortening rate and strain rate vary along the Himalaya arc in the Sub-Himalaya Group. Due to the differences in the formation length in the balanced sections and the onset of the deformation, strain rate had to be used for a comparative analysis. The strain rates correlate very well with the west-to-east increasing gradient of convergence rates, both with long-term plate reconstruction data, and with GPS data (Molnar and Stock, 2009; Banerjee et al., 2008) suggesting that the plate convergence rate is a primary factor controlling the shortening within the orogenic foreland fold-and-thrust belt.

These strain rates also correlate to the west-to-east increasing gradient of rainfall and inversely correlate to wedge width. According to the critical taper model, greater shortening of the wedge will occur where more erosion is taking place.

It is safe to say rainfall has an impact on the strain rates and wedge width of the Sub-Himalaya. Furthermore, the variation in strain rates along the Sub-Himalaya show the same trend as plate velocities and plate strain rates.

### **5.2. RECOMMENDATIONS AND FURTHER WORK**

This work has identified along strike changes in convergence and strain rates and wedge shape in the Sub-Himalaya of the Himalayan orogen. There is a clear correlation between the structural data and the long-term and short-term plate convergence rates

as well with the precipitation rates. However, the causative relationships could not be determined. In order to tackle the questions opened in this thesis it is recommended to fill in the gaps in the data and undertake numerical modeling. Further work may include:

- Detailed stratigraphic sections at all cross-section transects, including updated stratigraphic ages for sections with poor Upper/Middle Siwaliks boundary ages.
- Gaps to be filled in along the Sub-Himalaya. Identify the segments of the Sub-Himalaya where this would be possible according to the exposure of the Siwaliks and identify logistic feasibility.
- Obtain seismic data to constrain the depth and dip of the décollement as well as identify structures, both shortening structures and basement structures.
- Perform forward modeling to quantitatively estimate the sensitivity of the models to the two principal parameters, erosion and convergence rate.
- Construct a fence diagram like model of the fold-and-thrust belt using multiple cross-sections and seismic lines.

## 6. REFERENCES

- Avouac, J.P., 2003, Mountain building, erosion, and the seismic cycle in the Nepal Himalaya: *Advances in Geophysics*, v. 46, p. 1–80.
- Banerjee, P., Bürgmann, R., Nagarajan, B., and Apel, E., 2008, Intraplate deformation of the Indian subcontinent: *Geophysical Research Letters*, v. 35, no. 18, p. L18301, doi: 10.1029/2008GL035468.
- Barcilon, V., 1987, A note on “Noncohesive critical Coulomb wedges: An exact solution” by F. A. Dahlen: *Journal of Geophysical Research*, v. 92, no. B5, p. 3681, doi: 10.1029/JB092iB05p03681.
- Barr, T.D., and Dahlen, F.A., 1989, Brittle frictional mountain building: 2. Thermal structure and heat budget: *Journal of Geophysical Research*, v. 94, no. B4, p. 3923–3947, doi: 10.1029/JB094iB04p03923.
- Beaumont, C., 1981, Foreland basins: *Geophysical Journal of the Royal Astronomical Society*, v. 65, no. 2, p. 291–329.
- Bernet, M., van der Beek, P., Pik, R., Huyghe, P., Mugnier, J.-L., Labrin, E., and Szulc, A., 2006, Miocene to Recent exhumation of the central Himalaya determined from combined detrital zircon fission-track and U/Pb analysis of Siwalik sediments, western Nepal: *Basin Research*, v. 18, no. 4, p. 393–412, doi: 10.1111/j.1365-2117.2006.00303.x.
- Bilham, R., and England, P., 2001, Plateau Pop-up during the 1897 Assam earthquake: *Nature*, v. 410, p. 806–809.
- Bilham, R., Bendick, R., and Wallace, K., 2003, Flexure of the Indian plate and intraplate earthquakes: *Journal of Earth System Science*, v. 112, no. 3, p. 315–329.
- Biswas, S., Coutand, I., Grujic, D., Hager, C., Stöckli, D., and Grasemann, B., 2007, Exhumation and uplift of the Shillong plateau and its influence on the eastern Himalayas: New constraints from apatite and zircon (U-Th-[Sm])/He and apatite fission track analyses: *Tectonics*, v. 26, no. 6, p. TC6013, doi: 10.1029/2007TC002125.
- Bookhagen, B., and Burbank, D.W., 2010, Toward a complete Himalayan hydrological budget: Spatiotemporal distribution of snowmelt and rainfall and their impact on river discharge: *Journal of Geophysical Research*, v. 115, no. F3, p. F03019, doi: 10.1029/2009JF001426.

- Chakraborty, T., and Ghosh, P., 2010, The geomorphology and sedimentology of the Tista megafan, Darjeeling Himalaya: Implications for megafan building processes: *Geomorphology*, v. 115, no. 3-4, p. 252–266, doi: 10.1016/j.geomorph.2009.06.035.
- Chirouze, F., Huyghe, P., van der Beek, P., Chauvel, C., Chakraborty, T., Dupont-Nivet, G., and Bernet, M., 2012a, Tectonics, exhumation, and drainage evolution of the eastern Himalaya since 13 Ma from detrital geochemistry and thermochronology, Kameng River Section, Arunachal Pradesh: *Geological Society of America Bulletin*, doi: 10.1130/B30697.1.
- Chirouze, F.O., Dupont-Nivet, G., Huyghe, P., van der Beek, P., Chakraborti, T., Bernet, M., and Erens, V., 2012b, Magnetostratigraphy of the Neogene Siwalik Group in the far eastern Himalaya: Kameng section, Arunachal Pradesh, India: *Journal of Asian Earth Sciences*, v. 44, no. C, p. 117–135, doi: 10.1016/j.jseaes.2011.05.016.
- Clark, M.K., and Bilham, R., 2008, Miocene rise of the Shillong Plateau and the beginning of the end for the Eastern Himalaya: *Earth and Planetary Science Letters*, v. 269, no. 3, p. 337–351.
- Coward, M.P., and Butler, R., 1985, Thrust tectonics and the deep structure of the Pakistan Himalaya: *Geology*, v. 13, no. 6, p. 417–420.
- Dahlen, F.A., 1990, Critical taper model of fold-and-thrust belts and accretionary wedges: *Annual Review of Earth and Planetary Sciences*, v. 18, p. 55. Dahlen, F.A., 1984, Noncohesive critical Coulomb wedges: An exact solution: *Journal of Geophysical Research*, v. 89, no. B12, p. 10125–10,133
- Dahlen, F.A., and Barr, T.D., 1989, Brittle frictional mountain building: 1. Deformation and mechanical energy budget: *Journal of Geophysical Research*, v. 94, no. B4, p. 3906, doi: 10.1029/JB094iB04p03906.
- Dahlen, F.A., and Suppe, J., 1988, Mechanics, growth and erosion of mountain belts: *Geological Society of America Special Paper*, no. 218, p. 161–178.
- Dahlen, F.A., Suppe, J., and Davis, D., 1984, Mechanics of fold-and-thrust belts and accretionary wedges: Cohesive Coulomb theory: *Journal of Geophysical Research*, v. 89, no. B12, p. 10087–10–101.
- Davis, D., Suppe, J., and Dahlen, F.A., 1983, Mechanics of fold-and-thrust belts and accretionary wedges: *Journal of Geophysical Research*, v. 88, no. B2, p. 1153–1172. De, R., and Kayal, J.R., 2004, Seismic activity at the MCT in Sikkim Himalaya: *Tectonophysics*, v. 386, no. 3-4, p. 243–248, doi: 10.1016/j.tecto.2004.06.013.
- Fossen, H., 2010, *Structural Geology*: Cambridge University Press, New York, NY, USA.



- Gan, W., Zhang, P., Shen, Z.-K., Niu, Z., Wang, M., Wan, Y., Zhou, D., and Cheng, J., 2007, Present-day crustal motion within the Tibetan Plateau inferred from GPS measurements: *J Geophys Res*, v. 112, no. B8, p. B08416, doi: 10.1029/2005JB004120.
- Godin, L., Grujic, D., Law, R.D., and Searle, M.P., 2006, Channel flow, ductile extrusion and exhumation in continental collision zones: an introduction: Geological Society, London, Special Publications, v. 268, no. 1, p. 1–23, doi: 10.1144/GSL.SP.2006.268.01.01.
- Grujic, D., Coutand, I., Bookhagen, B., Bonnet, S., Blythe, A., and Duncan, C., 2006, Climatic forcing of erosion, landscape, and tectonics in the Bhutan Himalayas: *Geology*, v. 34, no. 10, p. 801, doi: 10.1130/G22648.1.
- Hodges, K., 2006, Climate and the Evolution of Mountains: *Scientific American*, v. 295, no. 2, p. 72–79, doi: 10.1038/scientificamerican0806-72.
- Hodges, K.V., 2000, Tectonics of the Himalaya and southern Tibet from two perspectives: *Geological Society of America Bulletin*, v. 112, no. 3, p. 324–350.
- Husson, L., Mugnier, J.L., Leturmy, P., and Vidal, G., 2004, Kinematics and sedimentary balance of the Sub-Himalayan zone, western Nepal: Thrust Tectonics and hydrocarbon systems: *AAPG Memoir*, v. 82, p. 115–130.
- Judge, P.A., and Allmendinger, R.W., 2011, Assessing uncertainties in balanced cross-sections: *Journal of Structural Geology*, v. 33, no. 4, p. 458–467.
- Lehner, F.K., 1986, Comments on “Noncohesive critical Coulomb wedges: An exact solution” by F. A. Dahlen: *Journal of Geophysical Research*, v. 91, no. B1, p. 793–796, doi: 10.1029/JB091iB01p00793.
- Long, S., McQuarrie, N., Tobgay, T., and Grujic, D., 2011a, Geometry and crustal shortening of the Himalayan fold-thrust belt, eastern and central Bhutan: *Geological Society of America Bulletin*, v. 123, no. 7-8, p. 1427–1447, doi: 10.1130/B30203.1.
- Long, S., McQuarrie, N., Tobgay, T., Rose, C., Gehrels, G., and Grujic, D., 2011b, Tectonostratigraphy of the Lesser Himalaya of Bhutan: Implications for the along-strike stratigraphic continuity of the northern Indian margin: *Geological Society of America Bulletin*, v. 123, no. 7-8, p. 1406–1426, doi: 10.1130/B30202.1.
- McQuarrie, N., Robinson, D., Long, S., Tobgay, T., Grujic, D., Gehrels, G., and Ducea, M., 2008, Preliminary stratigraphic and structural architecture of Bhutan: Implications for the along strike architecture of the Himalayan system: *Earth and Planetary Science Letters*, v. 272, no. 1-2, p. 105–117, doi: 10.1016/j.epsl.2008.04.030.

- Mitra, G., Bhattacharyya, K., and Mukul, M., 2010, The Lesser Himalayan duplex in Sikkim: Implications for variations in Himalayan shortening: *Journal of the Geological Society of India*, v. 75, no. 1, p. 289–301.
- Molnar, P., 1987, Inversion of profiles of uplift rates for the geometry of dip-slip faults at depth, with examples from the Alps and the Himalaya: *Ann. Geophys.*, v. 5, p. 663–670.
- Molnar, P., and Stock, J.M., 2009, Slowing of India's convergence with Eurasia since 20 Ma and its implications for Tibetan mantle dynamics: *Tectonics*, v. 28, no. 3, p. TC3001, doi: 10.1029/2008TC002271.
- Molnar, P., and Stock, J.M., 2009, Slowing of India's convergence with Eurasia since 20 Ma and its implications for Tibetan mantle dynamics: *Tectonics*, v. 28, no. 3, p. TC3001, doi: 10.1029/2008TC002271.
- Mugnier, J.-L., and Huyghe, P., 2006, Ganges basin geometry records a pre-15 Ma isostatic rebound of Himalaya: *Geology*, v. 34, no. 6, p. 445, doi: 10.1130/G22089.1.
- Mugnier, J.L., Leturmy, P., Huyghe, P., and Chalaron, E., 1999a, The Siwaliks of western Nepal: II. Mechanics of the thrust wedge: *Journal of Asian Earth Sciences*, v. 17, no. 5, p. 643–657.
- Mugnier, J.L., Leturmy, P., Mascle, G., Huyghe, P., Chalaron, E., Vidal, G., Husson, L., and Delcaillau, B., 1999b, The Siwaliks of western Nepal: I. Geometry and kinematics: *Journal of Asian Earth Sciences*, v. 17, no. 5, p. 629–642.
- Najman, Y., Carter, A., Oliver, G., and Garzanti, E., 2005, Provenance of Eocene foreland basin sediments, Nepal: Constraints to the timing and diachroneity of early Himalayan orogenesis: *Geology*, v. 33, no. 4, p. 309–312.
- Najman, Y., Clift, P., Johnson, M.R.W., and Robertson, A.H.F., 1993, Early stages of foreland basin evolution in the Lesser Himalaya, N India: *Geological Society, London, Special Publications*, v. 74, no. 1, p. 541–558, doi: 10.1144/GSL.SP.1993.074.01.36.
- Ojha, T.P., Butler, R.F., DeCelles, P.G., and Quade, J., 2009, Magnetic polarity stratigraphy of the Neogene foreland basin deposits of Nepal: *Basin Research*, v. 21, no. 1, p. 61–90, doi: 10.1111/j.1365-2117.2008.00374.x.
- Ojha, T.P., Butler, R.F., Quade, J., and DeCelles, P.G., 2004, Magnetic polarity stratigraphy of Siwalik Group sediments in Nepal: Diachronous lithostratigraphy and isochronous carbon isotope shift: *Himalayan Journal of Sciences*, v. 2, no. 4, p. 213, doi: 10.3126/hjs.v2i4.906.
- Ojha, T.P., Butler, R.F., Quade, J., DeCelles, P.G., Richards, D., and Upreti, B.N., 2000, Magnetic polarity stratigraphy of the Neogene Siwalik Group at Khutia Khola, far western Nepal: *Geological Society of America Bulletin*, v. 112, no. 3, p. 424–434.

- Powers, P.M., Lillie, R.J., and Yeats, R.S., 1998, Structure and shortening of the Kangra and Dehra Dun reentrants, sub-Himalaya, India: *Geological Society of America Bulletin*, v. 110, no. 8, p. 1010–1027.
- Quade, J., Cater, J.M.L., Ojha, T.P., Adam, J., and Harrison, T.M., 1995, Late Miocene environmental change in Nepal and the northern Indian subcontinent: Stable isotopic evidence from paleosols: *Geological Society of America Bulletin*, v. 107, no. 12, p. 1381–1397.
- Robinson, D.M., DeCelles, P.G., and Copeland, P., 2006, Tectonic evolution of the Himalayan thrust belt in western Nepal: Implications for channel flow models: *Geological Society of America Bulletin*, v. 118, no. 7-8, p. 865–885, doi: 10.1130/B25911.1.
- Robinson, D.M., DeCelles, P.G., Patchett, P.J., and Garzzone, C.N., 2001, The kinematic evolution of the Nepalese Himalaya interpreted from Nd isotopes: *Earth and Planetary Science Letters*, v. 192, no. 4, p. 507–521.
- Sanyal, P., Bhattacharya, S.K., Kumar, R., Ghosh, S.K., and Sangode, S.J., 2004, Mio–Pliocene monsoonal record from Himalayan foreland basin (Indian Siwalik) and its relation to vegetational change: *Palaeogeography, Palaeoclimatology, Palaeoecology*, v. 205, no. 1-2, p. 23–41, doi: 10.1016/j.palaeo.2003.11.013.
- Schelling, D., 1992, The tectonostratigraphy and structure of the eastern Nepal Himalaya: *Tectonics*, v. 11, no. 5, p. 925–943.
- Schelling, D., and Arita, K., 1991, Thrust tectonics, crustal shortening, and the structure of the far-eastern Nepal Himalaya: *Tectonics*, v. 10, no. 5, p. 851–862.
- Srivastava, P., and Mitra, G., 1994, Thrust geometries and deep structure of the outer and lesser Himalaya, Kumaon and Garhwal (India): implications for evolution of the Himalayan fold-and-thrust belt: *Tectonics*, v. 13, no. 1, p. 89–109.
- van der Beek, P., Robert, X., Mugnier, J.-L., Bernet, M., Huyghe, P., and Labrin, E., 2006, Late Miocene - Recent exhumation of the central Himalaya and recycling in the foreland basin assessed by apatite fission-track thermochronology of Siwalik sediments, Nepal: *Basin Research*, v. 18, no. 4, p. 413–434, doi: 10.1111/j.1365-2117.2006.00305.x.
- Whipple, K.X., 2004, Controls on the strength of coupling among climate, erosion, and deformation in two-sided, frictional orogenic wedges at steady state: *Journal of Geophysical Research*, v. 109, no. F1, p. F01011, doi: 10.1029/2003JF000019.
- Whipple, K.X., 2009, The influence of climate on the tectonic evolution of mountain belts: *Nature Geoscience*, v. 2, no. 2, p. 97–104, doi: 10.1038/ngeo413.

- Woodward, N.B., Boyer, S.E., and Suppe, J., 1989, Balanced geological cross-sections: An essential technique in geological research and exploration: v. 6, p. 132.
- Yin, A., 2006, Cenozoic tectonic evolution of the Himalayan orogen as constrained by along-strike variation of structural geometry, exhumation history, and foreland sedimentation: *Earth-Science Reviews*, v. 76, no. 1-2, p. 1–131, doi: 10.1016/j.earscirev.2005.05.004.
- Yin, A., Dubey, C.S., Webb, A.A.G., Kelty, T.K., Grove, M., Gehrels, G.E., and Burgess, W.P., 2010, Geologic correlation of the Himalayan orogen and Indian craton: Part 1. Structural geology, U-Pb zircon geochronology, and tectonic evolution of the Shillong Plateau and its neighboring regions in NE India: *Geological Society of America Bulletin*, v. 122, no. 3-4, p. 336–359, doi: 10.1130/B26460.1.
- Zhao, W.L., Davis, D.M., Dahlen, F.A., and Suppe, J., 1986, Origin of convex accretionary wedges: Evidence from Barbados: *Journal of Geophysical Research*, v. 91, no. B10, p. 10246–10,258, doi: 10.1029/JB091iB10p10246.

## **APPENDIX**

**THE APPENDIX CONTAINS EDITABLE FULL SIZE PDF IMAGES.**

### **FULL SIZE IMAGES INCLUDE:**

FIGURE 3.5 - LANDSAT GEOCOVER MAP OF THE HIMALAYAN ARC

FIGURE 2.11 - GEOLOGICAL OVERVIEW MAP OF THE HIMALAYA WITH STRATIGRAPHIC SECTION LOCATIONS

FIGURE 2.12 - MAGNETO STRATIGRAPHIC CORRELATION OF THE SIWALIK GROUP ACROSS THE HIMALAYAN ARC

FIGURE 1.1 - GEOLOGICAL OVERVIEW MAP OF THE HIMALAYA

FIGURE 3.6 - GEOLOGICAL OVERVIEW MAP OF THE HIMALAYA

FIGURE 3.7 - GEOLOGICAL MAP OF NORTH WESTERN INDIA (HIMACHAL PRADESH)

FIGURE 3.10 - MAP 2, DETAILED GEOLOGICAL MAP OF THE SIWALIKS FORMATION, WESTERN NEPAL

FIGURE 3.15 - MAP 3, DETAILED GEOLOGICAL MAP OF THE SIWALIKS FORMATION, EASTERN NEPAL

FIGURE 3.18 - MAP 4, DETAILED GEOLOGICAL MAP OF THE SIWALIKS FORMATION, EASTERN BHUTAN

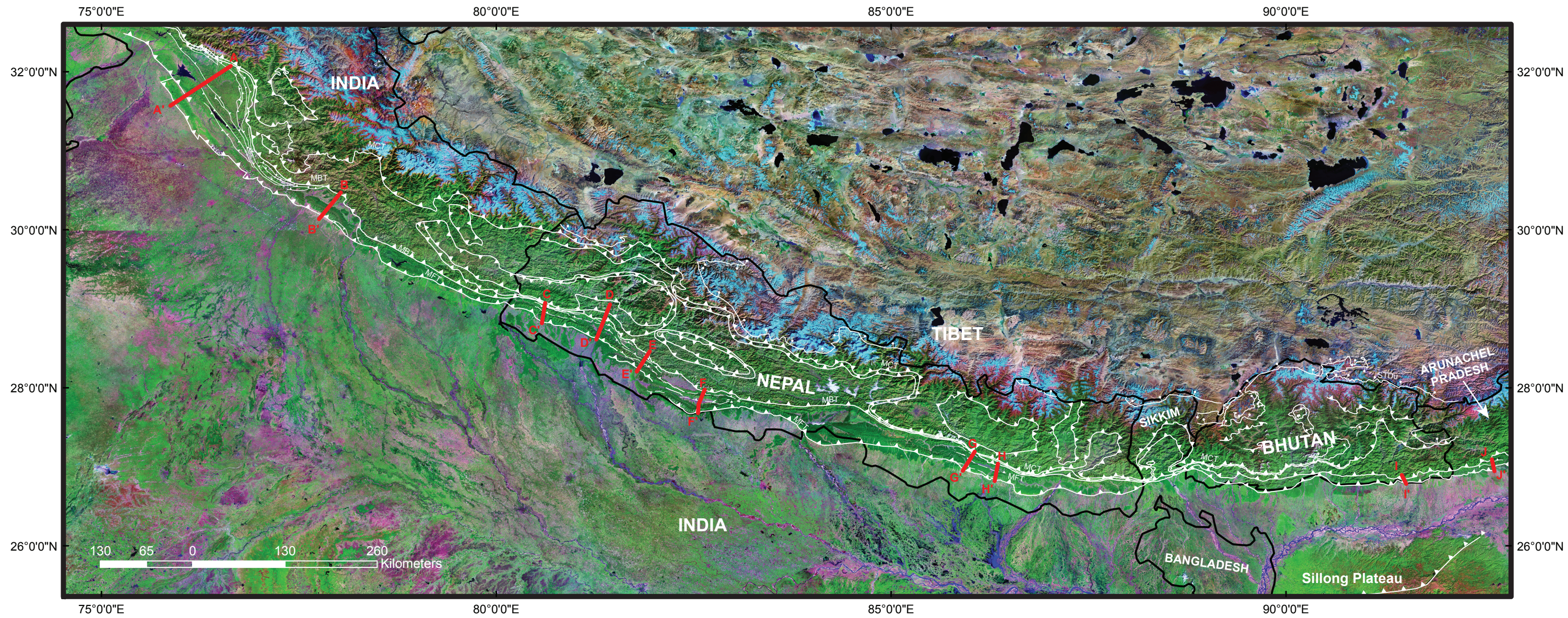
FIGURE 3.20 - MAP 5, DETAILED GEOLOGICAL MAP OF THE SIWALIKS FORMATION, ARUNACHEL PRADESH

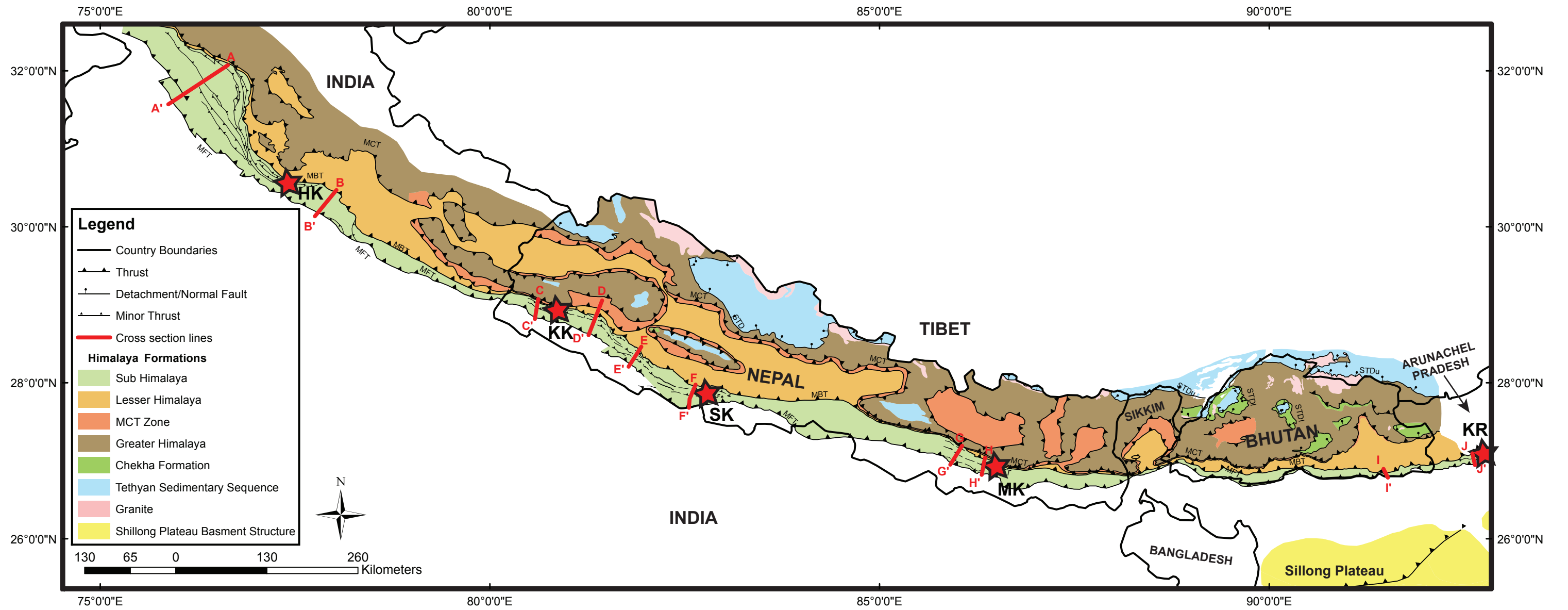
FIGURE 4.2 - MEAN ANNUAL RAINFALL AVERAGED OVER 10 YEARS

FIGURE 4.5 - TRANSFER ZONES IN WESTERN NEPAL, HIGHLIGHTED WITH TRANSPARENT BOXES

### **CROSS-SECTIONS ALL AT THE SAME SCALE**

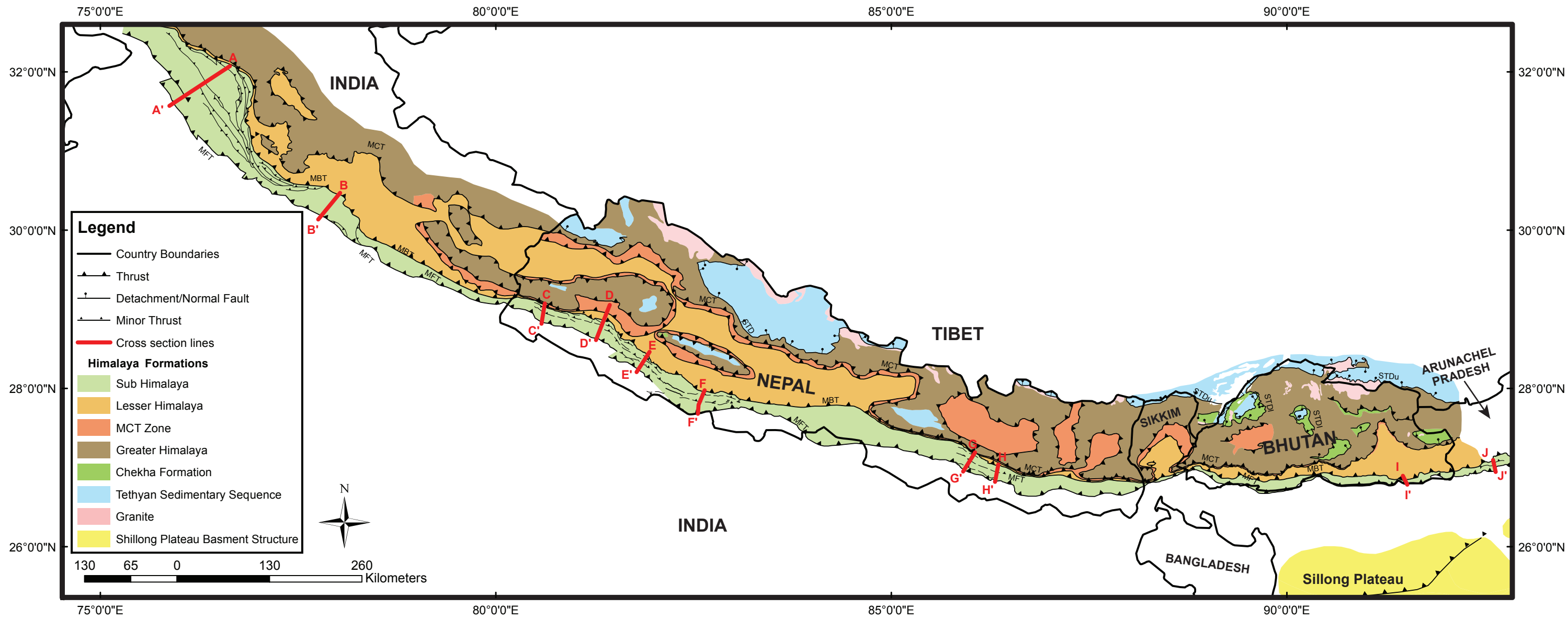
### **FULL PAGE VERSIONS OF RESULTS GRAPHS**

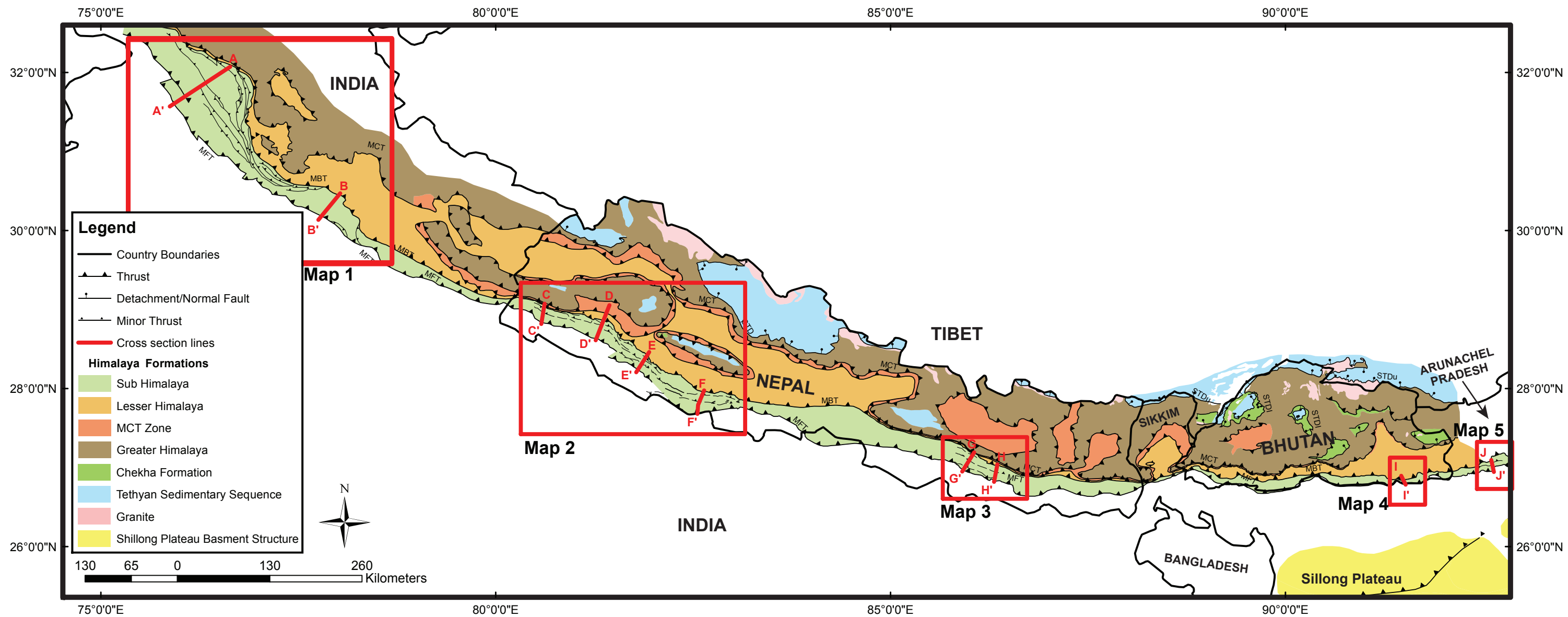


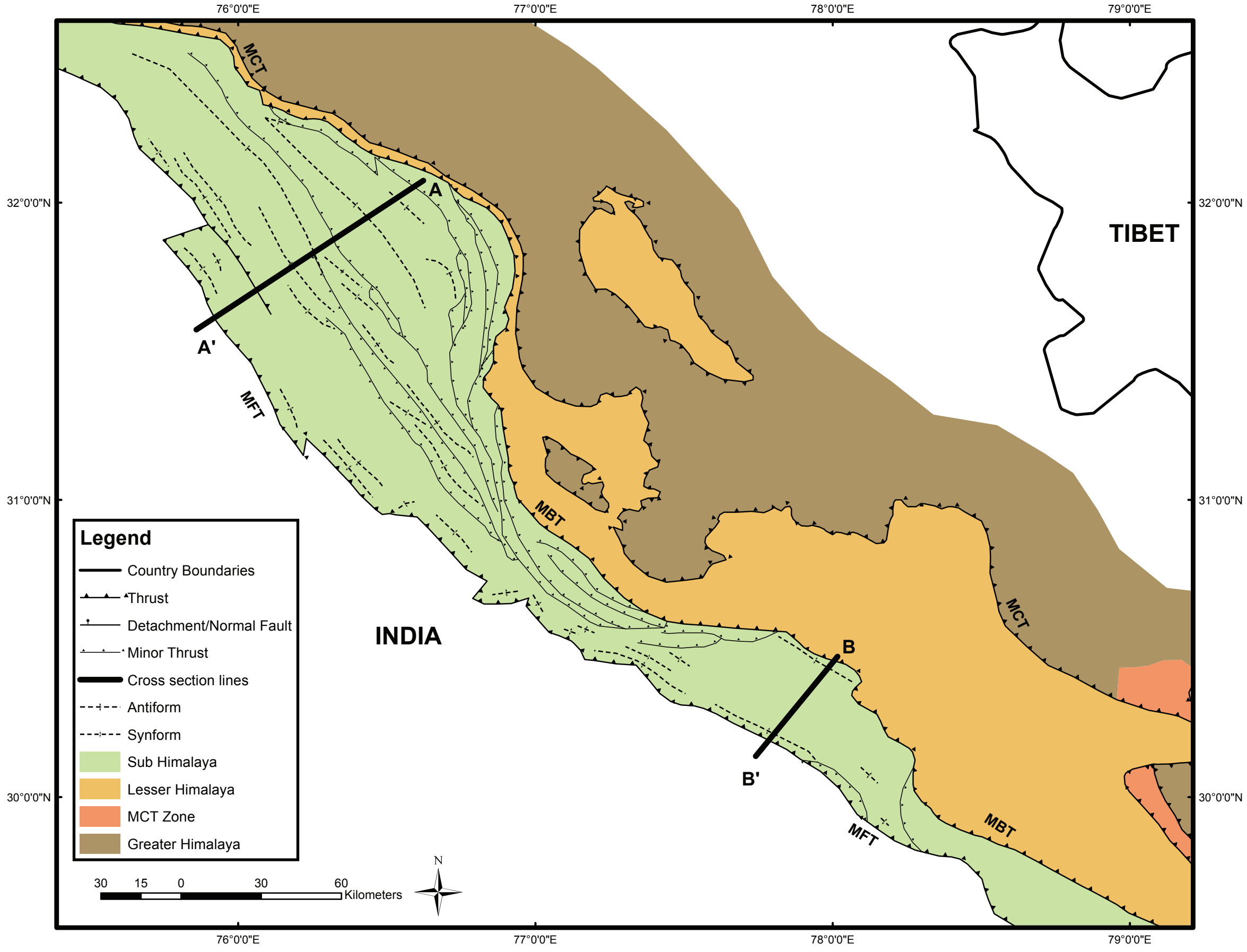


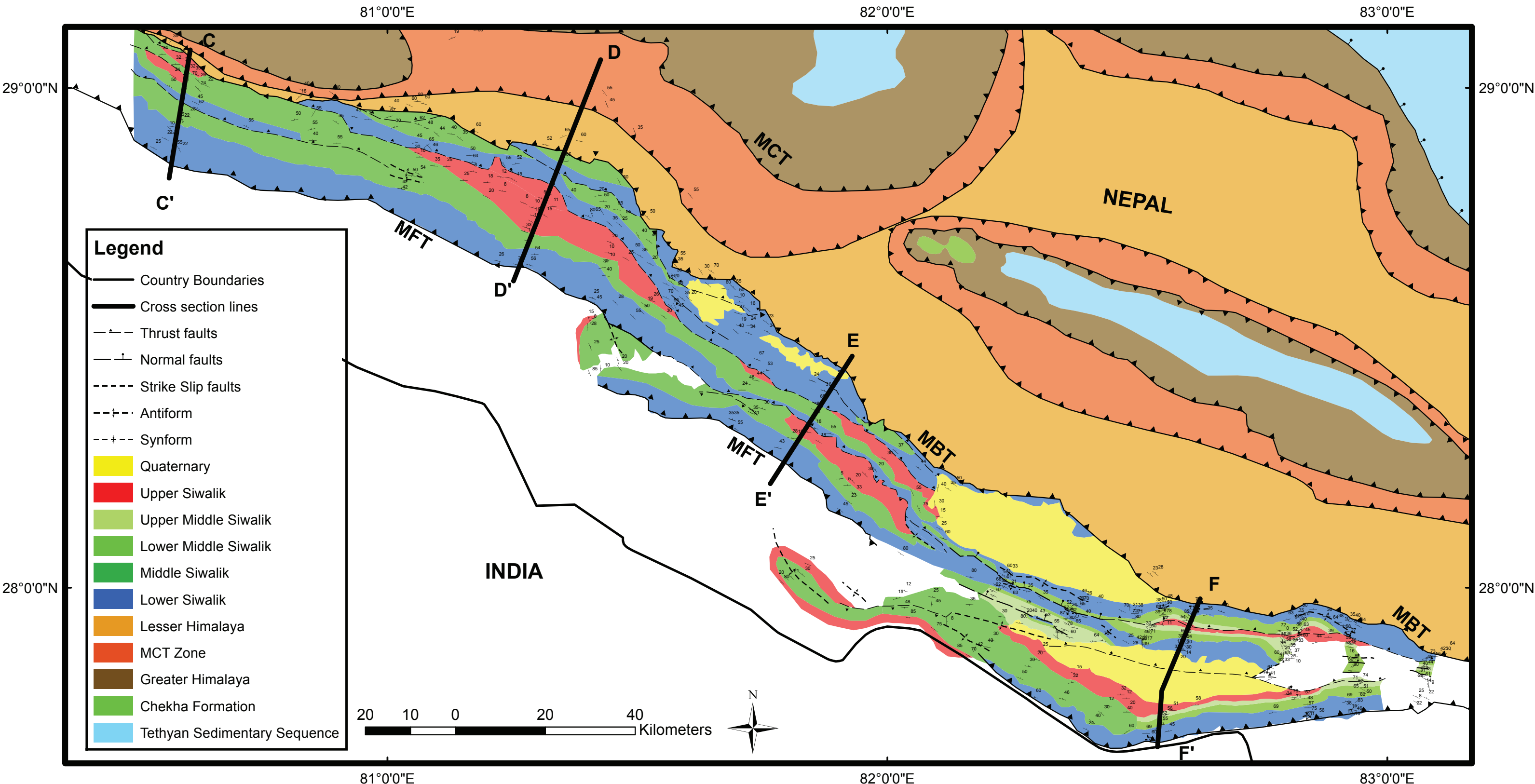






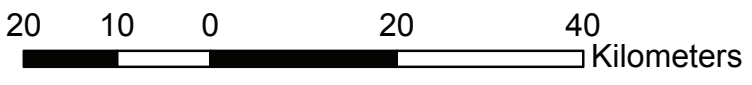


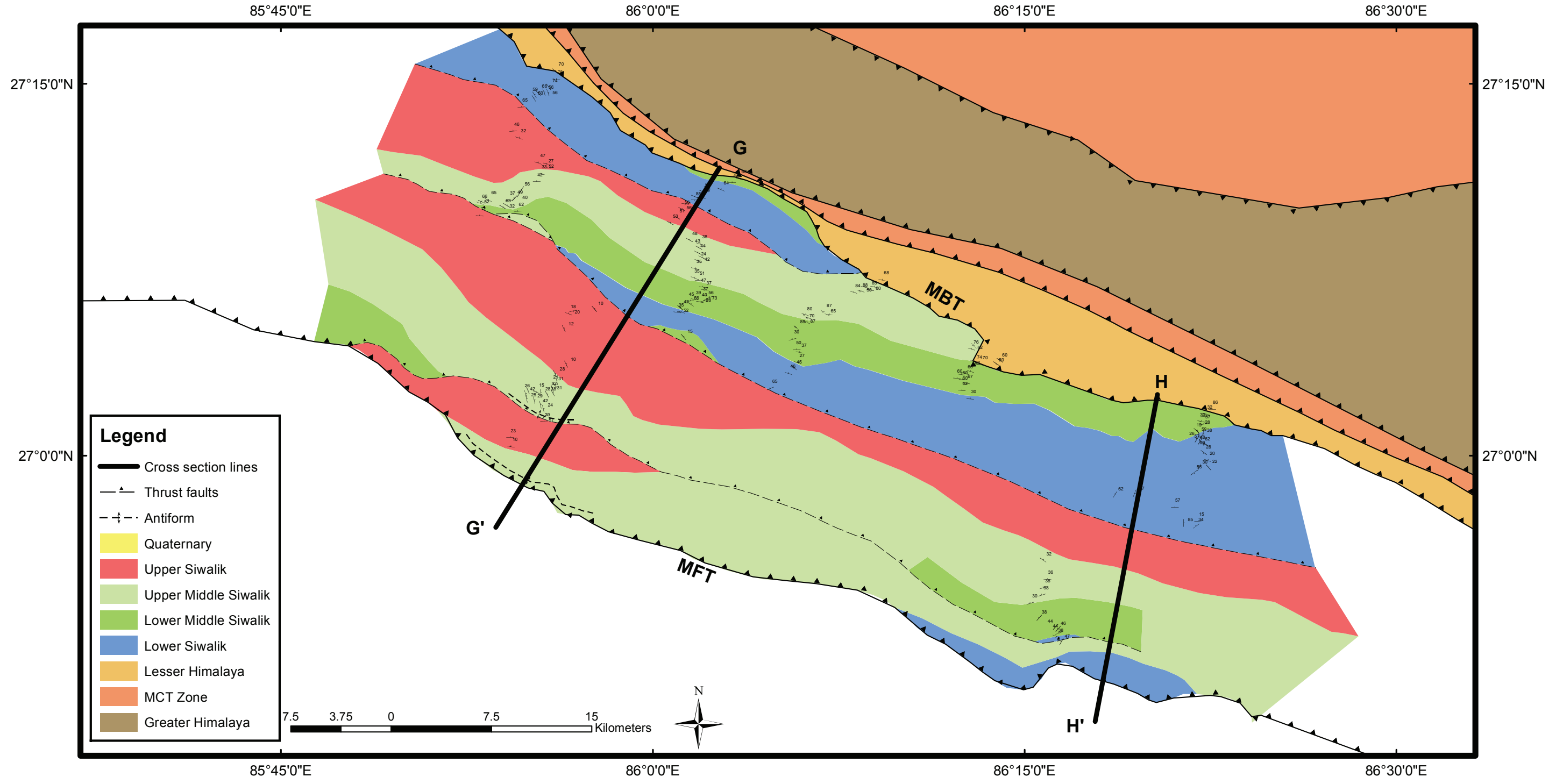




**Legend**

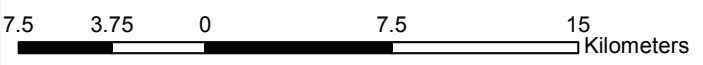
- Country Boundaries
- Cross section lines
- ▲- Thrust faults
- ┴- Normal faults
- - - Strike Slip faults
- + - Antiform
- - + - Synform
- Yellow box: Quaternary
- Red box: Upper Siwalik
- Light green box: Upper Middle Siwalik
- Green box: Lower Middle Siwalik
- Dark green box: Middle Siwalik
- Blue box: Lower Siwalik
- Orange box: Lesser Himalaya
- Dark orange box: MCT Zone
- Brown box: Greater Himalaya
- Light green box: Chekha Formation
- Light blue box: Tethyan Sedimentary Sequence

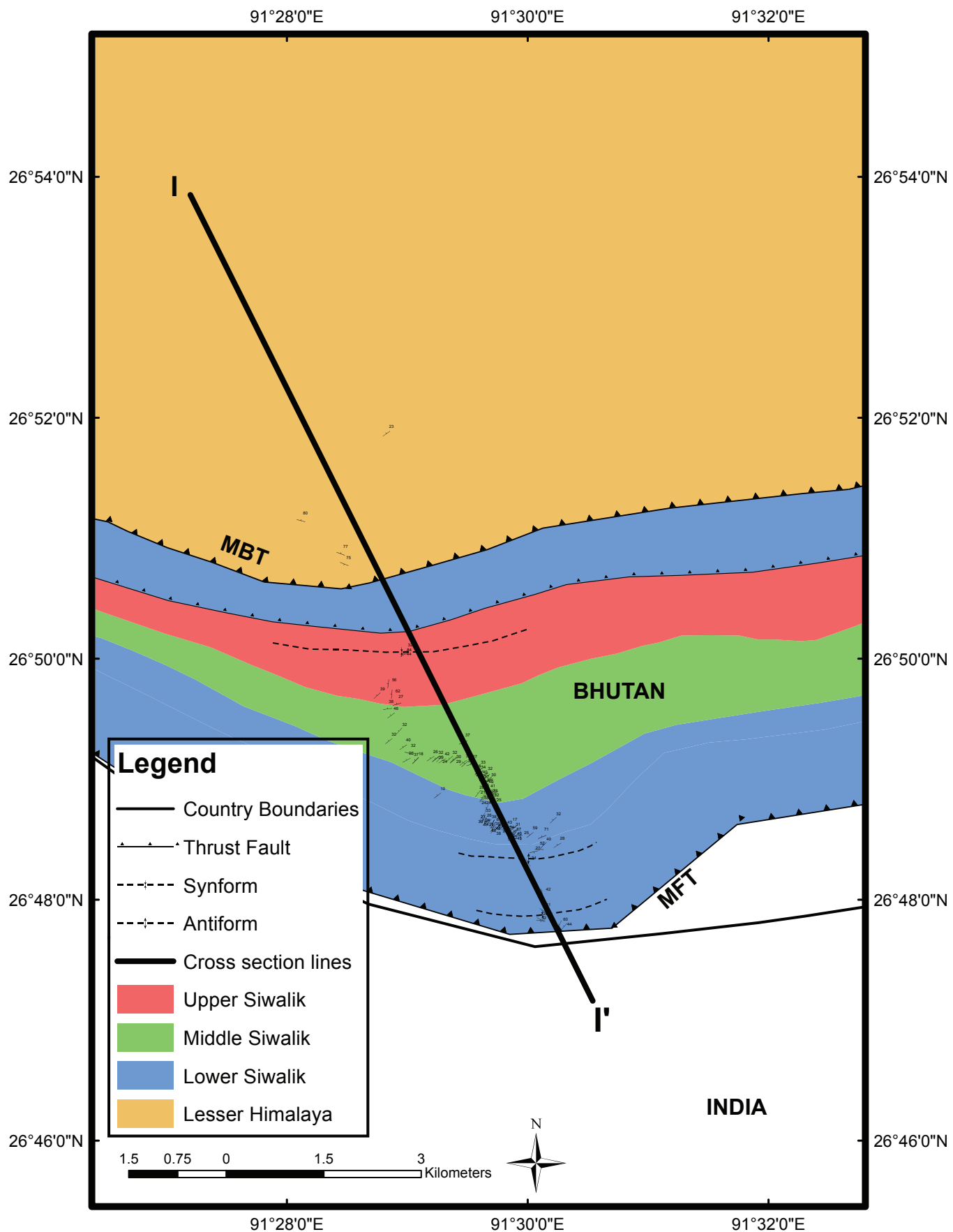


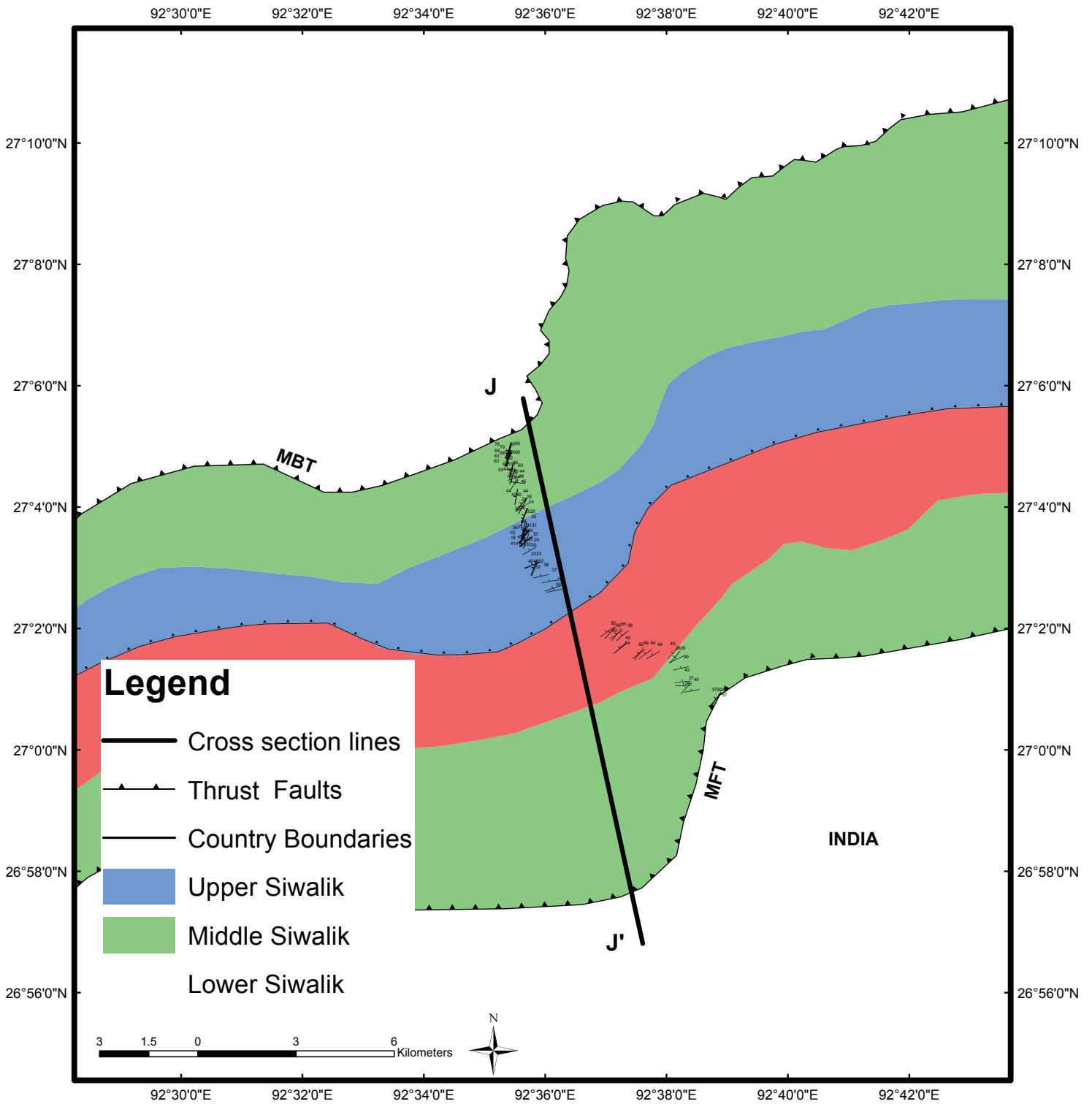


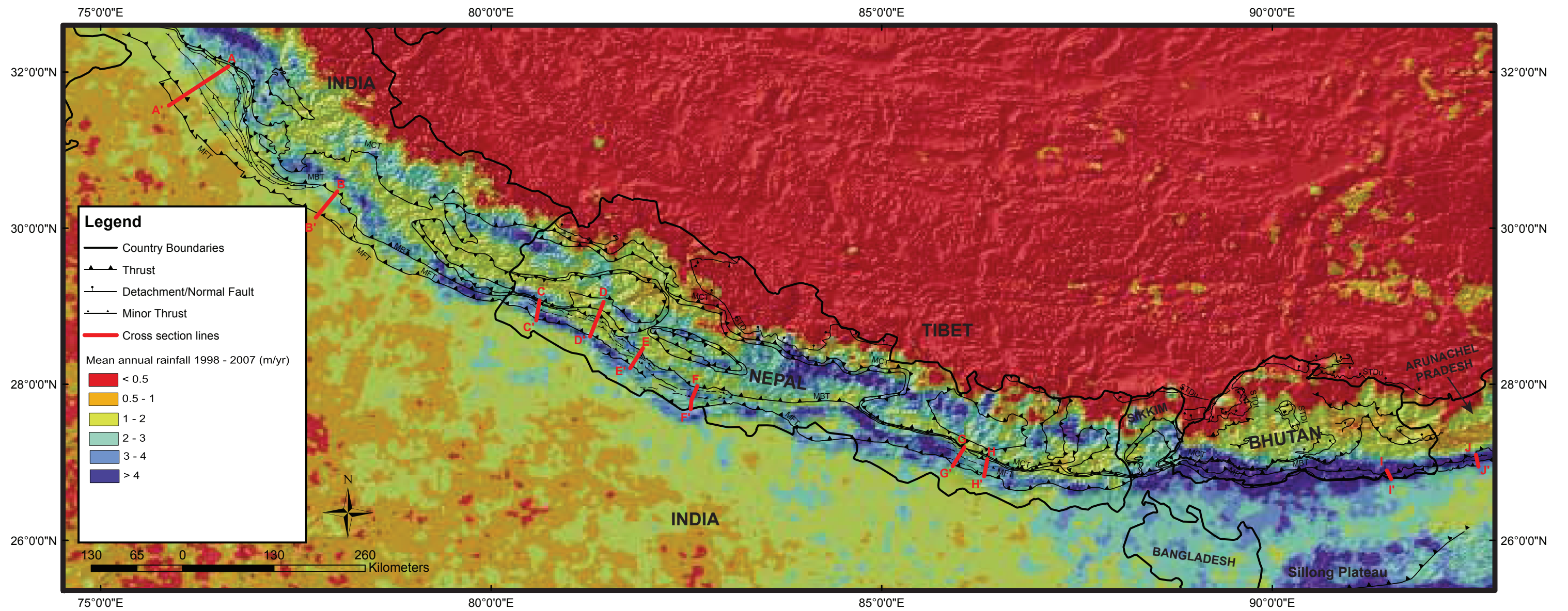
**Legend**

- Cross section lines
- Thrust faults
- Antiform
- Quaternary
- Upper Siwalik
- Upper Middle Siwalik
- Lower Middle Siwalik
- Lower Siwalik
- Lesser Himalaya
- MCT Zone
- Greater Himalaya

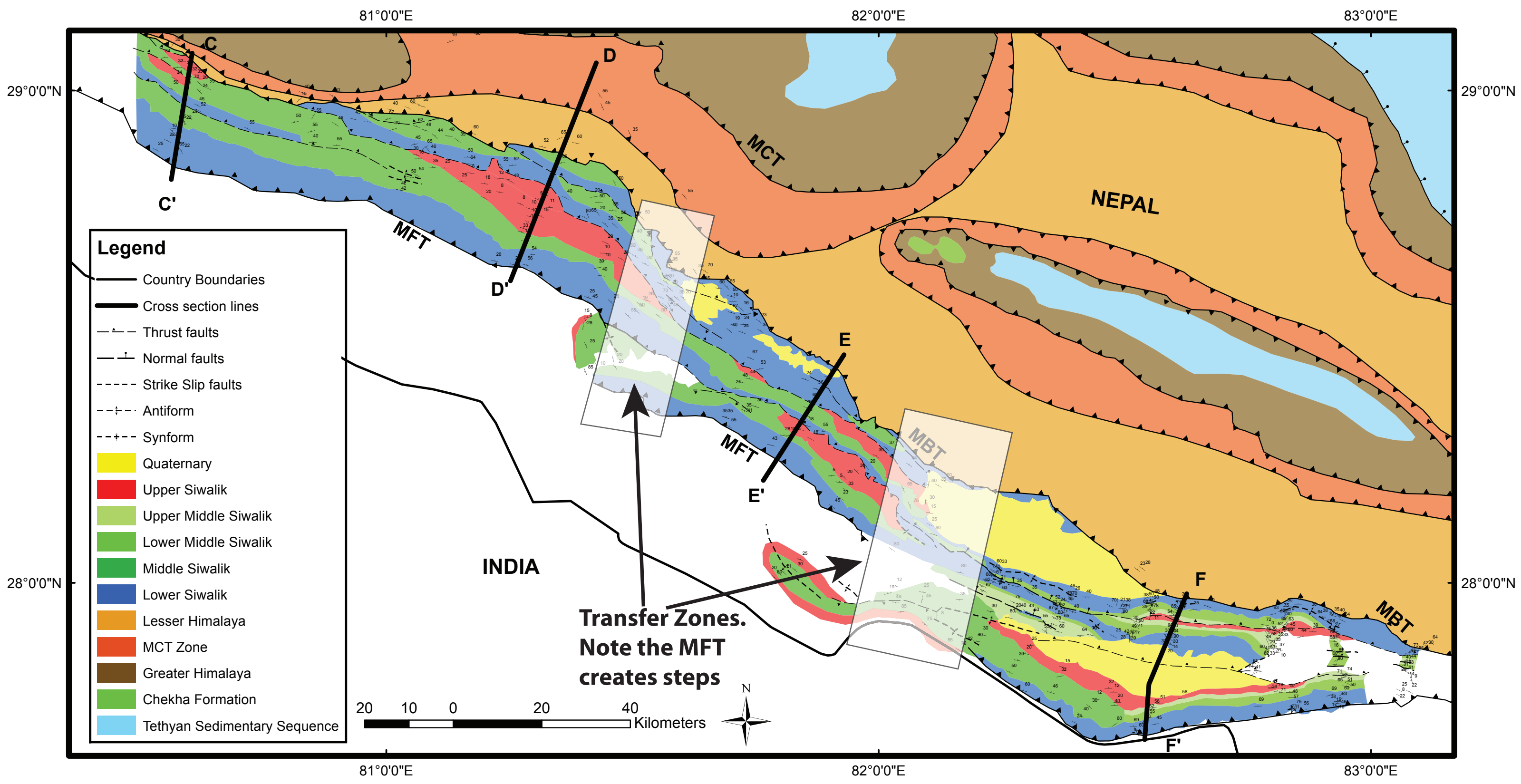








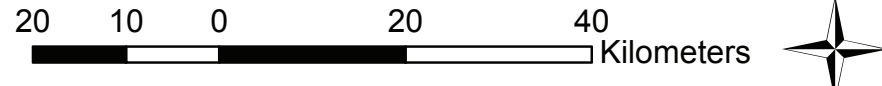


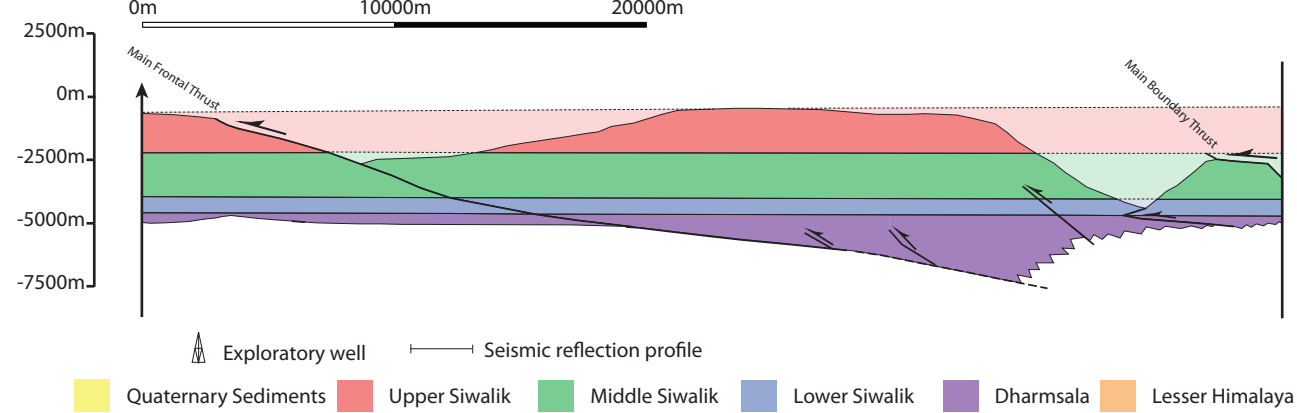
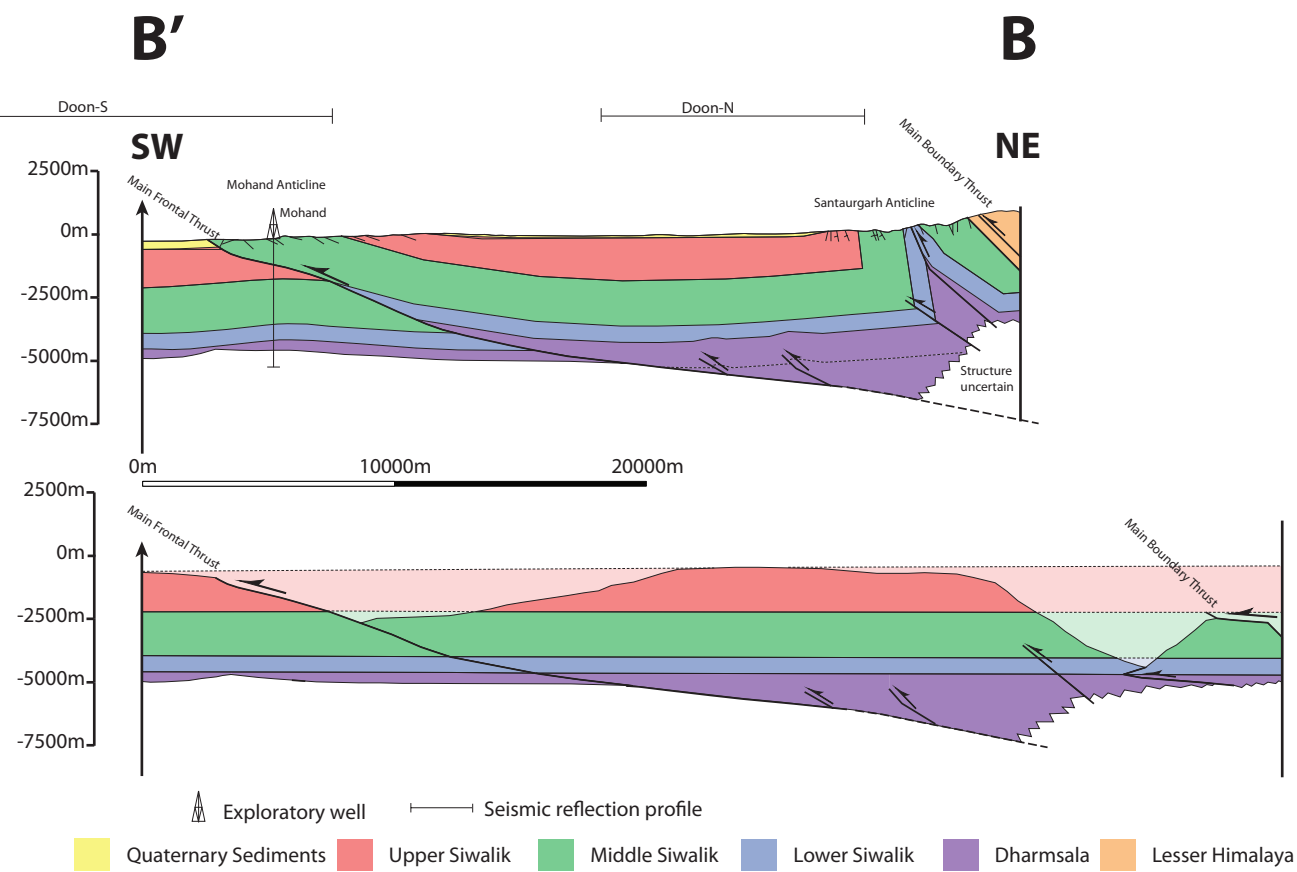
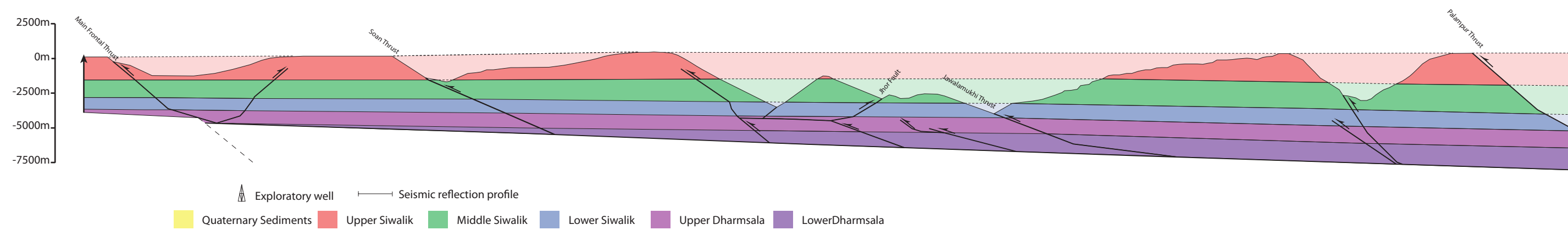
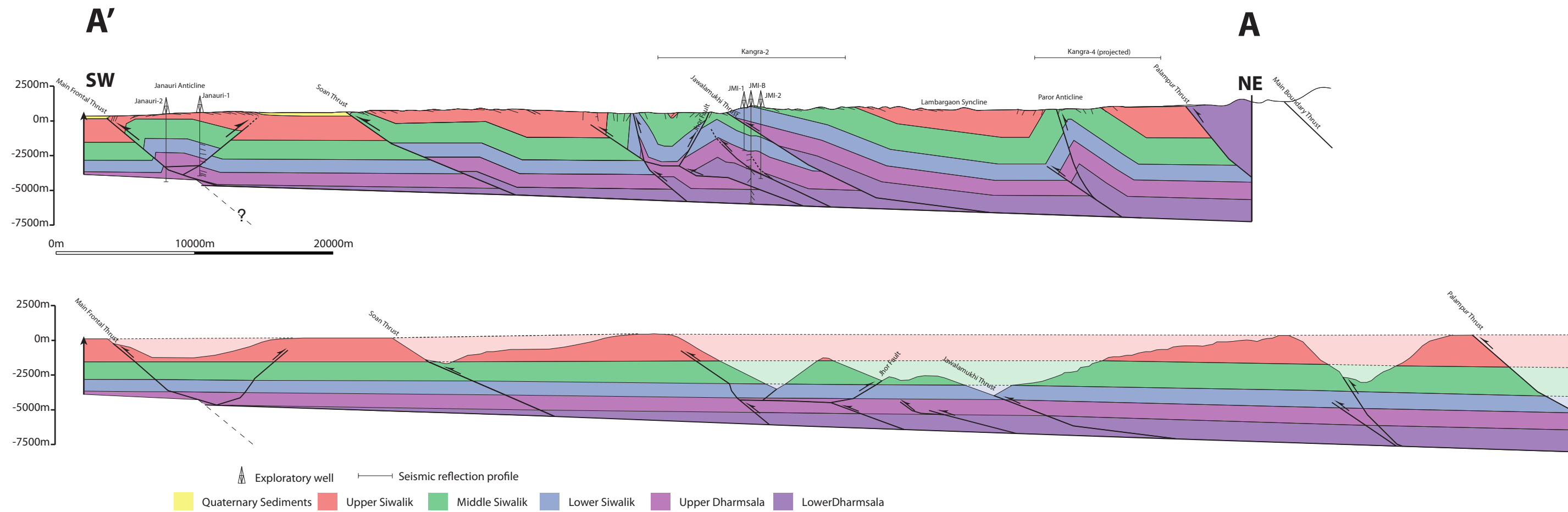


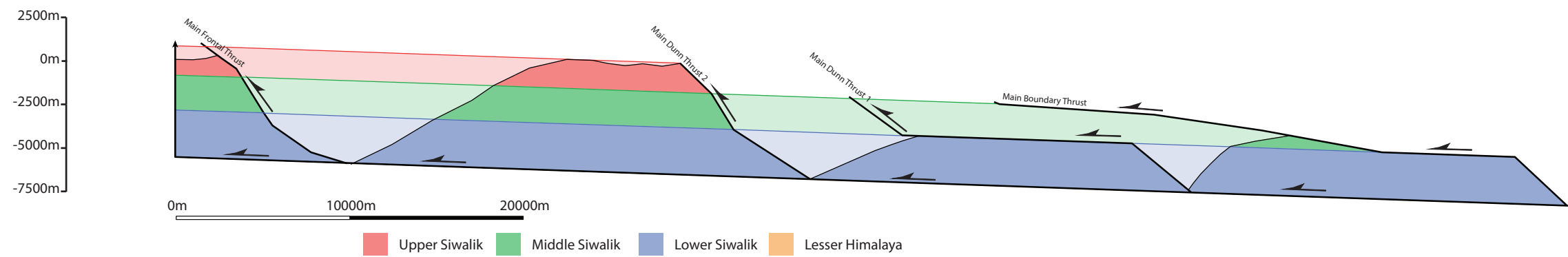
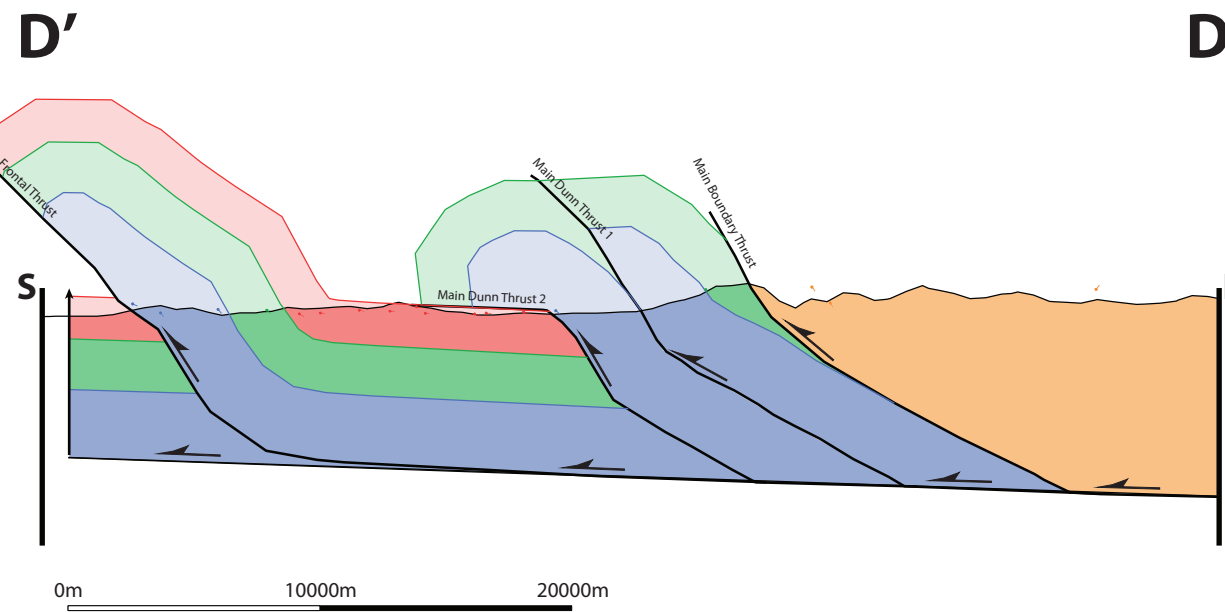
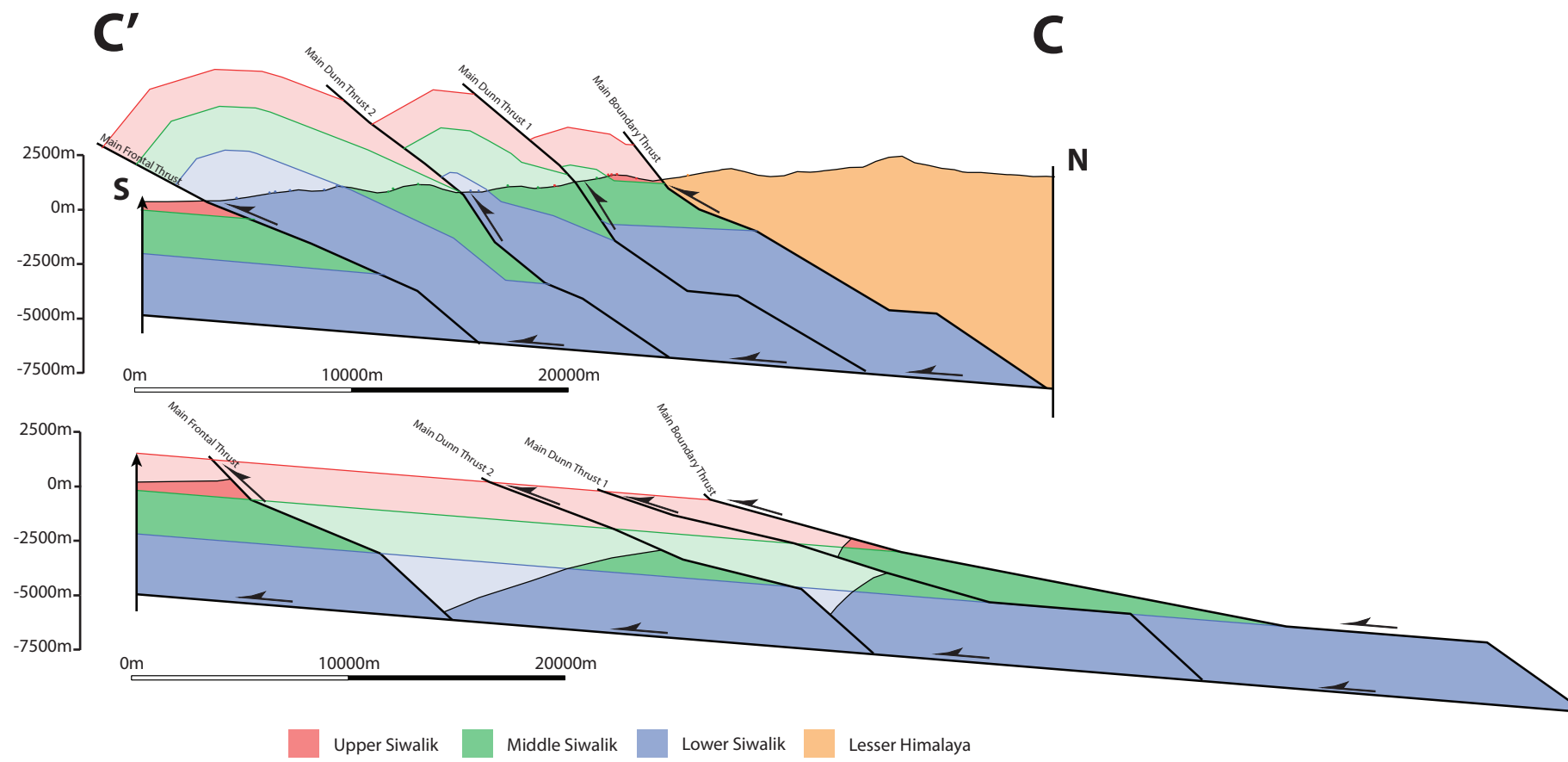
**Legend**

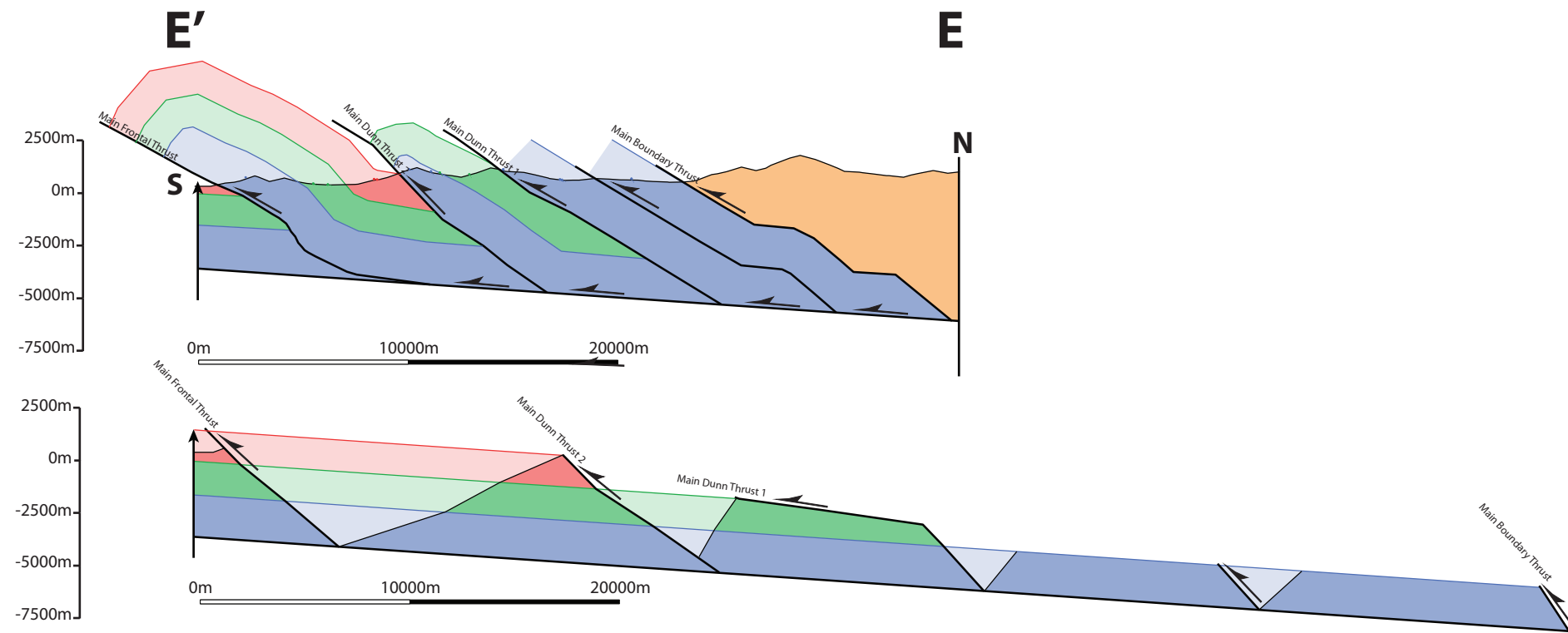
- Country Boundaries
- Cross section lines
- ▲- Thrust faults
- ┴- Normal faults
- - - Strike Slip faults
- - - Antiform
- - - Synform
- Yellow Quaternary
- Red Upper Siwalik
- Light Green Upper Middle Siwalik
- Medium Green Lower Middle Siwalik
- Dark Green Middle Siwalik
- Blue Lower Siwalik
- Orange Lesser Himalaya
- Orange MCT Zone
- Brown Greater Himalaya
- Light Green Chekha Formation
- Light Blue Tethyan Sedimentary Sequence

**Transfer Zones.  
Note the MFT  
creates steps**

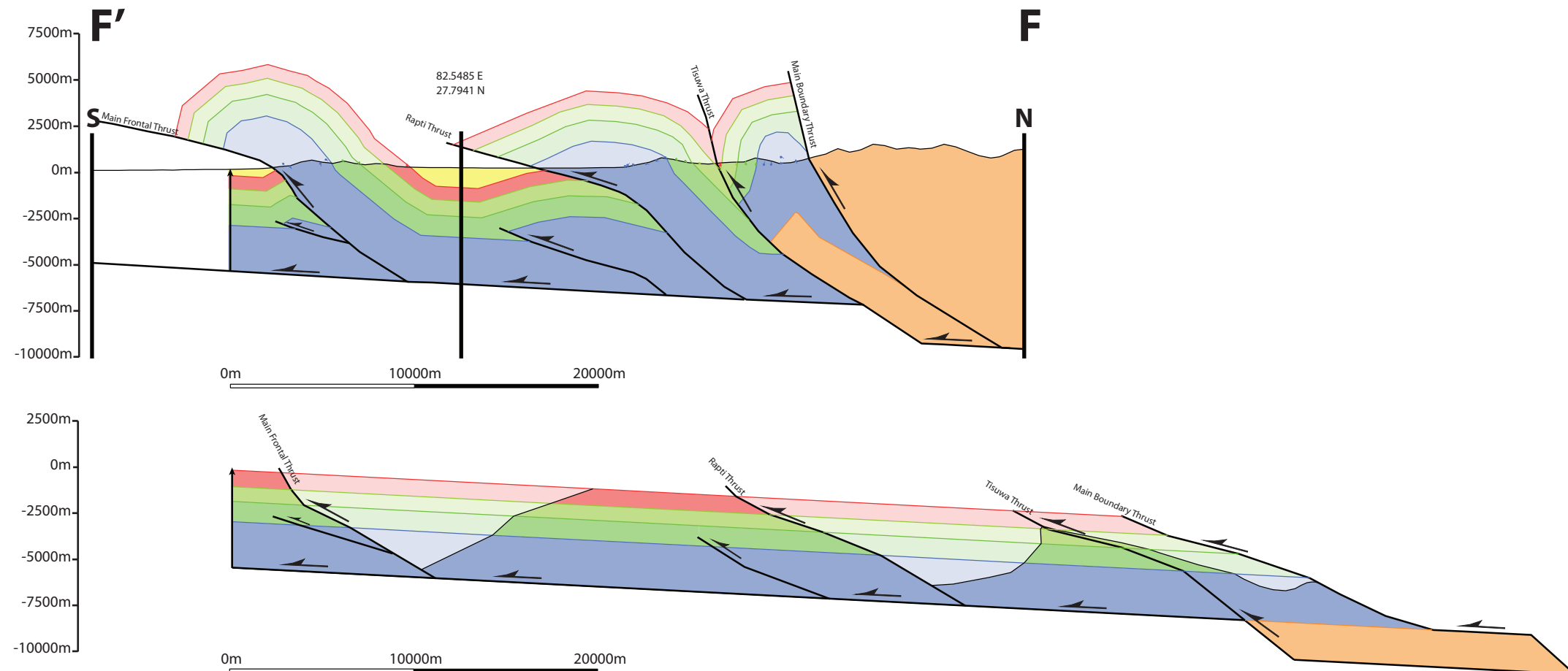




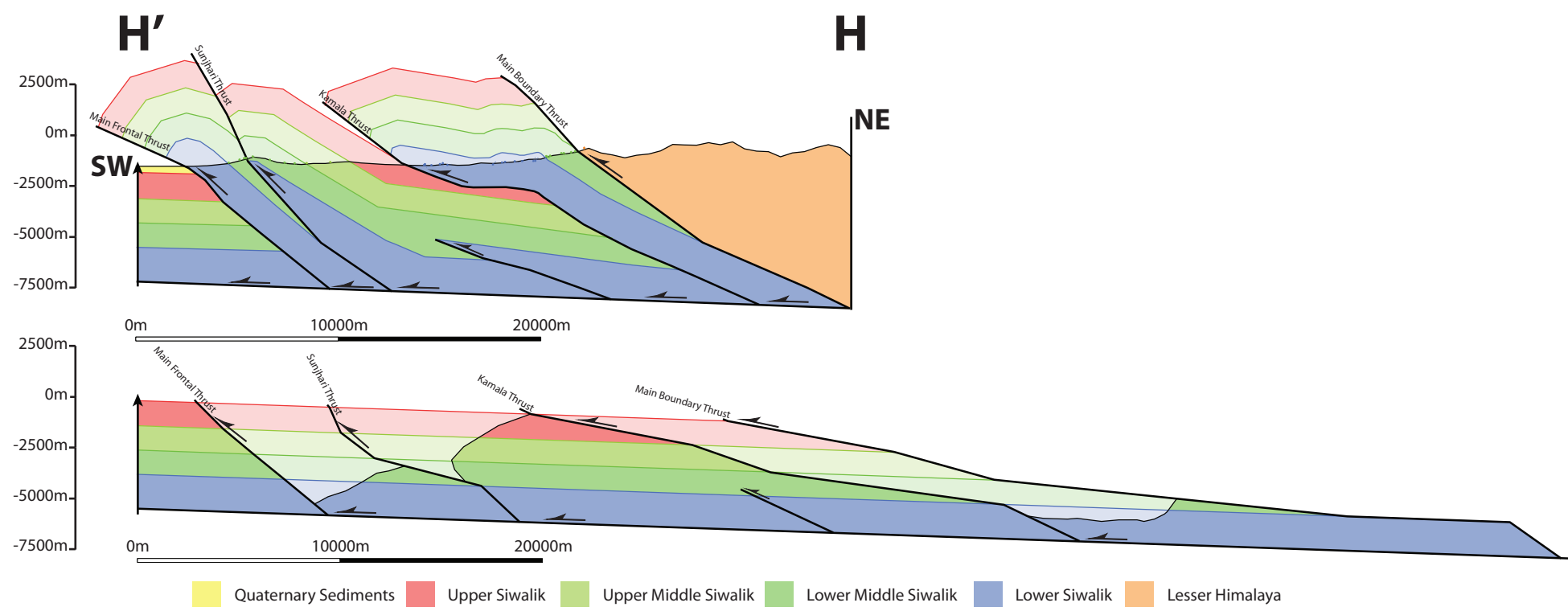
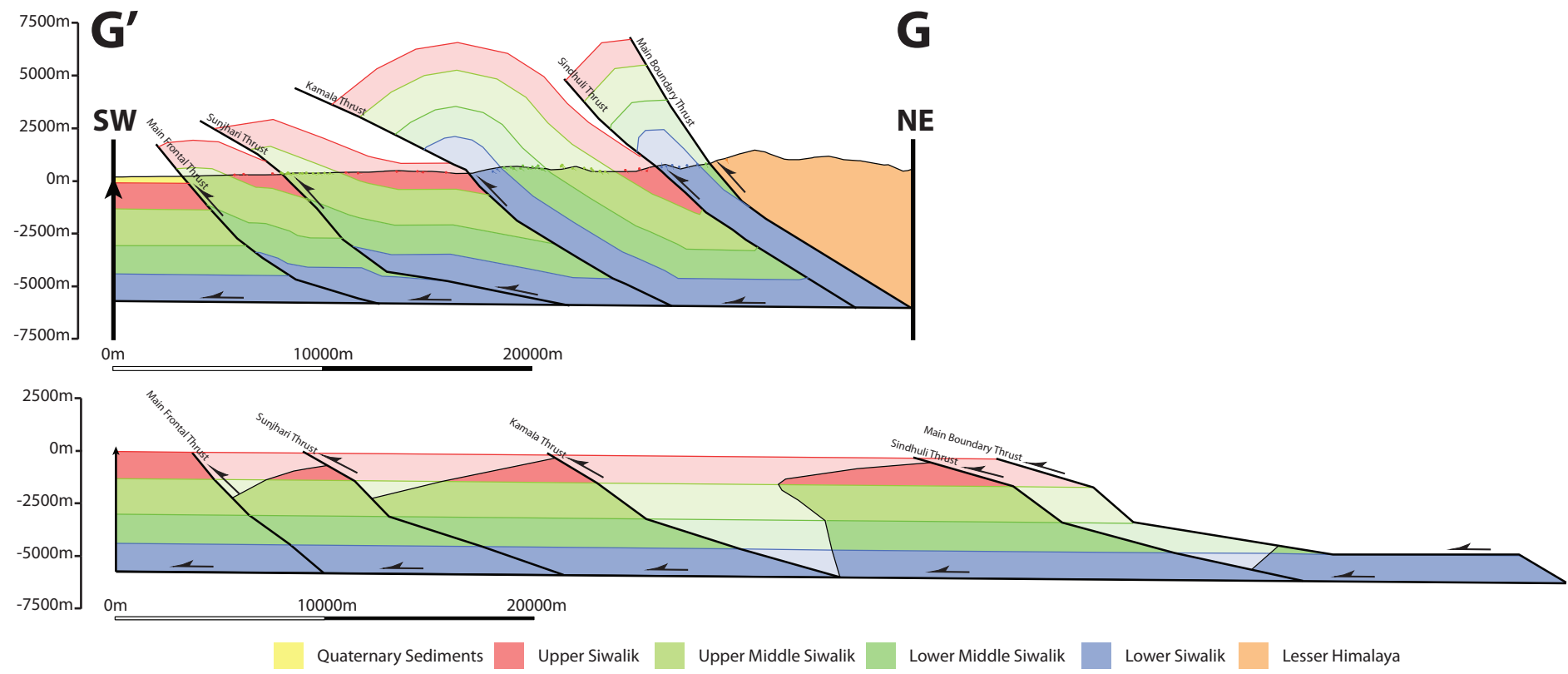


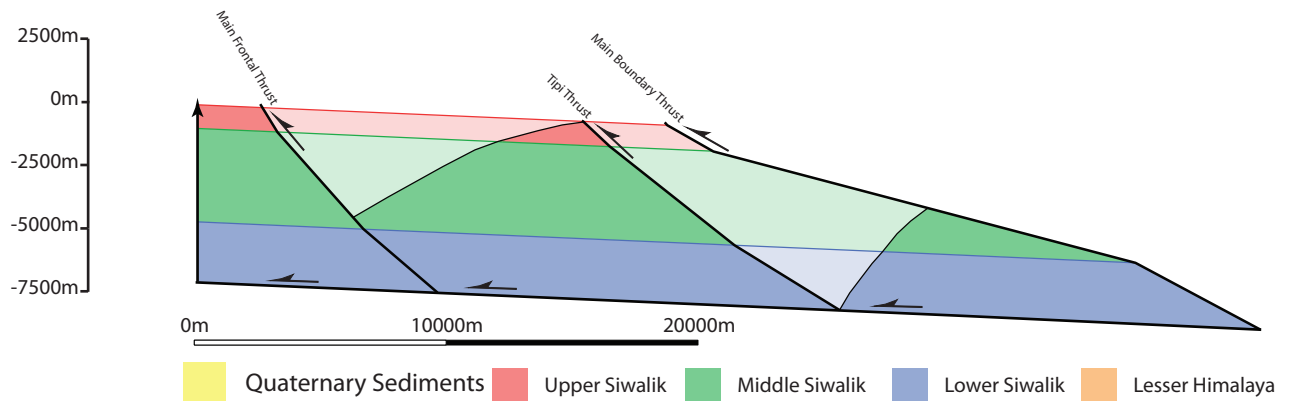
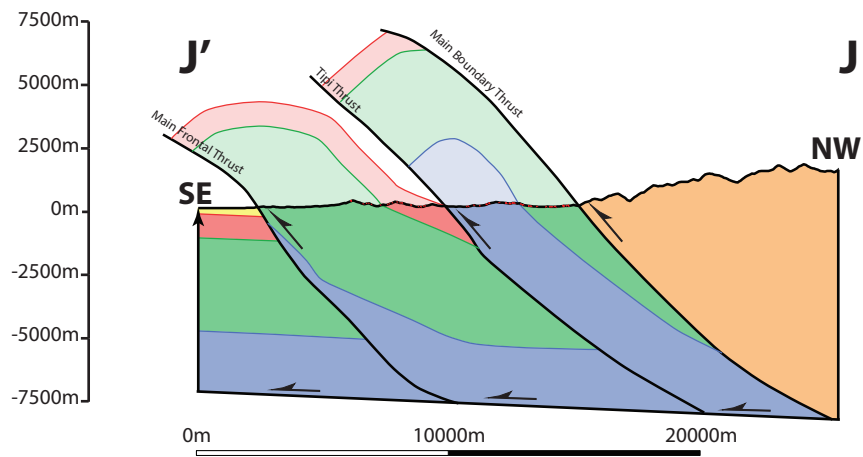
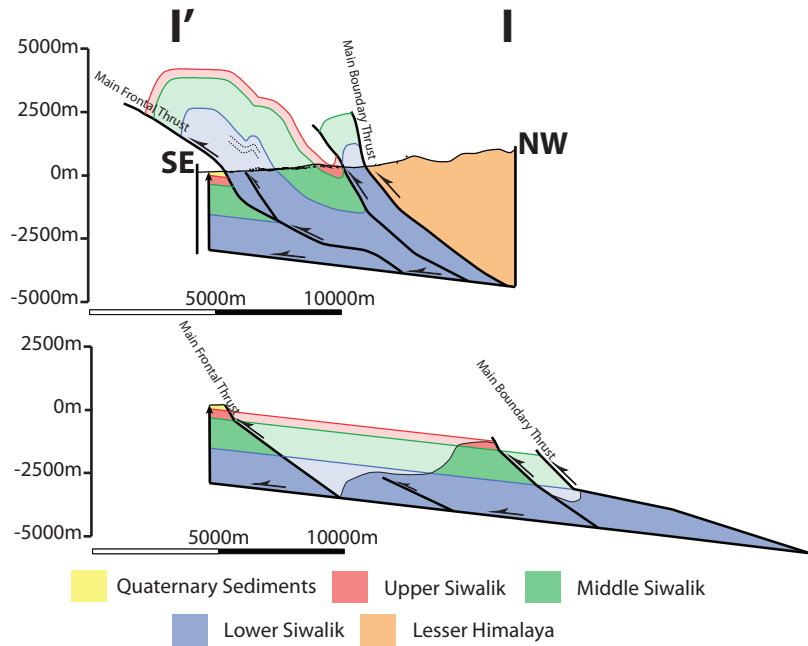


■ Upper Siwalik 
 ■ Middle Siwalik 
 ■ Lower Siwalik 
 ■ Lesser Himalaya



■ Quaternary Sediments 
 ■ Upper Siwalik 
 ■ Upper Middle Siwalik 
 ■ Lower Middle Siwalik 
 ■ Lower Siwalik 
 ■ Lesser Himalaya





<b>Section</b>	<b>Shortening km Lower Siwalik (km)</b>	<b>Shortening % Lower Siwalik (%)</b>	<b>Age of Upper/Middle Siwalik Boundary from Magnito Stratigraphy (Ma)</b>	<b>Shortening Rate from Age of Top of Middle Siwalik (Lower Siwalik Shortening) (mm/yr)</b>	<b>Strain Rate of the Lower/Middle Siwalik (strain/sec)</b>
<b>A</b>	<b>23.0 ± 3.47</b>	<b>21.5 ± 3.24</b>	<b>2.70 ± 0.30</b>	<b>8.52 ± 1.60</b>	<b>2.52E-15 ± 4.73E-16</b>
<b>B</b>	<b>10.6 ± 2.67</b>	<b>23.4 ± 5.89</b>	<b>2.70 ± 0.30</b>	<b>3.93 ± 1.08</b>	<b>2.75E-15 ± 7.56E-16</b>
<b>C</b>	<b>25.7 ± 2.21</b>	<b>41.1 ± 3.53</b>	<b>4.83 ± 1.00</b>	<b>5.32 ± 1.19</b>	<b>2.70E-15 ± 6.05E-16</b>
<b>D</b>	<b>37.7 ± 8.77</b>	<b>48.8 ± 11.4</b>	<b>4.83 ± 1.00</b>	<b>7.81 ± 2.43</b>	<b>3.20E-15 ± 9.97E-16</b>
<b>E</b>	<b>31.1 ± 3.22</b>	<b>48.2 ± 4.99</b>	<b>3.22 ± 0.30</b>	<b>9.66 ± 1.35</b>	<b>4.74E-15 ± 6.61E-16</b>
<b>F</b>	<b>27.0 ± 2.98</b>	<b>46.1 ± 5.09</b>	<b>3.22 ± 0.30</b>	<b>8.39 ± 1.21</b>	<b>4.54E-15 ± 6.55E-16</b>
<b>G</b>	<b>29.3 ± 1.52</b>	<b>43.5 ± 2.26</b>	<b>3.42 ± 0.60</b>	<b>8.57 ± 1.57</b>	<b>4.03E-15 ± 7.37E-16</b>
<b>H</b>	<b>32.6 ± 2.29</b>	<b>48.1 ± 3.38</b>	<b>3.42 ± 0.60</b>	<b>9.53 ± 1.80</b>	<b>4.46E-15 ± 8.42E-16</b>
<b>I</b>	<b>8.31 ± 1.45</b>	<b>57.1 ± 9.96</b>	<b>2.60 ± 0.30</b>	<b>3.20 ± 0.67</b>	<b>6.96E-15 ± 1.46E-15</b>
<b>J</b>	<b>16.5 ± 1.91</b>	<b>44.3 ± 5.13</b>	<b>2.60 ± 0.30</b>	<b>6.35 ± 1.04</b>	<b>5.40E-15 ± 8.82E-16</b>

